UNCLASSIFIED

CENTRAL RESEARCH LIBRARY
DOCUMENT COLLECTION

MARTIN MARIETTA ENERGY SYSTEMS LIBRARIES
3 4456 0361200 8

ORNL-2413 cy. 122
Physics and Mathematics
TID-4500 (13th ed. Rev.)

CENTRAL RESEARCH LIBRARY
DOCUMENT COLLECTION
LIBRARY LOAN COPY
DO NOT TRANSFER TO ANOTHER PERSON
If you wish someone else to see this document, send in name with document and the library will arrange a loan.

SOLID STATE DIVISION

ANNUAL PROGRESS REPORT

FOR PERIOD ENDING AUGUST 31, 1957

OAK RIDGE NATIONAL LABORATORY
OPERATED BY
UNION CARBIDE NUCLEAR COMPANY
Division of Union Carbide Corporation
UCC
POST OFFICE BOX X · OAK RIDGE, TENNESSEE

UNCLASSIFIED

Printed in USA. Price $3.50 cents. Available from the

Office of Technical Services
U. S. Department of Commerce
Washington 25, D. C.

LEGAL NOTICE

This report was prepared as an account of Government sponsored work. Neither the United States, nor the Commission, nor any person acting on behalf of the Commission:

A. Makes any warranty or representation, express or implied, with respect to the accuracy, completeness, or usefulness of the information contained in this report, or that the use of any information, apparatus, method, or process disclosed in this report may not infringe privately owned rights; or

B. Assumes any liabilities with respect to the use of, or for damages resulting from the use of any information, apparatus, method, or process disclosed in this report.

As used in the above, "person acting on behalf of the Commission" includes any employee or contractor of the Commission to the extent that such employee or contractor prepares, handles or distributes, or provides access to, any information pursuant to his employment or contract with the Commission.

UNCLASSIFIED

ORNL-2413
Physics and Mathematics
TID-4500 (13th ed. Rev.)

Contract No. W-7405-eng-26

SOLID STATE DIVISION

ANNUAL PROGRESS REPORT

For Period Ending August 31, 1957

D. S. Billington, Director
J. H. Crawford, Jr., Assistant Director

DATE ISSUED

NOV 11 1957

OAK RIDGE NATIONAL LABORATORY
Operated by
UNION CARBIDE NUCLEAR COMPANY
Division of Union Carbide Corporation
Post Office Box X
Oak Ridge, Tennessee

UNCLASSIFIED

3 4456 0361200 8

Reports previously issued in this series are:

ORNL-1025	Period Ending January 31, 1951
ORNL-1095	Period Ending April 30, 1951
ORNL-1128	Period Ending July 31, 1951
ORNL-1214	Period Ending October 31, 1951
ORNL-1261	Period Ending January 31, 1952
ORNL-1301	Period Ending May 10, 1952
ORNL-1359	Period Ending August 10, 1952
ORNL-1429	Period Ending November 10, 1952
ORNL-1506	Period Ending February 10, 1953
ORNL-1606	Period Ending August 31, 1953
ORNL-1677	Period Ending February 28, 1954
ORNL-1762	Period Ending August 30, 1954
ORNL-1851	Period Ending February 28, 1955
ORNL-1944	Period Ending August 30, 1955
ORNL-1945	Period Ending August 30, 1955
ORNL-2051	Period Ending February 29, 1956
ORNL-2052	Period Ending February 29, 1956
ORNL-2188	Period Ending August 30, 1956
ORNL-2189	Period Ending August 30, 1956

ORNL-2413
Physics and Mathematics
TID-4500 (13th ed. Rev.)

INTERNAL DISTRIBUTION

1. R. E. Adams
2. C. D. Baumann
3. R. G. Berggren
4. J. O. Betterton, Jr.
5. D. S. Billington
6. D. Binder
7. T. H. Blewitt
8. A. L. Boch
9. E. G. Bohlmann
10. C. D. Bopp
11. G. E. Boyd
12. H. Brooks (consultant)
13. W. A. Brooksbank
14. W. E. Browning
15. W. E. Brundage
16. D. W. Cardwell
17. R. M. Carroll
18. R. J. Carter
19. C. E. Center
20. R. A. Charpie
21. J. W. Cleland
22. R. J. Cleland (consultant)
23. R. R. Coltman
24. A. F. Cohen
25. J. H. Crawford, Jr.
26. F. L. Culler
27. J. E. Cunningham
28. O. L. Curtis
29. W. W. Davis
30. R. R. Dickison
31. S. E. Dismuke
32. L. B. Emlet (K-25)
33. J. H. Frye, Jr.
34. J. L. Gabbard
35. R. J. Gray
36. C. S. Harrill
37. H. L. Hemphill
38. N. E. Hinkle
39. A. Hollaender
40. D. K. Holmes
41. A. S. Householder
42. J. T. Howe
43. H. B. Huntington (consultant)
44. R. E. Jamison
45. L. H. Jenkins
46. L. K. Jetter
47. R. W. Johnson
48. R. J. Jones
49. W. H. Jordan
50. C. E. Klabunde
51. G. W. Keilholtz
52. C. P. Keim
53. M. T. Kelley
54. R. H. Kernohan
55. J. A. Krumhansl (consultant)
56. J. E. Lee
57. A. B. Lewis (consultant)
58. T. A. Lincoln
59. S. C. Lind
60. R. S. Livingston
61. H. G. MacPherson
62. C. J. McHargue
63. W. D. Manly
64. E. J. Manthos
65. A. J. Miller
66. E. C. Miller
67. J. G. Morgan
68. K. Z. Morgan
69. M. T. Morgan
70. E. J. Murphy
71. J. P. Murray (Y-12)
72. C. M. Nelson
73. M. L. Nelson
74. T. S. Noggle
75. R. B. Oliver
76. M. F. Osborne
77. V. Paré
78. W. W. Parkinson
79. D. Phillips
80. J. C. Pigg
81. T. A. Read (consultant)
82. P. E. Reagan
83. J. K. Redman
84. P. M. Reyling
85. A. E. Richt
86. H. E. Robertson
87. C. C. Robinson
88. M. T. Robinson
89. O. E. Schow
90. E. S. Schwartz

91. H. C. Schweinler
92. W. C. Sears (consultant)
93. F. Seitz (consultant)
94. S. T. Sekula
95. F. A. Sherrill
96. R. P. Shields
97. E. D. Shipley
98. R. H. Silsbee (consultant)
99. O. Sisman
100. M. J. Skinner
101. G. P. Smith
102. A. H. Snell
103. E. Sonder
104. R. L. Sproull (consultant)
105. E. E. Stansbury
106. J. O. Stiegler
107. C. D. Susano
108. J. A. Swartout
109. E. H. Taylor
110. D. O. Thompson
111. M. S. Wechsler
112. R. A. Weeks
113. A. M. Weinberg
114. E. P. Wigner (consultant)
115. G. C. Williams
116. J. C. Wilson
117. C. E. Winters
118. M. C. Wittels
119. F. W. Young
120. J. C. Zukas
121. Biology Library
122-124. Central Research Library
125. Health Physics Library
126-145. Laboratory Records Department
146. Laboratory Records, ORNL R.C.
147. ORNL, Y-12 Technical Library, Document Reference Section
148. Reactor Experimental Engineering Library

EXTERNAL DISTRIBUTION

149. R. F. Bacher, California Institute of Technology
150. W. W. Shaver, Corning Glass Works, Corning, New York
151. S. H. Liebson, Naval Research Laboratory, Washington, D.C.
152. Boeing Airplane Company
153. H. V. Klaus, Phillips Petroleum Company
154. Division of Research and Development, AEC, ORO
155. J. R. Johnson, Minnesota Mining and Manufacturing Co., St. Paul
156. R. N. Little, ANP Project Office, Fort Worth
157. G. L. Stiehl, Convair Division of General Dynamics Corp., San Diego
158. C. C. Webster, Engineering Center, Westinghouse Electric Corp., E. Pittsburgh
159. R. O. Bolt, California Research Corp., Richmond
160. Benjamin Lax, Lincoln Laboratory, Lexington, Massachusetts
161. George H. Wagner, Linde Air Products Company, Tonawanda Laboratory, East Park Drive and Woodward Avenue, Tonawanda, New York
162. D. K. Stevens, Materials and Metallurgy Branch, Division of Research, U.S. Atomic Energy Commission, Washington, D.C.
163. J. B. Trice, General Electric Company – ANPD, Applied Materials Research, Building D, Cincinnati 15, Ohio
164. R. I. Leininger, Battelle Memorial Institute, 505 King Avenue, Columbus, Ohio
165. L. F. Connell, Jr., Dept. of Physics, N. Texas State Col., Denton, Texas
166. Westinghouse Electric Corp., Research Laboratories, Pittsburgh, Pennsylvania
167. J. G. Castle, Jr., Physics Dept., Westinghouse Electric Corp., Research Laboratories, Pittsburgh, Pennslyvania
168-722. Given distribution as shown in TID-4500 (13th ed. Rev.) under Physics and Mathematics category

CONTENTS

Publications and Papers vii
Summary 1
Low-Temperature Bombardment of Metals 9
Theoretical Considerations on the Temperature Dependence of the Mechanical Properties of Metals 13
Young's Modulus and Internal-Friction Studies 16
Small-Angle X-Ray Scattering Studies of Fast-Neutron Irradiation Effects in an Aluminum-Silver Precipitate Alloy 18
Effect of Neutron Irradiation on Copper-Base Alloys 19
The Precipitation-Hardening Reaction in Nickel-Beryllium 22
Electron Microscope Studies 24
Chemical Properties of Metal Surfaces 25
Low-Temperature Irradiation of *n*-Type Germanium 28
Minority-Carrier Lifetime Studies in Germanium 31
Mobility Changes in Irradiated *n*-Type Germanium 32
Annealing Studies of Irradiated Germanium 34
Optical Absorption in Germanium 36
Activation Energies and Total Energies of Localized States in Semiconductors 38
Magnetic Properties of Arsenic-Doped Silicon 42
Magnetic Susceptibility of Molybdenum 47
Instrumentation for Susceptibility Studies 48
Magnetic Defects in Covalent and Ionic Crystal Systems 50
Superheterodyne Electron-Spin-Resonance Spectrometer 55
Optical Absorption Studies of Irradiated Solids 58
X-Ray Diffraction Studies 64
Low-Temperature Thermal Conductivity of Potassium Chloride Crystals, Including the Effects of Strain and Particle Irradiation 66
Low-Temperature Thermal Conductivity of Nonmetals 69
Low-Temperature Thermal Conductivity in Neutron-Irradiated Vitreous Silica 70
Proposed Reactor Bombardments at 4°K 72
Gamma-Source Facilities 73
Automatic Liquid-Gas Level Control 74
HRP Radiation Metallurgy 75
Radiation Stability of Ceramic Materials 80
Infrared Spectra of Plastics and Elastomers After Irradiation 83
Effect of High-Energy Radiation on Polymers 88
Analysis of Gases Evolved by Irradiation of Polymers 91
Effects of Radiation on Engineering Properties of Polymeric Materials 93

Miscellaneous Polymer Problems 98
High-Frequency Electrical Properties of Some Irradiated Plastic Materials 99
Attempt at the Separation of Neutron and Gamma-Ray Irradiation Effects by Means of a Hydrogenous Absorber 100
An Investigation of the Properties of Two Uranium-Bearing Zeolites 102
Forced-Cooling Ceramic-Fuels Experiment 109
High-Temperature Ceramic Fuels 110
Radiation Effects in Thermocouple Insulation 116
Chemical Effects of Nuclear Reactions 117
Adsorption of Fission Gases by Activated Charcoal 118
Investigation of Sulfur Contamination of a Dry Box by Neoprene Rubber 119
Neutron Flux Monitoring in High-Temperature In-Pile Experiments 120
ORR Experimental Facility 121
Fission Reactions as Threshold Detectors 122
Hot Lab Studies 125

PUBLICATIONS AND PAPERS

R. G. Berggren, S. E. Dismuke, M. J. Feldman, and J. C. Wilson
"Mechanics of Testing Irradiated Materials," *Am. Soc. Testing Materials, Spec. Tech. Publ. No. 208* (1957).

R. G. Berggren and J. C. Wilson
Recent Data on the Effects of Neutron Irradiation on Structural Metals and Welds, ORNL CF-56-11-1 (Jan. 30, 1957).

WASH-733 (Part 2) p 236–273 (secret).

D. S. Billington
"Radiation Damage in Reactor Materials," *Proc. Intern. Conf. Peaceful Uses Atomic Energy, Geneva, 1955* **7**, 421–432 (1956).

"Irradiation Effects in Reactor Materials," *Nuclear Metallurgy; A Symposium*, p 31–54, Special Report Series No. 3, AIMMPE, Institute of Metals Division, New York, 1956.

"Radiation Effects on Physical and Metallurgical Properties of Metals and Alloys," paper presented at the Office of Naval Research – Martin Company Colloquium on the Effects of Radiation on Materials, Baltimore, Md., March 1957.

"Neutron Irradiation Effects in Metals and Alloys," talk given at the Franklin Institute, Philadelphia, Pa., June 1957, and also at the Naval Ordnance Laboratory, Silver Spring, Md., June 1957.

D. Binder and W. J. Sturm
"Expansion of LiF Under Neutron Irradiation," *Phys. Rev.* **107**, 106 (1957).

T. H. Blewitt
"Low Temperature Irradiation Effects," paper presented at the American Physical Society Meeting, Cleveland Section, Cleveland, May 1957.

"Low-Temperature Irradiation Studies," paper presented at the Gordon Research Conference, Chemistry and Physics of Metals Session, Meriden, N. H., July 8–12, 1957.

T. H. Blewitt, R. R. Coltman, D. K. Holmes, and T. S. Noggle
"Mechanisms of Annealing in Neutron Irradiated Metals," *Creep and Recovery*, p 84, American Society of Metals, Cleveland, 1957.

T. H. Blewitt, R. R. Coltman, C. E. Klabunde, and T. S. Noggle
"Low-Temperature Reactor Irradiation Effects in Metals," *J. Appl. Phy.* **28**, 639–644 (1957).

T. H. Blewitt, R. R. Coltman, and J. K. Redman
"Low-Temperature Deformation of Copper Single Crystals," *J. Appl. Phy.* **28**, 651 (1957).

T. H. Blewitt and J. K. Redman
"Effect of Neutron Irradiation on Twinning in Copper," *Bull. Am. Phys. Soc.* **2**, Series II, 137 (1957).

C. D. Bopp, W. K. Kirkland, O. Sisman, and R. L. Towns
"Radiation Effects on Polymer Vibration Characteristics," *Ind. Eng. Chem.* **49**, 718 (1957).

R. Chang
"Etching Behavior of Pile-Irradiation Germanium and Silicon Single Crystals," *J. Appl. Phy.* **28**, 385–387 (1957).

J. W. Cleland and J. H. Crawford, Jr.
"Radiation Effects in Semiconductor Materials," paper presented by J. W. Cleland at the Symposium on Nuclear Radiation Effects in Semiconductor Devices and Materials, New York, N.Y., February 27–28, 1957.

A. F. Cohen
"Low Temperature Thermal Conductivity of Non-Metals Including Radiation Effects," paper presented at the International Low-Temperature Conference, Madison, Wis., August 1957.

A. F. Cohen and L. C. Templeton
"Effect of Fast Neutron and Gamma-Ray Bombardment on the Low-Temperature Thermal Conductivity of Non-Metals," *Bull. Am. Phys. Soc.* **2**, Series II, 186 (1957).

B. L. Cohen, A. F. Cohen, and C. D. Foley
"Energy Distribution of Mass-97 Fission Fragments from Thermal Neutron Fission of U-235," *Phys. Rev.* **104**, 1046 (1956).

R. R. Coltman
"Radiation Hardening. – Part I. Experiments," paper presented at the Gordon Research Conference, Chemistry and Physics of Metals Session, Meriden, N. H., July 8–12, 1957.

R. R. Coltman and T. H. Blewitt
"Reactor Irradiations at 15°K," *NBS Proceedings of the 1956 Cryogenic Conference*, p 110–115, University of Colorado, Boulder, 1957.

R. R. Coltman, T. H. Blewitt, and T. S. Noggle
"Techniques and Equipment Utilized in Low-Temperature Reactor Irradiations," *Rev. Sci. Instr.* **28**, 375–380 (1957).

J. H. Crawford, Jr.
"Magnetic Susceptibility of Semiconductors," paper presented at the Naval Ordnance Laboratory, Silver Spring, Md., February 14, 1957.

"The Nature of Radiation Damage in Crystalline Solids," *Bull. Am. Ceram. Soc.* **36**(3), 95–98 (1957).

"The Effects of Nuclear Environment on the Properties of Solids," talk given at the American Institute of Electrical Engineers–Institute of Radio Engineers Meeting, Philadelphia Section, Philadelphia, Pa., March 1957.

"Effects of Radiation on Semiconductors," paper presented at ORINS Radiation Chemistry Course, Oak Ridge, Tenn., April 6, 1957.

"Radiation Effects in Non-Metals," paper given at the Gordon Research Conference, Chemistry and Physics of Metals Sessions, Meriden, N. H., July 8–12, 1957.

J. H. Crawford, Jr., and J. W. Cleland
"Radiation Effects in Semiconductors," *Progress in Semiconductors*, vol 2, p 67–107, Heywood and Company, London, 1957.

O. L. Curtis, Jr., J. W. Cleland, and J. C. Pigg
"Effect of Irradiation on the Hole Lifetime of *n*-Type Germanium," *Bull. Am. Phys. Soc.* **2**, Series II, 157 (1957).

S. E. Dismuke, M. J. Feldman, G. W. Parker, and F. Ring, Jr.
"Hot Laboratory Facilities and Techniques for Handling Radioactive Materials," *Proc. Intern. Conf. Peaceful Uses Atomic Energy, Geneva, 1955* **7**, 67–81 (1956).

D. K. Holmes
"Radiation Hardening. Part II. Theory," paper given at the Gordon Research Conference, Chemistry and Physics of Metals Session, Meriden, N. H., July 8–12, 1957.

J. T. Howe, R. R. Coltman, and T. H. Blewitt
"Liquid Helium Temperatures in an Atomic Reactor," paper presented by J. T. Howe at the National Bureau of Standards 1957 Cryogenic Conference, Boulder, Colo., August 19–21, 1957.

R. E. Jamison
"Retardation of Zone Growth in an Al-Ag Precipitate Alloy by Previous Fast Neutron Irradiation," *Bull. Am. Phys. Soc.* **2**, Series II, 151–152 (1957).

C. E. Klabunde, T. H. Blewitt, R. R. Coltman, and T. S. Noggle
"Low-Temperature Annealing Process in Irradiated Metals. Part A. Effect of Defect Concentrations in Copper," *Bull. Am. Phys. Soc.* **2**, Series II, 137 (1957).

E. J. Manthos
ORNL CF-57-3-14 (secret).

ORNL CF-57-3-53 (secret).

J. G. Morgan
"Radiation Damage Effects," talk given at the Information Meeting on Thermal Neutron Shielding Materials, Oak Ridge National Laboratory, Oak Ridge, Tenn., September 20, 1956.

TID-7530 (Part 2) (confidential).

"Ceramics Irradiation Program," talk given at the ORNL–Army Reactor Branch, Metallurgy Information Meeting, Oak Ridge National Laboratory, Oak Ridge, Tenn., May 6–7, 1957.

C. M. Nelson and J. H. Crawford, Jr.
"Optical Absorption of Irradiated Quartz and Fused Silica," paper presented by C. M. Nelson at the Symposium on Defect Structure of Quartz and Glassy Silica, Mellon Institute, Pittsburgh, Pa., May 1957.

T. S. Noggle, T. H. Blewitt, R. R. Coltman, and C. E. Klabunde
"Low-Temperature Annealing of Irradiated Metals. Part B. Effect of Sample History," *Bull. Am. Phys. Soc.* **2**, Series II, 151 (1957).

"Thermal-emf-Free Vacuum Seal for Electrical Lead Wires," *Rev. Sci. Instr.* **28**, 464 (1957).

J. C. Pigg
"Effects of Irradiation on Electronic Components," talk presented at the American Institute of Electrical Engineers–Institute of Radio Engineers Symposium, Philadelphia, Pa., May 2, 1957.

J. C. Pigg and C. C. Robinson
"Effect of Radiation on Semiconductors," *Elec. Mf.* **59**(4), 116 (1957).

"Effects of Irradiation on Semiconductor Components," paper presented by J. C. Pigg at the Institute of Radio Engineers Meeting, San Diego, Calif., April 26, 1957.

A. E. Richt
ORNL CF-56-10-91 (secret).

ORNL CF-57-2-30 (secret).

ORNL CF-57-31-51 (secret).

ORNL CF-56-10-56 (secret).

ORNL CF-56-12-105 (secret).

ORNL CF-57-2-33 (secret).

ORNL CF-57-5-46 (secret).

A. E. Richt and J. O. Stiegler
Metallographic Examination of HRP In-Pile Loop L-4-11, ORNL CF-56-9-116.

M. T. Robinson
"The Reaction of Boric Acid with Some Pyridine Bases," *J. Phys. Chem.* **61**, 120–122 (1957).

"Molten Salt Research in the ORNL Solid State Division," paper presented at the Molten Salt Symposium, Oak Ridge National Laboratory, Oak Ridge, Tenn., July 1957.

M. T. Robinson, W. A. Brooksbank, S. A. Reynolds, H. W. Wright, and T. H. Handley
ORNL-2374 (secret).

M. T. Robinson and G. E. Klein
"Radiation Stability of Copper Phthalocyanine," *J. Phys. Chem.* **61**, 1004 (1957).

M. T. Robinson and J. F. Krause
"The Yields of Chemical Elements in Thermal Neutron Fission of Uranium-235," *Nuclear Sci. and Eng.* **1**, 216–221 (1956).

E. S. Schwartz
"Hot Cell Operation at the Oak Ridge National Laboratory Solid State Division," *Fifth Hot Laboratories and Equipment Conference*, p 91–97, Nuclear Congress, Philadelphia, 1957.

F. A. Sherrill, M. C. Wittels, and T. H. Blewitt
"X-Ray Determination of Conjugate Deformation Twins in Copper," *J. Appl. Phy.* **28**, 526 (1957).

O. Sisman
"The Effect of High Energy Radiation on the Physical Properties of Plastics and Elastomers," paper presented at the U.S. Naval Air Development and Material Center, Philadelphia, Pa., March 12, 1957.

O. Sisman, W. E. Brundage, and W. W. Parkinson
ORNL-1965 (secret).

D. K. Stevens, W. J. Sturm, E. Sonder, J. W. Cleland, and J. H. Crawford
"Magnetic Susceptibility of Silicon," *Bull. Am. Phys. Soc.* **2**, Series II, 134 (1957).

J. O. Stiegler
Metallographic Examination of HRP In-Pile Loop L-4-8, ORNL CF-56-12-113 (Dec. 28, 1956).

Metallographic Examination of HRP In-Pile Loop L-4-12, ORNL CF-57-2-88 (Feb. 19, 1957).

Metallographic Examination of HRP In-Pile Loop L-2-10, ORNL CF-57-3-42 (March 9, 1957).

Metallographic Examination of HRP In-Pile Loop "GG," ORNL CF-57-3-83 (March 19, 1957).

Metallographic Examination of HRP In-Pile Loop L-4-13, ORNL CF-57-3-140 (March 29, 1957).

Supplemental Metallographic Examination of HRP In-Pile Loop L-4-12, ORNL CF-57-8-54 (Aug. 9, 1957).

D. O. Thompson
"Irradiation Measurements of the Young's Modulus and Internal Friction of Copper During Irradiation," presented at the Gordon Research Conference, Chemistry and Physics of Metals Session, Meriden, N. H., July 8–12, 1957.

D. O. Thompson, T. H. Blewitt, and D. K. Holmes
"Low Temperature Measurements of the Young's Modulus and Internal Friction of Copper During Irradiation," *J. Appl. Phy.* **28**, 742 (1957).

D. O. Thompson and D. K. Holmes
"The Effect of Gamma Irradiation on the Young's Modulus of Copper," *Intern. J. Phys. Chem. Solids* **1**(4), 275 (1957).

M. S. Wechsler
"The Quenching-In of Lattice Defects in Gold-Cadmium," *Acta Met.* **5**, 150 (1957).

R. A. Weeks
"Paramagnetic Resonance of Lattice Defects in Irradiated Quartz," *J. Appl. Phy.* **27**, 1376–1381 (1956).

R. A. Weeks and D. Binder
"Effects of Neutron and Gamma-Ray Irradiation on the Dielectric Constant and Loss Tangent of Some Plastic Materials," paper presented by R. A. Weeks at the Institute of Radio Engineers Conference, San Diego, Calif., April 26, 1957.

R. A. Weeks, R. H. Silsbee, D. K. Stevens, and E. Sonder
"Magnetic Behavior of Defects in Irradiated Quartz and Silica," paper presented by R. H. Silsbee at the Symposium on Defect Structure of Quartz and Glassy Silica, Mellon Institute, Pittsburgh, Pa., May 1957.

J. C. Wilson
"The Effect of Intense Reactor Irradiation on Materials," paper presented at the 29th International Congress of Industrial Chemistry, Paris, France, November 1956.

"Modern Metallurgical Testing," talk presented at the American Society of Metals, New York City Chapter, New York, January 14, 1957.

"Experimental Approaches to Radiation Studies – Radiation Sources and Dosimetry," paper presented at Office of Naval Research – Martin Company Colloquium on the Effects of Radiation on Materials, Baltimore, Md., March 1957.

ORNL CF-57-5-82 (confidential).

J. C. Wilson and R. G. Berggren
"Will ASTM Standards Be Influenced by Radiation Effects in Metals?" paper presented by J. C. Wilson at the Symposium on Radiation Effects in Materials, Los Angeles, Calif., September 17–21, 1956, *Am. Soc. Testing Materials, Spec. Tech. Publ. No. 208* (1957).

M. C. Wittels
"Expansions in Reactor Irradiated Germanium and Silicon," *J. Appl. Phy* **28**, 921 (1957).

M. C. Wittels and F. A. Sherrill
"Fast Neutron Effects in Tetragonal Barium Titanate," *J. Appl. Phy.* **28**, 606 (1957).

"Effects of Neutron Irradiation on Silica Structures," paper presented by M. C. Wittels at the Symposium on Defect Structure of Quartz and Glassy Silica, Mellon Institute, Pittsburgh, Pa., May 23, 1957.

F. W. Young, Jr.
"Dislocations in Copper as Revealed by Etch Pits and Oxide Nuclei," paper given at the Gordon Research Conference, Chemistry and Physics of Metals Session, Meriden, N.H., July 8–12, 1957.

Members of the Solid State Division, ORNL
TID-7515 (Part 2) (confidential).

SOLID STATE DIVISION ANNUAL PROGRESS REPORT

SUMMARY

Low-Temperature Bombardment of Metals

The information obtained from the low-temperature bombardments seems to indicate that the nature of radiation damage in metals is considerably more complex than was thought earlier. The concept of a highly mobile defect such as the crowdion seems to meet the requirements of the present data. It is felt that experiments based upon an effort to understand the properties of the crowdion and its interactions with other lattice defects will offer a hopeful approach to the problem of describing the details of radiation damage in metals.

Theoretical Considerations on the Temperature Dependence of the Mechanical Properties of Metals

A method of treatment of the thermal activation of dislocation line motion has been applied to the temperature dependence of the internal friction and Young's modulus and of the critical shear stress after neutron irradiation of copper single crystals. The theory is regarded as satisfactory for the critical shear stress but only tentatively acceptable for the internal friction.

Young's Modulus and Internal Friction Studies

Measurements of low-temperature phenomena in the internal friction and Young's modulus curves of copper have been made during the past year. These studies have been devoted chiefly to measurements of the temperature dependence of these properties before and after neutron irradiation, and to the Bordoni relaxation peaks in cold-worked samples. From the temperature-dependent curves before and after irradiation it is possible to deduce the temperature dependence of the dislocation component in both the modulus and internal friction curves. The Bordoni studies have not yet yielded the expected results in terms of existing theory. It is planned to continue both these investigations in the coming year.

Small-Angle X-Ray Scattering Studies of Fast-Neutron Irradiation Effects in an Aluminum-Silver Precipitate Alloy

Measurements of rates of zone growth, measurements of zone size distributions, and studies of zone structure differences between irradiated and nonirradiated aluminum-silver have been continued. Recent results indicate that the retardation of zone growth by previous irradiation may be due to a changing distribution of vacant lattice sites in the silver-poor shells of the zones during early heat treatment following irradiation.

Effect of Neutron Irradiation on Copper-Base Alloys

The process that causes the electrical resistivity of certain alloys to decrease upon neutron irradiation is being studied. This effect has been found to be particularly prominent in the copper-rich α solid solutions of copper-aluminum and copper-zinc, but no appreciable effect was detected in the alloys of copper with silicon, gallium, germanium, arsenic, and tin. It is found that the magnitude of the effect in the copper-aluminum alloys increases with aluminum content. For the copper-aluminum alloy containing 15 atomic per cent aluminum, exposure to an integrated neutron flux of about 10^{18} neutrons/cm^2 at 40°C produces a decrease of 2 per cent resistivity, but upon further irradiation the resistivity increases linearly with time of exposure. However, when the irradiation is carried out at −120°C, no decrease is observed, although if the sample is subsequently heated to above 0°C in the absence of the neutron flux, the decrease in resistivity then takes place. The kinetics of the decrease in resistivity that occurs under these circumstances has been investigated, and an activation energy of 0.8 ev has been obtained for the process. Characteristic differences in the behavior of single crystals and polycrystals were noted.

The Precipitation-Hardening Reaction in Nickel-Beryllium

Two experiments on the alloy nickel-beryllium were completed. In the first experiment, supersaturated specimens irradiated at ambient temperature in the ORNL Graphite Reactor were subsequently heat-treated at 450°C. A definite suppression of the first stage of the precipitation process was observed. In the second experiment, specimens heat-treated and irradiated at 300°C were subsequently heat-treated at 450°C. In this case, a retardation in the precipitation process was observed which corresponds to the phenomenon of retrogression observed in other age-hardening alloys.

Electron Microscope Studies

A program of electron microscope studies on solids has recently been initiated. The main emphasis of this program will be the study of radiation effects in solids. Attempts will be made to "see" directly radiation effects in solids as well as to study indirect effects such as the changes in the surface structures developed by plastic deformation which result from irradiation with energetic particles. Preliminary work on the development of remote replication techniques applicable to highly radioactive materials has been started.

Chemical Properties of Metal Surfaces

The relationships between dislocations in copper single crystals and the chemical properties of the metal surface are being studied by observing (1) oxide films and nuclei formed by gaseous oxidation of the metal, (2) etch pits produced electrolytically in crystals containing certain impurities, and (3) pits resulting from thermal etching. Gaseous oxidation in a radiation field is also being investigated. Differences in surface processes as a function of crystal face are being considered by establishing the effects of orientation on reaction rates, activation energies, reaction mechanisms, etc. during the dissolution of copper in aqueous media by various chemical reagents.

Low-Temperature Irradiation of n-Type Germanium

The removal rate of conduction electrons in n-type germanium is increased during fast-neutron irradiation at $\sim$ 16°K over that previously observed at $\sim$ 100°K. No evidence of thermally activated annealing processes was observed below $\sim$ 100°K. Large-scale annealing occurred at higher temperatures as a consequence of successive escape of trapped holes from trapping levels.

Minority-Carrier Lifetime Studies in Germanium

The lifetime of excess carriers injected into germanium by an electrical pulse or light pulse is dependent on the number of recombination centers present. Irradiation introduces recombination centers in germanium, and lifetime measurements provide an understanding of the process of carrier recombination. This information is of importance for use of semiconducting devices in radiation fields. The dependence of hole lifetime in n-type germanium on irradiation has been determined. The dependence of electron lifetime in p-type germanium on irradiation is being studied.

Mobility Changes in Irradiated n-Type Germanium

The Hall mobility of fast-neutron- and gamma-irradiated single-crystal plates of n-type germanium has been determined from room temperature to $\sim$ 50°K for a series of irradiations. The effect of additional charge carrier scattering and minority-carrier trapping as a function of temperature following irradiation is being investigated.

Annealing Studies of Irradiated Germanium

The studies of annealing of irradiation-induced changes in the electrical properties of germanium have been continued. A circuit has been developed which will allow continuous monitoring of Hall constant, resistivity, and, thus, carrier concentration and mobility during pulse and isothermal annealing treatments.

Optical Absorption in Germanium

A theoretical expression was obtained for the bulk absorption coefficient of germanium for light in the near-infrared region. The parameters entering

into this expression can all be evaluated from independent experiments. The result is compared with the experimental measurements and is found to be gratifyingly close to the observations.

Activation Energies and Total Energies of Localized States in Semiconductors

The relationship between the total energy and the activation energy for localized states in semiconductors is analyzed. The localized states may be substitutional impurities, vacancies, or interstitial atoms. The relative concentration of localized states of different valences can be expressed as a Fermi-Dirac type of function, the parameters of which are explicitly given. Total-energy diagrams are presented for several substitutional impurities in germanium.

Magnetic Properties of Arsenic-Doped Silicon

A strong paramagnetic contribution to the total susceptibility is evident at low temperatures in silicon samples having between 5×10^{16} and 4×10^{18} arsenic donors per cubic centimeter. At higher impurity concentrations the paramagnetic contribution is absent, presumably due to a merging of the conduction and impurity bands. Comparison between the number of donors as obtained from measurements of the Hall effect and the number of magnetic centers at low temperatures shows that the data deviate from the simple theory, especially at higher (10^{18}) donor concentrations. Furthermore, the "freedom number" calculated from the magnetic susceptibility at room temperature is much smaller than would be expected. It is concluded that impurity banding influences the magnetic properties of n-type silicon and that the simple theory based on considering donors as independent and noninteracting magnetic centers does not apply at impurity levels greater than 10^{17} cm^{-3}.

Magnetic Susceptibility of Molybdenum

The temperature dependence of the magnetic susceptibility of pure molybdenum wire has been measured. The results differ from De Haas and Van Alphen's measurements (1933). The temperature-dependent paramagnetism of the presently available molybdenum is appreciably smaller than that of the material available in 1933. The difference may be due to a greater purity of currently available material.

Instrumentation for Susceptibility Studies

A liquid-helium cryostat was put into operation to permit measurement of magnetic susceptibility over the range 3 to 350°K. Making measurements in the liquid-helium temperature range also required modification of the magnet power supply to prevent the eddy-current heating in the cryostat that results from changes in the magnetic field when the latter is turned on and off too rapidly. In order to isolate the susceptibility balance from building vibration, a 5-ton concrete isolation pad was constructed.

Magnetic Defects in Covalent and Ionic Crystal Systems

Some progress has been made in identifying the magnetic defects in the quartz system produced by neutron irradiation. The hyperfine interaction of one of the defects with the 4.7%-abundant Si^{29} isotope (nuclear spin $I = \frac{1}{2}$) has been observed. A study of this hyperfine interaction as a function of crystal orientation may give a much more detailed model of the defect. Two of the magnetic defects have been tentatively related to two optical absorption bands. By consideration of the resonance, optical, and x-ray data, some preliminary deductions with respect to the radiation damage behavior have been made. One of the defects produced in magnesium oxide by neutron irradiation has been positively identified as an F center. Values of observed hyperfine interaction are compared with those calculated from theoretical F-center wave functions. The anisotropic hyperfine interaction calculated with these wave functions was one-half the observed value.

Superheterodyne Electron-Spin-Resonance Spectrometer

A superheterodyne spectrometer has been constructed which has a sensitivity approximately 100 times greater than that of the old system for similar operating conditions. With the increased sensitivity, detailed analysis of the structure of irradiation-produced defects in many crystal systems is possible.

Optical Absorption Studies of Irradiated Solids

Optical studies of crystalline quartz after Co^{60} gamma irradiation indicate little if any formation of the 2150-Å *C* band in contrast to neutron bombardment. A comprehensive series of fast-neutron bombardments have been completed covering the range 10^{17} to 2.9×10^{20} fast neutrons/cm^2. Neutron-irradiated specimens are much more difficult to bleach with either heat or ultraviolet light than those exposed to gamma rays. Thermal annealing of neutron-bombarded (5×10^{17} *nvt*) crystalline quartz produced another optical absorption band at 2000 Å. Pretreatment by fast-neutron bombardment and then annealing at 700°C followed by gamma irradiation indicate that the 700°C anneal removes the optical absorption but not the defects created by the fast neutrons.

X-Ray Diffraction Studies

The effects of fast pile neutrons upon solid crystalline structures were observed by use of x-ray diffraction techniques. These methods were also applied to deformation studies of metals and alloys. In the case of insulating materials, irradiation-induced phase transitions have been produced in natural ZrO_2 and single crystals of tetragonal $BaTiO_3$. It was also found that coesite, a high-density crystalline silica, is more stable than quartz under neutron irradiation. Lattice expansions of small magnitude have been observed in single crystals of germanium and silicon irradiated in the MTR. The measurements also indicated that the irradiation dose rate is a contributing factor to the freezing-in of lattice damage. By means of a unique spectrometer–Geiger counter technique, (111) twins have been observed in copper, silver, and gold single crystals deformed by tensile extension at 4.2°K.

Low-Temperature Thermal Conductivity of Potassium Chloride Crystals, Including the Effects of Strain and Particle Irradiation

It has been observed in high-purity KCl crystals that the scattering of phonons by strains introduced by cleaving may be considerable and that thermal annealing is effective in removing such thermal resistance. In addition, Co^{60} gamma rays are effective in annealing strains in such crystals. With annealed KCl crystals, Co^{60} gamma rays produce point defects at temperatures above the temperature, T_m, at which the thermal conductivity is a maximum. Below T_m, in the boundary scattering region, an additional scattering, possibly due to dislocations, is observed. Experiments with fast neutrons indicate that point-defect scattering is much less effective than with gamma rays, as evidenced by the fact that neutron bombardment produced almost no effect on the thermal conductivity of a KCl crystal at $T > T_m$ in the case where the crystal was shielded with lead during the irradiation.

Low-Temperature Thermal Conductivity of Nonmetals

The thermal conductivity, K, of the purest available crystals of KCl, SiO_2, LiF, CaF_2, MgO, Ge, and NaF has been measured at low temperatures. The value of the thermal conductivity maximum, K_m, and the temperature at which the maximum occurs, T_m, are given. Sodium fluoride was of particular interest because it is free of isotope scattering. The expected exponential K vs T dependence at $T > T_m$ was observed. However, the known impurities which were present were sufficient to prevent the theoretically expected values of K from being realized.

Low-Temperature Thermal Conductivity in Neutron-Irradiated Vitreous Silica

The thermal conductivity of fused silica at low temperatures increases by a factor of 2 after an irradiation of 5.8×10^{19} fast neutrons/cm^2, the increase being approximately linear with dose. On the other hand, the density saturates at 2.26 g/cm^3 (a density increase of ~3%) after exposure to 5.84×10^{19} neutrons/cm^2. Increases in the thermal conductivity and the density of fused silica upon irradiation can be interpreted as being due to an increase in order and are theoretically expected.

Proposed Reactor Bombardments at 4°K

In order to examine materials bombarded near 4°K, a helium liquefier system to be inserted in the hole No. 12 cryostat is under construction.

Gamma-Source Facilities

Two gamma-source facilities have been constructed for room- and liquid-nitrogen-temperature irradiation of various materials. One device employed ~960 curies of Cs^{137}, with a central

sample-exposure chamber 1 in. in inside diameter. The other device made use of underground storage of ~ 1880 curies of Co^{60}, with a central sample-exposure chamber $1\frac{13}{16}$ in. in inside diameter. Provision for liquid-nitrogen-temperature irradiation has been made.

Automatic Liquid-Gas Level Control

A device to maintain a level of liquid nitrogen in any Dewar vessel to within limits of $\pm\frac{1}{4}$ in. has been designed and has continuously operated for three months without failure. It is made of stock laboratory equipment and has sufficient flexibility for many applications.

HRP Radiation Metallurgy

The objectives and conclusions to date of the HRP radiation metallurgy program are summarized. Comparison of the properties of three different heats of A-212 grade B steel shows that there is a considerable spread in the properties of the metals in the irradiated condition. Irradiation of iron-carbon alloys (including a high-purity iron, a weld metal, and two low-manganese steels) containing 0.06% or less carbon results in reduction of the uniform elongation to the order of 1%. The uniform elongation in alloys having a carbon content of the order of 0.20% and higher is not so drastically reduced. Aluminum-killing and fine ferritic grain size alone are not sufficient to promote a high degree of resistance to radiation effects in carbon steels.

Radiation Stability of Ceramic Materials

Changes in density and in thermal conductivity were measured for ceramic materials irradiated for several operating cycles in the MTR. Changes in the Tukon hardness number were measured for some of these materials. No large annealing of the radiation changes occurred during aging at room temperature in the interval from one to two years after irradiation for materials irradiated for one operating cycle in the MTR. During exposure the materials were subject to corrosion by the reactor cooling water in which they were immersed. Another irradiation is being prepared in which the specimens are sealed in an inert atmosphere. Work is continuing on apparatus for measuring the elastic constants and the internal friction over the temperature range from −100 to 500°C.

Infrared Spectra of Plastics and Elastomers After Irradiation

Spectral measurements were made on polyethylene terephthalate before and after irradiation. A rupture in the ester linkage and a loss in crystallinity were observed, but loss of CO_2 could not be established definitely. No formation of –OH groups as a result of oxidation was noted, although saturation of the C=O peak masked any determination of this oxidation product. The absorption coefficients of several types of C=C groups have been measured on liquid standards, but these absorptivities were found to be unsuitable for application to solid films. Absorptivities are being determined from solid films of polybutadiene standards for analysis of other hydrocarbon polymers.

Effects of High-Energy Radiation on Polymers

Samples of polymethyl methacrylate of various average molecular weights were irradiated. The molecular weights after irradiation were determined by measuring the viscosities of dilute solutions of the polymer. The energy required per scission, calculated from the initial and final molecular weights, was not found to be constant for the samples of various molecular weights. The energy per scission was determined for samples of identical average molecular weights and identical average molecular weight distributions for various exposures. The energy per scission was not constant for various doses. It is thought that the relation between dilute-solution viscosity and average molecular weight varies with molecular weight distribution, which is subject to change during irradiation. Other methods of measuring molecular weight will be utilized. The energy per cross link in polystyrene was determined by viscosity measurement of molecular weight for samples of different average molecular weights. Within experimental error, the energy required per cross link was constant at about 1200 ev. Cross-linking was studied by means of solvent-swelling measurements in samples irradiated sufficiently to produce an insoluble network. A given quantity of absorbed energy in the higher-intensity field of the LITR was found to produce more cross-linking than did the same energy from the ORNL Graphite Reactor. This unexpected result may be due to higher sample temperatures in the LITR,

especially if the water-cooling facilities were not adequate to dissipate the nuclear heating.

Analysis of Gases Evolved by Irradiation of Polymers

A gas chromatography apparatus was calibrated and utilized for preliminary analyses of the gases evolved from several polyethylenes and from polypropylene.

Effects of Radiation on Engineering Properties of Polymeric Materials

The radiation resistance of fluorobutyl acrylate was investigated by the usual engineering properties tests. The electrical properties of the material were found to deteriorate very rapidly under irradiation. The change in electrical properties indicates chemical decomposition, while increases in hardness and density show that cross-linking occurred also. Asbestos sheet impregnated with various polymers improved in tensile strength after only moderate exposures to radiation. Only brittleness and elongation suffered unfavorable changes after large doses. Ordinary (low-density) polyethylene and high-density polyethylene were compared after irradiation for various exposures. There was no conclusive evidence at the dose levels employed that high crystallinity in the high-density material retarded cross-linking. The density and hardness changes did behave differently. The high-density material, already highly crystalline, reached its maximum density at lower radiation doses than did the ordinary polymer. One method of hardness measurement yielded values passing through a maximum for the highly crystalline polyethylene, while the ordinary type showed only increasing hardness values. Limited testing of polyethylene terephthalate showed its tensile properties to be relatively sensitive to radiation. Diisocyanate polyester elastomer, tested under conditions simulating actual use, proved to be superior to natural rubber for gasket applications.

Miscellaneous Polymer Problems

An apparatus is being built for studying stress-relaxation and stress-strain properties of polymers in a radiation field over a range of temperatures. The effect of radiation dose rate is being investigated. The energy absorbed in hydrocarbon materials in a reactor will be measured by means of hydrocarbon calorimeters.

High-Frequency Electrical Properties of Some Irradiated Plastic Materials

A survey of the effects of reactor and gamma-ray irradiation on the high-frequency electrical properties of some plastic materials has been completed. The materials selected for the survey were those in which the primary physical processes of chain cleavage and cross-linking have been shown to take place upon irradiation. Two others which are initially heavily cross-linked and one in which the energy imparted by irradiation with neutrons or gamma rays is absorbed without greatly altering the structure of the material were also examined.

Attempt at the Separation of Neutron and Gamma-Ray Irradiation Effects by Means of a Hydrogenous Absorber

The effect of reactor irradiation on the viscosity of polymethyl methacrylate was observed both in and outside a polyethylene shield. The samples in the shield had a smaller change in viscosity, leading to the conclusion that the gamma-ray effect is no greater than 60% of the total effect.

An Investigation of the Properties of Two Uranium-Bearing Zeolites

The physical and nuclear properties of two uranium-bearing zeolites are presented. Chemical and spectrographic analyses, combustion losses, microscopic examination, and differential thermal analyses were made on the materials as powders. Density changes and fission-gas retention were measured on the materials as powders and pressed compacts for short irradiation periods. The two materials readily evolved the gaseous fission products formed during irradiation. Both, however, selectively retained proportionately more of the Xe^{135}.

Forced-Cooling Ceramic-Fuel Experiment

An experiment is being designed to study radiation effects on ceramic fuels generating 75,000 to 500,000 Btu/hr·ft^2 at surface temperatures of 1800 to 2500°F.

High-Temperature Ceramic Fuels

Radiation damage studies were continued on ceramic and metal-ceramic fuel systems at high temperatures. Postirradiation examinations were completed on two fuels, ThO_2–UO_2 and SiC–Si–UO_2. Irradiations were started on a Cr–Al_2O_3–UO_2 clad fuel plate. The ThO_2–UO_2 material retained dimensional stability. The elastic modulus and specific heat also remained unchanged as the result of irradiation. Fuel plates containing UO_2 and clad with siliconized silicon carbide were dimensionally stable after irradiation. A measurement of the Xe^{133} escape indicated good fission-product retention.

Radiation Effects in Thermocouple Insulation

A number of types of thermocouple wire insulation were tested in the LITR in both air and helium and at various temperatures. Of the insulation tested only one material, a glass-insulated, unimpregnated pair in a tubular sheath, was found to be unusable under irradiation because of low leakage resistance.

Chemical Effects of Nuclear Reactions

The conservation of chemical valency in the fission process is described, and the current status of determinations of the structures of K_2SO_4 and K_2PO_3F is discussed.

Adsorption of Fission Gases by Activated Charcoal

An investigation is being made of the holdup of fission gases by activated-charcoal adsorption beds. Theoretical and experimental studies have been conducted which are applicable to the Homogeneous Reactor Test and to future homogeneous reactors. Various factors which influence the adsorption process have been investigated. This work is being conducted to provide information for the design of adsorption beds for fission gases from reactors.

Investigation of Sulfur Contamination of a Dry Box by Neoprene Rubber

An investigation was made of deposits of Cu_2S which were observed on copper inside a vacuum-type dry box. The source of the sulfur was traced to neoprene gloves.

Neutron Flux Monitoring in High-Temperature In-Pile Experiments

A method has been developed for the measurement of thermal neutron flux in high-temperature in-pile experiments, the cobalt impurity in Inconel being used as the flux monitor.

ORR Experimental Facility

The auxiliary equipment being designed for use with in-pile experiments in the Oak Ridge Research Reactor is described.

Fission Reactions as Threshold Detectors

Measurements of the neutron flux in hole 51N of the ORNL Graphite Reactor were made with the Pu^{239}, Np^{237}, and U^{238} fission reactions, the detector foils being enclosed in a B^{10} shield. The variation of the measured fluxes with position in the hole indicates that the neutron converter adds a fission spectrum to the spectrum outside the converter. A catcher technique is described which allows the use of the Np^{237} reaction with only a cadmium cover.

Hot Lab Studies

During the last year approximately 400 radioactive metallographic specimens were processed, and 53 experiments were completed. Improvements were made to some of the equipment and facilities.

LOW-TEMPERATURE BOMBARDMENT OF METALS

T. H. Blewitt R. R. Coltman C. E. Klabunde J. K. Redman

The primary purpose of the research work by this group is that of obtaining a basic understanding of the mechanisms by which reactor neutrons change the properties of metals. It has been shown previously[1] that an annealing process takes place in many pure metals at a temperature as low as 30°K. Consequently, efforts have, for the most part, been devoted to a study of samples bombarded at temperatures below 20°K so that various low-temperature annealing treatments could be studied. Most of the work was done on copper single-crystal samples with a relatively low density of radiation-induced defects. For these bombardments the regions affected by the neutrons are relatively far apart, and the chance of interaction between them is small.

One of the first experiments performed by this group, after establishing that about 50% of the radiation-induced resistivity is recovered in the range from 30 to 50°K, was the determination of the energy associated with this annealing peak in copper. It was natural to suppose that a recovery in this temperature region was to be associated with the migration of interstitial atoms resulting from the neutron bombardment. Earlier calculations by Huntington[2] indicated that interstitials have an activation energy for migration which is considerably lower than that of vacancies and, in fact, is of the order of magnitude necessary to account for the annealing at 30 to 50°K. Since the energy of formation of an interstitial is quite high, a considerable amount of energy should be liberated by a vacancy-interstitial annihilation. Subsequent measurements of the stored energy showed that the amount of energy liberated in a 30 to 50°K range is smaller, by a factor of approximately 5, than that expected from the number of defects as determined from the electrical resistivity. This measurement was viewed with skepticism by some people, and as a result several measurements have been made during the past year to verify the stored energy results on copper and to measure this property in aluminum. The following measuring techniques were used: The sample was held at 20°K during bombardment by maintaining thermal contact with the wall of the cryostat, was bombarded for about 150 hr, and then was isolated from the wall of the cryostat. The sample was then heated by gamma rays, and the specific heat as a function of temperature was determined from the slope of the recorded time-temperature curve. In the first run made after the bombardment the sample was heated by both the gamma rays and the release of stored energy, but in the subsequent runs it was warmed by only the gamma heat. The stored energy was calculated from the difference between the two runs. The main experimental difficulty involved making and breaking thermal contact between the sample and the cryostat wall. Initially, thermal contact was maintained by mechanically holding the sample in contact with the bottom of the cryostat by means of a lead weight. This method was not sufficient to maintain a bombardment temperature of 20°K, and therefore about 20 μ of helium exchange gas had to be added. However, helium exchange gas was unsatisfactory for this purpose because of the difficulty in pumping it from a container which is at a low temperature. To eliminate the possibility of adsorbed helium gas being evolved from the sample during the first warmup run, the apparatus illustrated in Fig. 1 was devised for measuring the stored energy. In this method the interior of the bellows is always highly evacuated (pressure is of the order of a few hundredths of a micron). During the period of bombardment, when it is desirable that the sample be in thermal contact with the cryostat wall, the region between the bellows and the cryostat wall is filled with helium exchange gas to a pressure of 2 or 3 atm. This causes the bellows to collapse and maintain contact on each side of a pillbox-shaped sample. The sample is then kept cold since the helium exchange gas maintains the bellows at temperatures near that of the cryostat wall. When it is desired to isolate the sample from the cryostat, the helium exchange gas is pumped out to a pressure of about 100 μ, which allows the bellows to return to its initial shape

[1] T. H. Blewitt *et al.*, "Mechanism of Annealing in Neutron Irradiated Metals," p 84–110, in *Creep and Recovery*, American Society for Metals, Cleveland, 1957.

[2] H. B. Huntington, *Phys. Rev.* 91, 1092 (1953).

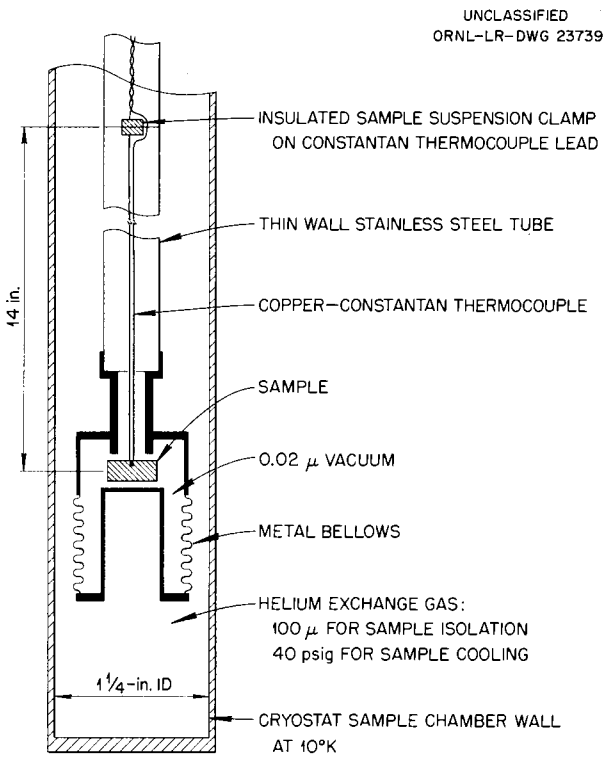

Fig. 1. Apparatus for the Measurement of Stored Energy.

and isolates the sample. The remaining 100 μ of exchange gas holds the bellows at the ambient temperature of the cryostat wall and thereby prevents the release of any condensed gas which may have collected on the wall of the bellows. This technique has been used to make two runs with different levels of gamma heating. In one run the sample was heated by the gamma rays that resulted from the reactor being held at one-tenth normal power. Approximately 40 min was required to warm the sample from 20°K to 60°K, and approximately 0.3 cal/mole of stored energy was released. In the other run the sample was heated by the gamma rays produced by the reactor operating at normal power. Approximately 4 min was required to heat the sample from 20°K to 60°K, and the stored energy was estimated to be about 0.2 cal/mole. Both measurements of the stored energy were made after a 150-hr bombardment (4×10^{17} neutrons/cm^2). These values are in substantial agreement with the previous experiments. It would thus appear that either the number of defects annihilated is much smaller than that estimated from the electrical resistivity, or that a value somewhat smaller than 5 ev is to be associated with each annihilation. The method used in the previous experiments, a description of the hole No. 12 cryostat, and other experimental techniques have been reported.[3]

Resistivity measurements have been made to attempt to determine the kinetics of the annealing process. It has been possible to deduce that there is more than one activation energy associated with the 30 to 50°K annealing. Studies have also been made of the effect of bombardment time on the low-temperature annealing. It was found that the annealing kinetics observed for a sample bombarded for 3 hr were the same as those for one bombarded for 150 hr. These results imply that the low-temperature annealing occurs by the first-order process. It was possible to estimate the spectrum of activation energies from the above data, and it was found that a single band of activation energies ranging from 0.08 to 0.15 ev occurs in a low-temperature annealing. The nonuniqueness of the activation energy for this low-temperature recovery indicated that a highly complicated process takes place. In like fashion, the fact that the decrement of copper single crystals was decreased at 20°K in the reactor was an indication of a complicated process.[4] It was possible to estimate from decrement data that some of the defects produced by bombardment were displaced a distance of the order of 200 times the lattice parameter. These facts led to the suggestion that perhaps defects more complicated than simple point defects were formed during neutron bombardment. In order to test this hypothesis, the low-temperature recovery of copper samples doped with various impurity atoms was studied,[5] and it was found that both undersized and oversized atoms would suppress the annealing. The addition of 0.1 at. % impurity did not affect the annealing in the vicinity of 30 to 35°K, but the addition of 1.0 at. % impurity completely suppressed the annealing which normally takes place in pure copper in the region from 30 to 50°K. This implies that under- or oversized atoms in the amount of 0.1 at. % have the ability to suppress the processes with the higher activation energies,

[3] R. R. Coltman, T. H. Blewitt, and T. S. Noggle, *Rev. Sci. Instr.* 28, 375–380 (1957).

[4] D. O. Thompson, T. H. Blewitt, and D. K. Holmes, *J. Appl. Phy.* 28, 742 (1957).

[5] T. H. Blewitt *et al.*, *J. Appl. Phy.* 28, 639 (1957).

leaving those processes with the lower activation energies unaffected. On the other hand, the addition of more impurity atoms will result in the further suppression of these lower energy migrations. These experimental facts are very difficult to explain, and any scheme which would explain the phenomenon might well be unique.

Experiments on the mechanical properties of metals bombarded at low temperatures have also been made. The surprising result was that radiation hardness is spontaneously introduced at 20°K. Subsequent annealing at 80°K did not affect the critical shear stress. This result appears to indicate that an annihilation process is not to be associated with the low-temperature annealing; otherwise the mechanical hardness would be expected to decrease. In fact, the evidence obtained by this group would seem to indicate that the annealing occurring in the range from 30 to 50°K is not to be associated with vacancy-interstitial annihilation.

Electrical resistivity measurements were made on beryllium, graphite, magnesium, aluminum, iron, cobalt, nickel, copper, zinc, molybdenum, silver, antimony, tungsten, platinum, gold, lead, and bismuth. The resistivity of these metals was studied as a function of neutron bombardment, and rates of increase varying by as much as a factor of 10,000 were observed. It is possible to understand these data if the number of conduction electrons and the mass of the atoms are taken into consideration.

An interesting experiment has recently been performed on graphite. The number of current carriers, which are thought to be electrons, is known to be very small, possibly 10^{-4} or 10^{-5} per cubic centimeter. This is of the same order as the number of defects produced in a week's bombardment in the ORNL Graphite Reactor. Since it is believed that radiation damage produces defects which expand and contract the lattice, it may be that the defects act as donors or acceptors of the current carriers. Some evidence that this may be the case was obtained from the study of the change in electrical resistivity of graphite irradiated at 20°K. It was found that the electrical resistivity of the graphite was increased by approximately 50% by pulse annealing at a temperature of about 150°K. It is believed that this increase is associated with the trapping of current carriers at the radiation-induced defects. Further tests are now being made to establish this hypothesis.

It is proposed that future experiments include a more detailed study of the damage rates and annealing processes in the semimetals graphite, bismuth, and antimony. In addition, it is planned to examine bombarded copper for stored energy in the range of 80 to 300°K. For this experiment, specimens will be removed from the reactor at liquid-nitrogen temperature, and their specific heat will then be measured in an isothermal cavity, with thermal radiation used as a heat supply. Of particular interest is the temperature range of 250 to 300°K, where a number of investigators have reported a unique annealing process. Further investigation of the mechanical properties of pure metals bombarded at very low temperatures is contemplated.

Listed below are the abstracts of two recently published papers which describe in detail many of the methods used by the group for low-temperature bombardment work and the results obtained from recent experiments.

Techniques and Equipment Utilized in Low-Temperature Reactor Irradiations.[3] R. R. Coltman, T. H. Blewitt, and T. S. Noggle. – A cryostat used in hole No. 12 of the graphite reactor at Oak Ridge National Laboratory is described in detail. The cryostat which is made almost entirely of aluminum is supplied with cold helium gas from an Arthur D. Little helium refrigerator. Bombardments have been made in the cryostat at temperatures as low as 15°K for periods as long as two weeks. A discussion of the equilibrium temperature attained by a specimen in the cryostat is given taking into account the reactor gamma ray heating effects. A method for measuring stored energy and specific heats of materials bombarded in the cryostat utilizing gamma ray heating is described. A method for pulse annealing specimens at low temperatures employing the discharge of the energy stored in a bank of condensers is also described. Relatively sharp and quite reproducible thermal pulses can be obtained with this method (which is also suitable for use in the laboratory). The hazard of cryogenic devices in high radiation fields is discussed. It is believed that when air is allowed to condense on a cold surface in the presence of intense ionizing radiations, a hazardous condition results.

Low-Temperature Reactor Irradiation Effects in Metals.[5] T. H. Blewitt, R. R. Coltman, C. E. Klabunde, and T. S. Noggle. – The effects of structural and chemical defects on the low-temperature (30–50°K) annealing peak in low-temperature reactor-irradiated aluminum and copper were studied. From the fact that the density of reactor-induced defects did not affect the annealing kinetics, it was possible to conclude that the low-temperature annealing process was of the first order without a unique activation energy. The fact that both oversized and undersized atoms could suppress this annealing peak led to the conclusion that the radiation-induced defects were more complicated than simple point defects. The suggestion is made that a defect similar to a crowdion must be created by low-temperature neutron irradiation. This data also supports to some degree the viewpoint that a radiation-induced defect, possibly a crowdion, has sufficient knock-on energy to migrate several hundred atomic distances. The experiments also contain evidence which rules out all forms of vacancy-interstitial annihilation.

THEORETICAL CONSIDERATIONS ON THE TEMPERATURE DEPENDENCE OF THE MECHANICAL PROPERTIES OF METALS

D. K. Holmes

Thermally Induced Oscillations of Dislocation Lines

Experimental observations have been made[1,2] on the temperature dependence of two sets of mechanical properties of metals: the critical shear stress (CSS) of irradiated single crystals (observations principally on copper) and the internal friction and elastic modulus under an oscillatory stress of very low amplitude (observations principally on copper single crystals). In both cases the basic mechanism under study is the motion of dislocations in the metal. Consequently, the temperature dependence in both cases has been considered from the viewpoint of an analysis of thermal activation of dislocation line motion which was suggested by G. Leibfried.[3]

Briefly, Leibfried's analysis is as follows. Consider a length of dislocation line between two pinning points, as shown below.

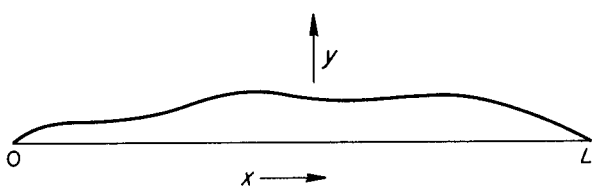

Let the displacement of the line from its rest position be $Y(x,t)$; then the equation of motion is

$$\mathcal{E}Y'' = \rho_D \ddot{Y} \quad , \tag{1}$$

where

$\mathcal{E}$ = the line tension
= $\frac{1}{2}\mu b^2$,

ρ_D = the line density
= ρb^2,

μ = the shear modulus of the crystal,

b = the Burgers vector.

Now, represent Y as a series of harmonics in x

$$Y(x,t) = \sum_{n=1,2,\ldots} a_n(t) \sin k_n x \quad . \tag{2}$$

From the condition that the line be fixed at the ends

$$k_n = \frac{n\pi}{L} \quad , \tag{3}$$

and from Eq. 1

$$\ddot{a}_n + \omega_n^2 a_n = 0 \quad , \tag{4}$$

where

$$\omega_n^2 = \frac{\mu}{2\rho} \frac{n^2\pi^2}{L^2} \quad . \tag{5}$$

Thus, each mode acts like an independent harmonic oscillator of frequency ω_n. Then the average amplitude of each mode, in a crystal at temperature T, may be calculated in the usual manner for linear harmonic oscillators in thermal equilibrium by use of the quantum mechanical result:

$$\overline{a_n^2}\omega_n^2 = \frac{2}{\rho_D L}\left(\frac{\hbar\omega_n}{2} + \frac{\hbar\omega_n}{e^{\hbar\omega_n/kT} - 1}\right) \quad . \tag{6}$$

The physical quantity of interest is the average force with which the dislocation line pulls on the anchoring points. For small displacements of the line, the force tending to release the dislocation from the pinning point (say, at $x = 0$) at any time is

$$F(t) = \mathcal{E}\frac{\partial Y(0,t)}{\partial x} \quad . \tag{7}$$

With the use of the results given above, the average force squared is

$$\overline{F^2} = \frac{2\rho\mathcal{E}^2}{\mu} \sum_{n=1}^{N} \overline{a_n^2}\omega_n^2 \quad . \tag{8}$$

---

[1] T. H. Blewitt *et al.*, "Mechanism of Annealing in Neutron Irradiated Metals," p 84–110, in *Creep and Recovery*, American Society for Metals, Cleveland, 1957.

[2] D. O. Thompson and D. K. Holmes, *J. Appl. Phy.* **27**, 713 (1956).

[3] G. Leibfried, paper presented at the Lake Placid Conference on Dislocations in Metals, Lake Placid, N.Y., September 1956.

Here a cutoff, N, has been introduced, since extremely short wavelength oscillations are not allowable; a convenient choice for N is

$$N = \frac{L}{a} \quad , \tag{9}$$

where a is the interatomic spacing. With the use of Eq. 6, the average force squared may be calculated in two limiting cases:

$$\overline{F^2} = \begin{cases} \left(\frac{2\mathcal{E}}{a}\right) kT & \text{(high temperature)}, \\ \left(\frac{2\mathcal{E}}{a}\right)(0.14)\, k\Theta & \text{(low temperature)}, \end{cases} \tag{10}$$

where Θ is the Debye temperature of the lattice, and the limits of high and low temperature are in comparison with the Debye temperature.

Application to Experiments

Critical Shear Stress. – It has been observed[1] that neutron irradiation not only increases the CSS of a metal single crystal but also increases the temperature dependence of the CSS. As a suggested explanation of this behavior, consider the model of randomly spaced barriers (created by fast-neutron hits) impeding the motion of dislocation lines. Suppose that each barrier can withstand a force F_0, without allowing the dislocation to break through; then the condition for flow is

$$F_0 = F_\sigma + F_T \quad , \tag{11}$$

where F_σ is the force on the barrier from the dislocation line due to the applied shear stress σ, and F_T is the force on the barrier due to the thermally induced motion of the line.

If the average separation of the barriers is $L(nvt)$ at any stage of the irradiation as measured by the integrated fast neutron flux, nvt, then

$$F_\sigma = bL \quad . \tag{12}$$

Using the Leibfried analysis above, we may take (at high temperatures)

$$F_T = \sqrt{\overline{F^2}} = \sqrt{\frac{2\mathcal{E}k}{a}}\,\sqrt{T} \quad . \tag{13}$$

Combining Eqs. 11, 12, and 13 results in:

$$\text{CSS} = \sigma = \frac{F_0}{bL}\left(1 - \sqrt{\frac{2\mathcal{E}k}{aF_0^2}}\,\sqrt{T}\right) , \tag{14}$$

which indicates that, at least in the high-temperature range, the CSS should vary as the square root of the absolute temperature. This law is found to fit the experimental results very well over a large range of integrated fast flux. The numerical values are such as to indicate a value for the strength of the barriers of 3.5×10^{-5} dyne.

An interesting prediction of the model is that the CSS should deviate from the square-root law and approach a constant value at lower temperatures as given by Eq. 10. It might be expected that this effect would be significant in the range of temperatures between that of liquid helium and that of liquid nitrogen.

Internal Friction and Young's Modulus. – It has proved possible to explain in detail the changes due to neutron irradiation in the internal friction and Young's modulus of well-annealed single crystals of copper on the basis of a model in which some of the defects produced by the neutron hits wander to the dislocation lines and effectively pin them at low stress levels.[2] At higher irradiations (say, 10^{17} neutrons/cm^2) it would then be reasonable to suppose that the dislocations are completely tied up, so that the observed Young's modulus is just the elastic modulus of the crystal and the observed internal friction is the non-dislocation background. To the extent that this assumption is valid, it is possible to obtain the dislocation contribution to the Young's modulus and to the internal friction by a subtraction process between the unirradiated and the fully irradiated values of these properties. Experiments to date have shown that, if E_d is the dislocation component of the Young's modulus, Δ_d is the dislocation contribution to the internal friction, and n is the number of pinning points per unit length along a dislocation line,

$$\begin{aligned} E_d &\propto n^2 \quad , \\ \Delta_d &\propto \frac{1}{n^4} \quad . \end{aligned} \tag{15}$$

Measurements of E_d and Δ_d have been made as a function of temperature over the range from liquid-nitrogen to room temperature. The variation of these quantities is such that (approximately)

$$E_d^2 \times \Delta_d = \text{constant} \quad . \tag{16}$$

The direction of the variation is such as to indicate that the effective number of pinning points per unit length *decreases* with rising temperature. (Note that the pinning points under discussion here are those in the well-annealed, unirradiated crystal, presumably impurity atoms.)

Again an attempt may be made to use the Leibfried analysis by imagining that at absolute zero there is a certain number of pinning points per unit length, n_0, which can withstand a force, F_0. Then as the temperature rises, the force on a given pinning point due to the thermal fluctuations may exceed F_0, so that it will no longer serve as an effective anchoring point. The problem is, then, to calculate the number of pinning points which *are* effective at any temperature.

The force on a given point will fluctuate in such a manner that the probability that the force lies in the range $F \to F + dF$ is given by

$$P(F)\,dF = \frac{1}{\sqrt{2\pi\overline{F^2}}}\, e^{-F^2/2\overline{F^2}}\, dF \quad . \tag{17}$$

That fraction of the pinning points on which the magnitude of the force is less than F_0 will be effective at any time; that is,

$$n_{\text{eff}} = 2n_0 \int_0^{F_0} P(F)\,dF = n_0\, E_2\left(\frac{C_1}{\sqrt{T}}\right) , \tag{18}$$

where $E_2(x)$ is the error integral of argument x and

$$\frac{C_1}{\sqrt{T}} \equiv \frac{F_0}{\sqrt{2}\sqrt{\overline{F^2}}} = \frac{F_0}{2\sqrt{\mathcal{E}k/a}\,\sqrt{T}} \tag{19}$$

if the high-temperature limit from Eq. 10 is used.

The experimental results for E_d and Δ_d do not fit well with the forms indicated by Eqs. 15 and 18 at low temperatures; however, in the temperature range from 200 to 300°K, a fairly good fit is obtained. At the present time this is regarded as indecisive since the experimental accuracy to date is probably not adequate for the subtraction process in the low-temperature range. The present numerical values lead to the result

$$n_0 F_0 = 0.54 \text{ dyne/cm} \quad , \tag{20}$$

which is reasonable. For example, if the force for these pinning points is an order of magnitude lower than that for the barriers considered above in the CSS case, $F_0 = 3.5 \times 10^{-6}$ dyne (say), then Eq. 20 yields, for the average distance between pinning points at 0°K, $l_0 = 8 \times 10^{-6}$ cm.

YOUNG'S MODULUS AND INTERNAL-FRICTION STUDIES

D. O. Thompson

During the past year an elastic-constant–internal-friction spectrometer has been developed and more or less perfected. Although details of this instrument will be published in the open literature, a brief description of its operation may be helpful to an understanding of the experiments already performed with it and of those planned. The metal sample, in the shape of a right cylindrical rod, is held in constant oscillation at a given, preset strain amplitude at the resonant frequency of the sample. Under these conditions it can be shown[1] that the square of the resonant frequency is proportional to the Young's modulus and that the current in the sample driver which is necessary to maintain a constant amplitude of oscillation is proportional to the internal friction. These two quantities are measured continuously, along with other appropriate parameters. The instrument makes possible a much greater resolution of internal friction phenomena and also greatly increases the rate at which such data may be obtained.

A study has been made during the past year of the Bordoni internal-friction peaks in copper[2–4] with the above-described equipment. Briefly, these peaks appear in the internal friction vs temperature curves of heavily cold-worked copper and other metals at low temperatures (about 78°K at 16 kilocycles per second). An appreciable amount of theory has been developed to explain these phenomena, chiefly by Seeger.[5] He interprets the peaks as basically a relaxation mechanism in which segments of dislocation lines lying along particular crystallographic directions flop over an intervening potential barrier into equivalent neighboring troughs under the influence of an alternating stress. The formation of the kinks connecting the dislocations is then the origin of the relaxation process. One of the predictions of the theory is contained in the flop-over mechanism. A certain free length of dislocation line, of the order of 100 atoms, is necessary in order for this mechanism to operate. Consequently, it was felt that a test of the theory could be made by measuring the peaks after neutron bombardment. In view of past experience[6,7] it was anticipated that the bombardment would pin the dislocations through dislocation-defect interactions and consequently eliminate the peaks.

Although the experiments have not been completed, to date they have not shown the anticipated results. In the first place, a study of the peaks before irradiation, with the spectrometer described above, has revealed a complex structure. These data are supported by the measured modulus curves, which have not been previously reported. This behavior would not be anticipated in a single relaxation process without some complicating factors. Coupled with this result is the fact that the peaks are about three times too broad with respect to temperature to be consistent with the activation energy of the process as determined by measuring the phenomena at different frequencies and observing the shift in temperature of the maximum. Bombardments up to 5×10^{17} *nvt* have not been effective in reducing the peak magnitudes to any appreciable extent. As a consequence of the negative results with respect to the existing theory, further study of the Bordoni peaks will be made during the present year. It is planned to extend the bombardment tests at least an order of magnitude in flux. This has to be done in such a fashion that the samples will not be annealed during the bombardment as the result of a temperature rise.

Another set of experiments begun during the past year and still in progress is the measurement of the Young's modulus and internal friction of copper as a function of temperature from liquid-helium to room temperature. These experiments had their

[1] W. G. Cady, *Piezoelectricity; an Introduction to the Theory and Application of Electromechanical Phenomena in Crystals*, 1st ed., McGraw-Hill, New York, 1956.

[2] P. G. Bordoni, *Ricerca Sci.* 19, 851 (1949).

[3] P. G. Bordoni, *J. Acoust. Soc. Am.* 26, 495 (1954).

[4] D. H. Niblett and J. Wilks, *Phil. Mag.* 1, Series 8, 415 (1956).

[5] A. Seeger, *Phil Mag.* 1, Series 8, 651 (1956).

[6] D. O. Thampson and D. K. Holmes, *J. Appl. Phy.* 27, 713 (1956).

[7] D. O. Thompson, T. H. Blewitt, and D. K. Holmes, *J. Appl. Phy.* 28, 742 (1957).

origin in the observations that the total change in Young's modulus for room-temperature neutron bombardments was greater than for bombardments at low temperatures.[6,7] The spectrometer described above was utilized in these experiments also. With neutron irradiation of the samples as a tool for elimination of the dislocation components of both the modulus and internal friction, it is possible by subtraction to obtain the dislocation components themselves as a function of temperature. This has been done for samples in various states of anneal prior to irradiation. The most significant result to date from these experiments is the demonstration that the product $E_d^2\Delta_d$ is a constant over the temperature range investigated; E_d is the dislocation component of the Young's modulus, and Δ_d is the internal friction which arises from dislocation motion. This result is quite fundamental to a theory of dislocation motion and an interpretation of how thermal fluctuations affect the dislocation lines. It should be mentioned that this result is entirely consistent with earlier interpretations of line pinning during neutron bombardment at a given temperature.

It is planned to continue these experiments during the next year. The hope, of course, is to obtain a sufficient amount of significant data so that a fundamental theory of the dislocation internal friction phenomena at very low strain amplitudes can be developed. Other experiments which will contribute to this understanding are being planned. One is a study of the internal friction and Young's modulus behavior in copper at very high frequencies (5 to 200 megacycles per second) during irradiation. The outcome of such experiments will be very important to any theoretical understanding of the damping process. It is also planned to extend the measurements to low frequencies (about 50 cycles per second).

It is possible that the motion of certain types of irradiation-induced defects in an alternating stress field will appear as stress relaxation peaks in the internal friction curves. This is particularly true for any polarized defect, such as a divacancy or a crowdion, in a face-centered cubic type of metal. In a body-centered cubic metal the motion of an interstitial atom should show up as a relaxation peak. Consequently, it is presently planned to begin experiments during the coming year which will reveal these peaks if they are present. An experimental determination of them would yield a considerable amount of information about the kinetics of motion of the defect involved, such as its activation energy, relaxation time, etc.

SMALL-ANGLE X-RAY SCATTERING STUDIES OF FAST-NEUTRON IRRADIATION EFFECTS IN AN ALUMINUM-SILVER PRECIPITATE ALLOY

R. E. Jamison

A year ago it was reported[1] that fast-neutron irradiation of a quenched aluminum-silver alloy caused retardation of zone growth during heat treatment following irradiation. This result has been confirmed, and the work has been continued with the object of learning more about the individual neutron-affected region.

Reported here are the effect of previous irradiation on advanced aging at higher temperatures, the apparent effect on the activation energy for diffusion, and something of the effect on the size distribution and structure of the zones during advanced aging. A description of the neutron-affected region in metals in general, or even in this alloy in particular, cannot yet be given, nor can a well-substantiated argument for or against the existence of displacement spikes in irradiated samples. However, the work is at the point where each experimental result seems to be nearer this goal.

The retardation of zone growth of course indicates an apparent lowering of the diffusion rate. This observation is in conflict with the general view that fast-neutron irradiation increases, among other things, the number of vacancies in a metal, thus increasing the diffusion rate. By assuming a reasonable function for the rate of increase in zone size as a function of time at temperature, and changing the temperature of treatment, it is possible to determine activation energies for the process of zone growth. Activation energies of about 26 kcal/mole were obtained in the unirradiated sample, and the value remained nearly constant throughout heat treatment. After 78 hours at 100°C the activation energy for the process in the irradiated sample was about 34 kcal/mole; it decreased on heating until, after an additional heat treatment of 4.5 hours at 130°C, it was about equal to the value of 26 kcal/mole for the unirradiated sample. After further heat treatment at higher temperatures (166°C and 196°C), where there would be more annealing of the existing irradiation effect, this activation energy for the irradiated sample was measurably less than that for the nonirradiated sample.

There are two reasons why these results do not indicate a real lowering of the activation energy for diffusion in this alloy. First, from results by previous workers, it can be assumed that the measured zone growth occurs by resolution of the smallest (subcritical) silver-rich zones, their silver then diffusing, through a downhill potential gradient, to and enlarging the larger zones. It can be argued that the irradiation effectively stabilizes these smallest zones, thus limiting the supply of silver atoms for the process without necessarily changing the activation energy for diffusion. Second, without consideration of time at temperature, the plot of number of zones versus predominant zone size as aging progresses in the irradiated case falls considerably above the same plot for the nonirradiated case. This indicates something other than a simple decrease of diffusion rate.

Some very recent measurements indicate that an earlier result may be more meaningful than it was first thought to be. It was reported earlier that some irradiated specimens showed a tendency to lose their ring-type x-ray pattern after very short heat treatments following irradiation. Our latest results show that this effect carries throughout heat treatment; that, even after heat treatment at 196°C for a period long enough to give the irradiated sample the same predominant zone size as the nonirradiated, the ring-type x-ray pattern is still less pronounced in the irradiated than in the nonirradiated sample. This is the result that would be expected if, during early heat treatment, aluminum were diffusing into vacant lattice sites in the silver-poor shell surrounding each silver-rich zone. As required by the previous results, this aluminum would thus, on further heat treatment, retard diffusion of silver through the shell by reducing the vacancy concentration there. If this is a valid explanation of the effect, then the previous irradiation must enhance diffusion of aluminum in the alloy in preference to diffusion of silver. This can be concluded without considering the relative abundance and ordinary diffusion coefficients of the aluminum and silver.

Future experiments will show the dependence of the various effects on initial zone size and possibly on the temperature of irradiation. Although weeks of heat treatment and x-ray time will be required, the activation energy for the annealing of the irradiation effect can also be determined.

[1] R. E. Jamison, *Solid State Semiann. Prog. Rep. Aug. 30, 1956*, ORNL-2188, p 98.

EFFECT OF NEUTRON IRRADIATION ON COPPER-BASE ALLOYS

R. H. Kernohan M. S. Wechsler

It has been shown previously[1-4] that large decreases in the resistivity of certain copper-rich binary solid solution alloys take place upon neutron irradiation. This behavior is in contrast to the effect on pure metals, in which case an increase in resistivity proportional to the integrated neutron flux is observed even at very low temperatures.[5] The previous experiments on copper-base alloys were of two types. In the first of these,[2] resistivity measurements were made on copper alloyed in the solid-solution range with aluminum, silicon, zinc, gallium, germanium, arsenic, and tin before and after a neutron exposure of 2×10^{18} neutrons/cm^2 at about 45°C. The resistivities of the aluminum and zinc alloys decreased significantly upon irradiation, whereas the effects on the other alloys were rather slight. In general, the effects were larger for samples with higher alloy content. In the second type of experiment,[3] the resistivity of a brass wire containing 12.9 atomic percent zinc was measured in-pile at ambient pile temperature. The resistivity was observed to decrease sharply in the early stage of the irradiation, reaching a minimum after an exposure of 2×10^{18} neutrons/cm^2. The resistivity then increased linearly with time in the reactor and eventually exceeded the original pre-irradiation value.

It was decided on the basis of these earlier experiments to study in more detail the nature of the process whereby decreases in resistivity are induced by neutron bombardment in the copper-aluminum and the copper-zinc alloys. Of these two alloys, somewhat greater attention has been given to the copper-aluminum alloy system for the following reasons: (1) larger changes in resistivity upon irradiation were observed for this alloy than for any of the other materials investigated in the earlier work,[2] (2) the reactor-induced radioactive isotopes of aluminum have short half lives, and (3) copper and aluminum are fairly well separated in the periodic table, and their atomic scattering powers for x rays are significantly different. This last factor is of special importance since, as will be discussed below, the effects being studied here appear to be related to the change in the relative atomic arrangements of the two constituents of the alloys. This rearrangement is thought not to be the immediate result of bombardment-produced displacements, but rather to be brought about by a diffusion-controlled solid-state reaction, which is triggered or accelerated by the irradiation in a way that is not yet very well understood. In any case, in studying the copper-aluminum alloys one has the opportunity to perform x-ray scattering experiments in order to detect changes upon irradiation in the relative arrangement of the copper and aluminum atoms.

In-pile measurements of the resistivity of α-phase copper-aluminum alloys containing various amounts of aluminum have been carried out for single-crystal and polycrystalline samples and for one-eighth-inch-diameter and wire samples. In each case, when the neutron exposure is made at ambient pile temperature (about 40°C), the sample experiences a sharp decrease in resistivity, reaching a minimum after about 500 hours in the reactor and then increasing linearly with further exposure. The amount of the decrease at the minimum and the slope of the linear increase are approximately proportional to the aluminum content. No such decrease in resistivity is observed for pure copper. For the samples with the largest aluminum concentration (15 atomic per cent), the decrease amounts to about 0.2 μohm-cm, or about 2 per cent. In-pile measurements on the alloy containing 15 atomic per cent aluminum have been carried out at about 40°C in three facilities in the Graphite Reactor: hole 1768 (hollow fuel element), hole C, and hole 52. The curves of resistivity vs in-pile exposure time superimpose fairly closely for the

[1] R. H. Kernohan, A. B. Lewis, and D. S. Billington, *Solid State Semiann. Prog. Rep. Feb. 28, 1955*, ORNL-1852, p 50.

[2] R. H. Kernohan and D. S. Billington, *Solid State Semiann. Prog. Rep. Aug. 30, 1955*, ORNL-1945, p 63.

[3] R. H. Kernohan and D. S. Billington, *Solid State Semiann. Prog. Rep. Feb. 29, 1956*, ORNL-2051, p 37.

[4] R. H. Kernohan, R. E. Jamison, and D. S. Billington, *Solid State Semiann. Prog. Rep. Aug. 30, 1955*, ORNL-1945, p 64.

[5] T. H. Blewitt *et al.*, *Solid State Semiann. Prog. Rep. Aug. 30, 1956*, ORNL-2188, p 52.

three experiments. Since the instantaneous fast-neutron flux in hole 1768 is thought to be several times greater than that in either of the other two holes, it appears that the reaction is not dependent upon neutron flux at the levels used in these experiments. In each experiment, however, the resistivity of the single-crystal samples was observed to decrease more rapidly in the early stage of the irradiation than that of the polycrystalline samples. Furthermore, the decrease in resistivity at the minimum was somewhat smaller for the single crystals. Single-crystal and polycrystalline samples were heated in the reactor during a pile shutdown period after the minimum was reached, and it was found that the original resistivity was recovered upon step-annealing to temperatures near 200°C. No significant difference was noted between the behavior of the one-eighth-inch-diameter rod samples and that of wire samples about 44 mils in diameter.

A series of experiments have been performed on the alloy containing 15 atomic per cent aluminum in the refrigeration facility at hole 52. It was found that when the irradiation was carried out at −120°C no decrease in resistivity took place; instead a linear increase was observed that began at the outset of the irradiation. However, upon subsequent warming of the sample to above 0°C during a pile shutdown period, the decrease in resistivity was observed to set in. A similar kind of annealing experiment was performed in which a number of samples were irradiated at −120°C for three weeks in hole 52. These samples were then removed from the reactor without being allowed to warm and were stored in liquid nitrogen until they could be handled in the laboratory. Then they were isothermally annealed at a number of temperatures in the range from 0°C to 175°C. It was found that most of the decrease in resistivity would take place in a reasonable time at temperatures between 0°C and 34°C. The annealing at several temperatures in this range was studied, and the time τ for a given fractional amount of decrease in resistivity was found to be given by an expression of the type

$$\tau = \tau_0 e^{\epsilon_M/kT} ,$$

where the activation energy ϵ_M is about 0.8 ev.

One question of importance in this work is whether the observed changes in resistivity are due to changes in the residual resistance or to changes in the temperature-dependent contribution to the resistivity. For this reason, measurements were made at temperatures down to liquid helium temperatures on an alloy containing 15 atomic per cent aluminum in its pre-irradiated condition, after irradiation for three weeks at −120°C, and after annealing at 0°C for a sufficient time to induce the decrease in resistance. The results of these experiments indicate that the observed changes are due to changes in the residual resistivity. The same conclusion was reached earlier[4] as regards irradiation-induced changes in the resistivity of copper-zinc alloy.

In-pile resistivity measurements were made on one-eighth-inch-diameter copper-zinc samples of compositions 13, 20, and 30 atomic per cent zinc. In contrast to the composition dependence of the decrease in resistivity for copper-aluminum, there was little difference in the depth of the minimum in the curve of resistivity vs neutron exposure for the three zinc-alloy samples. In each case the minimum occurred at $\Delta\rho = -0.04$ μohm-cm, which accounts for a decrease of about 0.7 per cent. The linear increase in resistivity upon further exposure was greater for the samples with higher zinc content, however. The results for the sample containing 13 atomic per cent zinc were in agreement with those obtained earlier[3] for a 38-mil wire of the same composition. In-pile measurements were also made on samples alloyed with silicon, gallium, germanium, arsenic, and tin. However, the changes in resistivity upon irradiation were small, as was found to be the case for the before-and-after experiments reported earlier.[2]

We may summarize the observations on the copper-aluminum samples as follows:

1. Upon irradiation at ambient pile temperature (~40°C), the resistivity decreases, reaches a minimum at about 10^{18} neutrons/cm^2, and then increases linearly upon further neutron exposure. The depth of the minimum is approximately proportional to the aluminum content; there is no decrease for pure copper, whereas $\Delta\rho = -0.2$ μohm-cm (2 per cent) for copper-aluminum containing 15 atomic per cent aluminum.

2. When the irradiation is carried out at −120°C, no decrease in resistivity is observed. However, upon subsequent warming of the sample the decrease in resistivity will set in. The major part of the decrease takes place between 0°C and

34°C with an activation energy of about 0.8 ev. Upon heating above 175°C, the resistivity increases again to its normal value.

For purposes of analyzing the data and designing future experiments, it seems reasonable to regard the observed changes in resistivity upon irradiation at ambient pile temperature as being due to the superposition of two processes. The first of these is a linear increase due to displacements produced directly by the neutron bombardment. This effect is thought to be largely temperature independent (or perhaps to decrease somewhat when the temperature is raised, due to simultaneous annealing of the displacements) and to occur for pure metals as well as alloys, although not to the same degree. The second process produces a decrease in resistivity, which saturates after about 10^{18} neutrons/cm^2 at 40°C. This process depends upon the presence of two constituent atomic species and is related to changes in their relative arrangements, for example, a clustering or ordering phenomenon. Thus it is diffusion-controlled and, therefore, goes on much more rapidly at higher temperatures. This is in accord with the fact that no decrease occurs for pure metals, nor for the alloys when the irradiation is conducted at −120°C. In this investigation, it is the process responsible for the decrease in resistivity that is of major concern, and future experiments are being planned in an attempt to shed some light on the essential mechanism of the atomic rearrangements that cause this decrease in resistivity of alloys upon irradiation. In particular, measurements of diffuse x-ray scattering are planned in order to make a direct determination of local atomic arrangements in the copper-aluminum alloys. It is felt that an understanding of the essential nature of this reaction and the reasons for its enhancement by neutron irradiation will contribute appreciably to our understanding of the ways in which neutron irradiation affects the properties of solids.

THE PRECIPITATION-HARDENING REACTION IN NICKEL-BERYLLIUM

R. H. Kernohan M. S. Wechsler
D. S. Billington A. B. Lewis

The study of the effect of neutron irradiation on the precipitation reaction in nickel-beryllium alloy containing 14.5 atomic per cent beryllium is being continued. In order to understand better the nature of the precipitation process in this alloy, the course of the precipitation in unirradiated solution-quenched samples was measured[1] at a number of temperatures in the range of 300 to 500°C. It was found that the precipitation appeared to occur in three stages. The suggestion was made that the three stages correspond to (1) nucleation of the precipitate particles, (2) growth of the particles, and (3) agglomeration of the particles (overaging).

The previous experiments on the effect of neutron bombardment gave several important results. First, specimens irradiated for one month at ambient reactor temperature (~35°C) showed no evidence of precipitation. This observation tends to cast doubt on the thermal spike interpretation of radiation effects on solids. Second, subsequent precipitation heat treatment of these specimens at four aging temperatures showed faster formation of the first stage, although there was little or no difference between the unirradiated and irradiated specimens in the later stages. Third, a specimen irradiated and aged at 300°C in the reactor for one month showed a depletion of 1.3 atomic per cent more beryllium from solid solution than a similar specimen aged at 300°C for one month outside the reactor.[2] These long heat treatments at 300°C were sufficient to bring the process into the second stage.

In this report, we wish to discuss two additional experiments which shed more light on the effect of neutron irradiation on the precipitation process. The first of these experiments indicated that the amount of precipitation at the end of the first stage was dependent on the neutron flux. Two similar supersaturated specimens were irradiated in the ORNL Graphite Reactor at ambient reactor temperature. The first remained in an empty fuel channel for three weeks, while the second was inside a hollow fuel element (greater fast-neutron flux) for four weeks. The kinetics of precipitation at 450°C of these two specimens were then studied and compared with that of an unirradiated sample. Again it was found that the irradiated specimens precipitated a little faster. However, the amount of precipitate at the end of the first stage was 2.4 atomic per cent for the unirradiated specimen, 1.8 atomic per cent for the first specimen (hollow channel), and 0.8 atomic per cent for the second specimen, which received a higher fast-neutron flux. Thus, it appears that neutron irradiation *decreases* the amount of beryllium precipitated in the first stage, although this precipitation occurs somewhat more rapidly for the irradiated specimens.

In the second experiment, the two specimens previously heat-treated at 300°C for one month (one irradiated at 300°C, the other a control) were heat-treated at 450°C. The precipitation of these two specimens is shown in Fig. 2. The precipitation of a solution-quenched specimen not previously heat-treated is also shown in this figure for comparison purposes.

From the curves it can be seen that there is a retardation in the precipitation of the two specimens previously heat-treated at 300°C. However,

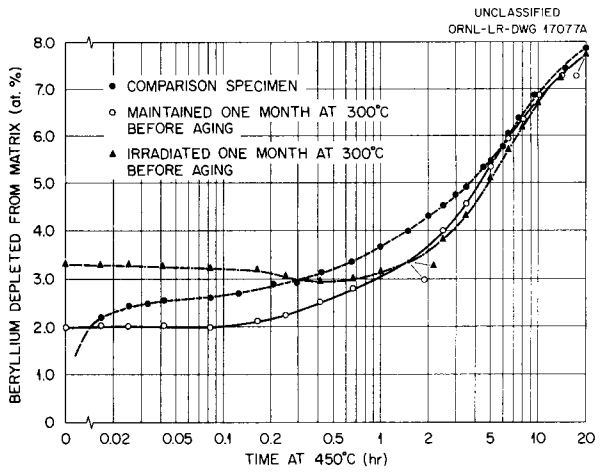

Fig. 2. Ni-Be Precipitation at 450°C.

[1] R. H. Kernohan, A. B. Lewis, and D. S. Billington, *Solid State Semiann. Prog. Rep. Aug. 30, 1956*, ORNL-2188, p 92.

[2] R. H. Kernohan, A. B. Lewis, and D. S. Billington, *Solid State Semiann. Prog. Rep. Feb. 29, 1956*, ORNL-2051, p 37.

near the end of the second stage, that is, after 20 hours at 450°C, little difference can be seen in the amount of precipitate for all three specimens. The behavior of the two specimens in the second experiment is typical of the retrogression phenomena observed in a number of other precipitation-hardening alloys. In general, precipitate particles formed at lower heat-treatment temperatures are not stable at higher temperatures. They must dissolve before the precipitate particles characteristic of the higher heat treatment can begin to form.

Although the precipitation process in nickel-beryllium has been divided into the three stages previously mentioned, it is entirely possible that these stages may be related to certain steps in the precipitation processes observed in other materials.[3,4] In particular, the first stage may be the formation of Guinier-Preston zones, while the second may be the formation of the precipitate itself. However, there is as yet insufficient information to identify the exact mechanism in the case of nickel-beryllium.

It is planned to study further the initial precipitation of irradiated supersaturated specimens and also to investigate the effect of neutron irradiation on specimens that have already been heat-treated. These latter specimens will then contain a definite amount of precipitate before they are irradiated. Whether neutron irradiation will further the precipitation process or result in the solution of some of the existing precipitate remains to be seen.

---

[3] A. Guinier, *Acta. Cryst.* 5, 121 (1952).

[4] A. Guinier, *Trans. Am. Inst. Mining, Met. Petrol. Engrs.* 206, 673 (1956).

ELECTRON MICROSCOPE STUDIES

T. S. Noggle

Installation of an RCA EMU-3B electron microscope was started in April 1957, and a program of electron microscope studies on solids has been initiated. To date, efforts have been directed to preliminary work on replica techniques applicable to the study of the surfaces of solids, and the work in progress is not sufficiently advanced to warrant reporting on at this time. The research program planned covers a range of interests, the most important of which are discussed briefly below.

Structural Changes Associated with Radiation Damage. – Electron microscope observations on structural changes arising from irradiation with energetic particles represent a virtually unexplored field of study. In particular, it is of interest to look for direct manifestations of radiation damage arising from fast-neutron bombardment. It has not been established at the present time whether it will be possible to "see" radiation damage directly; however, recent developments in electron microscopy have led to the observation of dislocations in metals[1] and the resolution of lattice planes in several metal-organic compounds;[2] and these developments suggest that it may be possible to see radiation effects in solids, at least for a limited number of materials, and perhaps with special techniques. A variety of materials and preparations will be examined for direct evidence of radiation damage. The indirect manifestations of radiation damage in multiphase alloys will also be studied, for example, precipitation in age-hardening alloys.

Surface Studies. – This general title covers the cooperative studies with the Surface Group in the Solid State Division and will use the microscope as a tool for direct observations on the effect of chemical, electrochemical, and thermal treatments on the surfaces of solids.

Plastic Deformation. – Recent work by the Low-Temperature Physics Group in the Solid State Division has established that, under suitable conditions of straining, copper and irradiated copper show different mechanisms of plastic deformation than heretofore observed;[3] the study of the surface structures produced by discontinuous slip and twinning is of considerable importance in obtaining further understanding of these mechanisms of plastic deformation. Initially, the studies of the surface structures developed by plastic deformation will be made on copper, but they will be extended to other metals at a later time.

Hot-Cell Techniques. – The high level of radioactivity induced in structural and fuel materials used in reactors makes it necessary that any electron microscope preparations on these materials must be carried out in hot cells employing remote handling techniques. Evaporated metal or inorganic films seem to offer the best approach to this problem, and vacuum evaporation equipment to be operated in the hot cells is being designed for this purpose. Investigation of several one- and two-step replica techniques is being carried out with the intent of adapting some of these techniques for remote manipulation. In general, the techniques under consideration will permit the removal of nonradioactive replicas from the surfaces to be studied, and further processing will be carried out in the usual manner.

---

[1] P. B. Hirsch, R. W. Horne, and M. J. Whelan, *Phil Mag.* 1, Series 8, 677 (1956).

[2] J. W. Menter, *Proc. Roy. Soc. (London)* **A236**, 119 (1956).

[3] T. H. Blewitt, R. R. Coltman, and J. K. Redman, *J. Appl. Phy.* **28**, 651 (1957).

CHEMICAL PROPERTIES OF METAL SURFACES

F. W. Young, Jr. L. H. Jenkins

Studies of the chemical properties of metal surfaces were initiated in the Solid State Division during the past year. Investigations are in progress on gaseous oxidation, observation of dislocations as etch pits, thermal etching in high vacuum, and dissolution of metals in aqueous media. Perforce, much of the time to date has been used in outfitting a laboratory for these studies, in collecting equipment, and in performing preliminary experiments. Many of these experimental systems will be used in the future to investigate the effect of irradiation on the chemical properties of surfaces.

Gaseous Oxidation of Metals

A previous investigation[1] indicated that, on oxidizing copper at 150°C in the presence of a radiation field, the oxidation process was changed in character and speeded up somewhat. This experiment is being repeated as the first part of a more comprehensive study on the effect of irradiation on the gaseous oxidation of metals. This program is being carried out in conjunction with J. V. Cathcart of the Metallurgy Division.

Harris[2] and others[3] have shown that the oxide film formed on a crystal face of copper during oxidation in oxygen at temperatures from 25°C to 250°C is not of uniform thickness. Rather it consists of a base film in which are dispersed nuclei of oxide of much greater thickness than the base film. It is proposed that these oxide nuclei may be related to dislocations in the metal, the points where dislocations end at the surface being points of enhanced oxidation rate. Investigations are in progress to correlate the oxide nuclei with dislocations as revealed by etch pits.

Observations of Dislocations as Etch Pits

Several methods of etching copper to obtain etch pits which correspond to dislocations were devised: (1) thermal etching in a vacuum, (2) thermal etching in hydrogen, (3) etching in an aqueous solution of KCl (10%), and (4) electrolytic etching in a phosphoric acid bath. The number of pits observed on as-grown crystals was 2×10^7 to 5×10^7 per square centimeter. In order to determine the correspondence between these pits and dislocations, copper crystals were bent so as to obtain a known increase in the number of dislocations. The movement of these dislocations on subsequent annealing was studied. A previous preliminary investigation[4] indicated that oxygen-free high-conductivity copper (~99.99%) would undergo a partial polygonization on annealing, whereas purer copper (99.999%) did not polygonize. The investigation is being continued with crystals which are grown and bent with an orientation, [512], such that slip occurs in a single slip system.

In order to obtain etch pits electrolytically, it was necessary that some impurity be present in the copper. The kind and amount of impurity which was necessary was determined by evaporating various impurities on copper and annealing at high temperatures to diffuse them into the crystal. It was found that 0.01 to 0.001% sulfur, selenium, tellurium, silicon, germanium, and tin in copper would cause etch pits to be formed electrolytically. Gold, silver, zinc, aluminum, phosphorus, arsenic, antimony, bismuth, iron, cobalt, and nickel did not cause electrolytic etch pitting.

It is of interest to speculate on the role played by impurities in the mechanical and chemical properties of dislocations. Since impurities in the metal can affect the ease with which dislocations climb, as suggested in the experiments on polygonization of copper, it is not unreasonable to assume that the geometrical arrangement of the dislocation in the metal is influenced by impurities. Seeger[5] has proposed that dislocations in copper would split into partial dislocations separated by a stacking fault of energy such

[1] F. W. Young, Jr., *On the Effect of Reactor Exposure on the Rate of Oxidation of Copper Single Crystals*, ORNL CF-55-3-70 (March 9, 1956).

[2] W. W. Harris, F. L. Ball, and A. T. Gwathmey, *Acta Met.* (in press).

[3] K. R. Lawless, F. W. Young, Jr., and A. T. Gwathmey, *J. chim. phys.* 53, 667 (1956).

[4] F. W. Young, Jr., and N. Cabrera, *J. Appl. Phy.* 28, 787 (1957).

[5] G. Schoeck and A. Seeger, *Conference on Defects in Crystalline Solids*, p 340, Physical Society, London, 1955.

as to stabilize them, and thus climb would not be possible. If the theory of Seeger is correct, it would appear that impurities allow the partial dislocations to recombine and climb at high temperature.

The necessity for the presence of certain impurities for the formation of electrolytic etch pits at dislocations in copper indicates the importance of the impurities in the chemical properties of dislocations. There are at least two ways in which the impurities could act to promote chemical activity at dislocations. An atom at an edge dislocation would have a residual charge compared with atoms not at a dislocation, because of the difference in number of nearest neighbors. In many cases, this charge is not large enough to cause observable differences in chemical activity at the dislocation, since impurities are often necessary for the formation of etch pits at dislocations. There may be some electrochemical interaction between the dislocation and the impurity which causes increased activity for the combination of impurity plus dislocation. Another possibility is that the impurity may be chemically active alone and the dislocation merely acts as a line source of impurity. It appears possible to decide between these two alternatives. The dislocations can be caused to move away from the impurities by mechanical force, and the line of impurities left behind can be investigated for chemical activity. Another question which is being studied is whether different kinds of dislocations have different chemical properties. If a crystal of the proper orientation is bent, the dislocations introduced will all be of edge character on one face, while on the face perpendicular to this one they will be of screw character. Thus difference in the activity of the dislocations on the two faces can be observed.

Thermal Etching

Previous experiments[6] showed that, when spherical copper crystals were heated to high temperatures in high vacuum, facets parallel to close-packed faces were developed. The size and type of facet developed was a function of the temperature of etching. Under certain conditions etch pits were formed which apparently correspond to dislocations. It was also found that there was a striking difference in the etching behavior of 99.99% and 99.999% copper, the less pure crystal developing much larger facets. These investigations will be continued on copper and on crystals of other metals.

Dissolution of Copper in Aqueous Media

A study of the dissolution of copper metal into aqueous media by means of various chemical reactions has been initiated. By a careful choice of reagents the dissolution should reveal the relationships between crystal face and certain surface processes. In general, an attempt is being made to gain an understanding of the processes involved when an atom leaves the surface of a metal and to determine if mechanisms of such processes vary as a function of crystal face. Specifically, the objectives of this program are to determine (1) the effect of crystal face on certain reactions which do not cover the metal with a protective film, (2) activation energies of these reactions as a function of crystal face, (3) differences in mechanisms, if any, of dissolution of various faces, (4) the equilibrium position of reactions with respect to different surface orientations, (5) the electrode potentials of various faces in systems in which the problem of oxide contamination has been eliminated, (6) effects of dislocations, chemical impurities, etc. on the foregoing phenomena, (7) how radiation damage affects these surface processes.

Two types of reactions have been considered to date:

$$(1)\quad Cu^0 + H_2O + 4CN^- \rightleftharpoons Cu(CN)_4^{---} + OH^- + \tfrac{1}{2}H_2$$

$$(2)\quad Cu^0 + Cu(\text{complex})^{++} \rightleftharpoons 2Cu(\text{complex})^+$$

The major effort has been placed on the first system. Copper (99.999%) single-crystal plates approximately 2 × 1 × 0.1 cm, grown by the Bridgman method, are electropolished to reduce the thickness of the sample and to produce a smooth surface. The finished specimen is about 0.5 mm thick, so that the sides present a very small reaction area as compared with the other surfaces. The sample is suspended in 50 ml of

[6] F. W. Young and A. T. Gwathmey (to be published).

dilute aqueous KCN, which is stirred constantly and which is maintained at desired temperatures by a thermostatically controlled water bath. Periodically, aliquots are withdrawn from the cyanide solution and analyzed for copper by the spectrophotometric neo-cuproine method of Smith.[7] Analytical techniques have been refined so that the dissolution of 10 Å of metal from the copper surface (~3 atomic layers) can be observed. Preliminary results show that the system does yield information useful in attaining the first four objectives.

Reactions of the second type will assume more importance as mechanisms are emphasized. Preliminary data have been gathered on the copper-ammonia and copper-ethylenediamine systems. By observing the change in reaction rates of crystal faces as a function of the complexing ligand employed, the mechanism of the electron transfer between the metal atoms will be better understood.

[7] G. F. Smith and W. H. McCurdy, Jr., *Anal. Chem.* **24**, 371 (1952).

LOW-TEMPERATURE IRRADIATION OF *n*-TYPE GERMANIUM

J. W. Cleland J. H. Crawford, Jr.

Studies of irradiation effects in germanium at temperatures well below the temperature of liquid nitrogen have been conducted in order to examine the thermal stability of radiation-induced defects and the importance of minority-carrier trapping processes. Previous studies have indicated that the rate of conductivity decrease in *n*-type germanium during reactor exposure is temperature sensitive. Under the assumption that the primary process is conduction-electron removal by vacant localized states, the removal rate has been determined as ~3.2 electrons per incident fast neutron at 300°K (ref 1) and ~5 electrons per incident fast neutron at 120°K (ref 2) in the ORNL Graphite Reactor.

It is not clear whether this variation is due to thermal stability of defects or to the fact that some defect acceptor states, which lie close to the conduction band, are more effective in removing conduction electrons at lower temperatures. Extensive relaxation processes occur when germanium specimens, irradiated in the liquid-nitrogen temperature range, are warmed. Two thermally unstable traps have been observed in *n*-type germanium subsequent to fast-neutron irradiation at 120°K. These are presumably minority-carrier traps that empty upon warming to ~134 and 165°K, respectively. Subsequent recooling indicates that these traps were thermally unstable and had disappeared during the warming cycle. Pulse annealing of *p*-type specimens of germanium following irradiation by fast neutrons at 100°K also indicates the annealing of thermally unstable minority-carrier traps[3] at a temperature of ~120°K. Electron and deuteron[4] irradiation experiments have indicated the production of a vacant electronic state about 0.11 ev below the conduction band that would presumably be more efficient at these low temperatures.

Single-crystal plates of *n*-type germanium ($n_0 \sim 10^{18}$ electrons/cm^3 at 77°K) have been irradiated in the hole-12 cryostat of the ORNL Graphite Reactor.[5] The temperature of exposure was ~16°K, and the conductivity, σ, was continuously recorded. Annealing studies subsequent to exposure were conducted by utilizing a pulse technique described in detail elsewhere.[5] The sample chamber was heated by successive condenser discharges to each pulse temperature in about 20 sec, held at temperature 1 to 3 min, and then returned rapidly to a reference temperature of 10°K.

A typical plot of σ vs the integrated fast-neutron flux, nvt_f, is shown in Fig. 3. Although the absolute value of the fast-neutron flux (a weighted

[1] J. H. Crawford, Jr., and K. Lark-Horovitz, *Phys. Rev.* **78**, 815 (1950).

[2] J. W. Cleland, J. H. Crawford, Jr., and J. C. Pigg, *Phys. Rev.* **98**, 1742 (1955); *Solid State Quar. Prog. Rep. Feb. 10, 1953*, ORNL-1506, p 43; *Solid State Semiann. Prog. Rep. Feb. 28, 1955*, ORNL-1852, p 15.

[3] J. W. Cleland, J. H. Crawford, Jr., and J. C. Pigg, *Phys. Rev.* **99**, 1170 (1955).

[4] H. Y. Fan and K. Lark-Horovitz, *Conference on Defects in Crystalline Solids*, p 232 ff., Physical Society, London, 1955.

[5] R. R. Coltman, T. H. Blewitt, and T. S. Noggle, *Rev. Sci. Instr.* **28**, 375 (1957); T. H. Blewitt *et al.*, *Solid State Semiann. Prog. Rep. Aug. 30, 1956*, ORNL-2188, p 45.

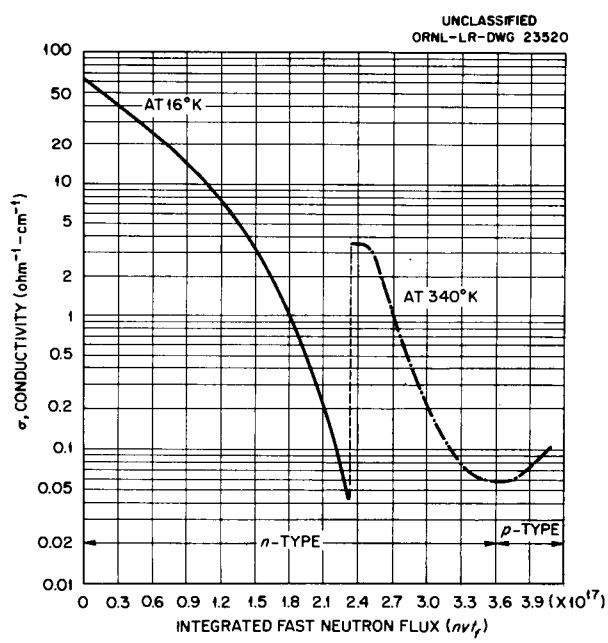

Fig. 3. *n*-Type Germanium Conductivity vs nvt_f at 16°K.

average of the flux of neutrons capable of displacing germanium atoms) may be in error by as much as a factor of 2, the calibration used here is consistent with that employed previously.[1-3] The initial rate of conductivity decrease per incident fast neutron, $[d\sigma/d(nvt)]_i$, is $\sim 8 \times 10^{-16}$ ohm^{-1}-cm^{-1} at 16°K for several samples. Annealing studies following irradiation are shown in Fig. 4. The sample remained *n*-type upon warming to reactor ambient temperature (340°K), and Fig. 3 shows the continued approach to intrinsic behavior and the conversion to *p*-type under subsequent exposure.

Under the assumption that the mobility is not appreciably changed initially, the variation of σ with exposure yields an initial rate of conduction-electron removal of ~9 per incident neutron for several specimens. As indicated above, however, the determination of the initial rate of electron removal, $[dn/d(nvt)]_i$, and hence the rate of defect introduction from the initial rate of conductivity change, is no longer a straightforward calculation at these temperatures. For example, the assumption, made for room-temperature exposures, that the change in mobility is insignificant early in the bombardment is no longer valid. Brooks[6] has pointed out that, for the James–Lark-Horovitz model of the defect-energy-level structure,[7] the conductivity change resulting from the decrease in mobility will be twice that caused by the decrease in electron concentration in the impurity scattering range. The problem of determining the rate of defect introduction is further complicated by the extensive minority-carrier trapping process, which tends to reduce the rate of conductivity decrease below the rate expected if the conduction electrons are in thermal equilibrium with the defect states. Consequently, care must be exercised when using the value of $[dn/d(nvt)]_i$. The rate of defect introduction obtained at ~16°K is three times that observed at room temperature; however, it is not certain how this should be divided among a true increase in the rate of defect formation, the greater effectiveness in removing electrons by the shallow vacant state, and an enhanced effect due to an appreciable decrease in mobility.

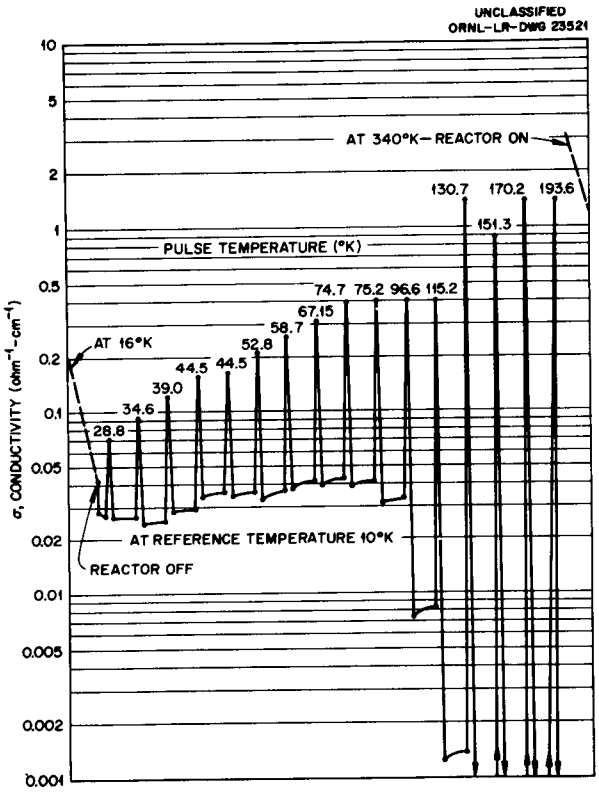

Fig. 4. *n*-Type Germanium Pulse-Annealing Studies.

The extensive relaxation during pulse annealing, as shown in Fig. 4, suggests strongly that the rate of defect introduction is considerably higher at the low temperature and that an appreciable fraction of these defects are thermally unstable above ~95°K. Minority-carrier trapping effects are the index of these unstable defects, and hence the relationship between the conductivity and the defect concentration is much more obscure than would be the case when the conduction electrons are in thermal equilibrium. Annealing of a large portion of the minority-carrier traps is indicated by the irreversible behavior of σ during temperature pulsing. The background of ionizing radiation within the reactor, even during reactor shutdown, should be amply sufficient that any minority-carrier traps remaining after a temperature pulse should be reoccupied within a short time after a recooling to the reference temperature. The time at the reference temperature between pulses was 30 min to 1 hr, a period much greater than that expected to be required for reoccupation. Since no restoration of conductivity to or near its value at 10°K was observed once the pulse temperature exceeded ~95°K, it is concluded that the decrease in σ at 10°K results from the disappearance of minority-

[6] H. Brooks, *Ann. Rev. Nuclear Sci.* 6, 215 (1956).

[7] H. M. James and K. Lark-Horovitz, *Z. physik. Chem. (Leipzig)* 198, 107 (1951).

carrier traps, either by a rearrangement of the configuration of defects or by defect annihilation. Insufficient information is available at present to permit further speculation on the exact nature of the annealing process.

The principal result of this experiment is the observation that little or no thermal relaxation of bombardment-produced defects occurs at temperatures between ~16 and 95°K. This result is in marked contrast with the behavior of many pure metals, which show a marked relaxation of electrical resistivity change between 30 and 50°K after exposure to electrons, neutrons, or deuterons at temperatures below 20°K. The absence of extensive annealing at very low temperatures simplifies considerably the studies of radiation effects in germanium, since there is now some assurance that liquid-nitrogen temperature is a sufficiently low exposure temperature to preserve for subsequent examination essentially all the defects that can be introduced at temperatures even as low as 16°K.

MINORITY-CARRIER LIFETIME STUDIES IN GERMANIUM

O. L. Curtis J. W. Cleland

Irradiation is being used as a tool to provide a better understanding of the process of carrier recombination in germanium. Recombination centers are introduced by reactor or gamma-ray irradiations, and these centers influence the lifetime of minority carriers. A known number of recombination centers can be introduced by a certain amount of irradiation. Samples of different initial carrier concentration can be studied after irradiation from a variety of sources. Although such experiments are designed to aid in understanding the fundamental processes of carrier recombination, the information received is also of practical importance to those who desire to use semiconducting devices in radiation fields.

The method of measurement used is an observation of the exponential decay of excess conductivity following an injection pulse. Injection is produced by an electrical pulse, with the use of a surface barrier contact, or by a light pulse. While a light pulse serves to inject carriers into either *n*-type or *p*-type material, electrical injection is suitable only for *n*-type germanium.

A study has been made of the dependence of hole lifetime in *n*-type germanium upon irradiation, and this work has been accepted for publication. The following is an abstract of the paper.

The Effect of Irradiation on the Hole Lifetime of *n*-Type Germanium.[1] O. L. Curtis, Jr., J. W. Cleland, J. H. Crawford, Jr., and J. C. Pigg. – The minority-carrier lifetime of germanium is very sensitive to certain types of irradiation. The results of irradiating large single-crystal samples of *n*-type germanium with fast neutrons and Co^{60} gamma rays are presented and discussed. Lifetime was determined from a transient measurement of the decay of holes following an injection pulse. The effect of initial carrier concentration has been considered. According to the James–Lark-Horovitz model, four energy levels are introduced by irradiation into the forbidden band of germanium, one above and three below the center of the band. Using the upper level, a one-level recombination model serves to explain the experimental results approximately. The determination of the recombination level agrees well with the position of the first ionization level of the interstitial produced by irradiation at about 0.2 ev below the conduction band. On this basis, the effective cross section for hole capture by these recombination centers is found to be about 4×10^{-15} cm^2 and 5×10^{-16} cm^2 for neutron and gamma irradiated germanium, respectively. A lower level may also be responsible for the recombination process.

A similar study of electron lifetime in irradiated *p*-type material is now being made, with utilization of a light-pulse technique. The *p*-type samples of 28 and 8 ohm-cm have been irradiated for a total of 16 hr in the new Solid State Division Co^{60} source; this corresponds to a total flux of $\sim 6 \times 10^{16}$ photons/cm.^{2} The rate of decrease of lifetime is roughly the same as that for *n*-type material previously observed. A similar decrease is observed in the lifetime of an essentially intrinsic sample. Annealing studies and additional experiments on the temperature dependence of the minority-carrier lifetime in irradiated germanium are expected to aid in a determination of the position of the irradiation-introduced energy levels that cause recombination.

[1] O. L. Curtis, Jr., *et al.*, *J. Appl. Phy.* **28**, 1161 (1957).

MOBILITY CHANGES IN IRRADIATED *n*-TYPE GERMANIUM

L. F. Connell, Jr.[1] J. W. Cleland

A systematic investigation of the variation of the Hall mobility of gamma- and fast-neutron-irradiated single-crystal plates of *n*-type germanium has been conducted. The apparatus employed consisted of a Consolidated Engineering Corp. electromagnet operated at ~4000 gauss and the liquid-nitrogen-temperature cryostat[2] originally constructed for magnetic susceptibility measurements. The Hall coefficient and the resistivity were determined as a function of temperature from room temperature to ~50°K by utilizing pumped liquid nitrogen. The mobility was then calculated from the relation $\mu = 8R/3\pi\rho$ $cm^2 \cdot v^{-1} \cdot sec^{-1}$, where R is the measured Hall coefficient in units of cm^3/coulomb, and ρ is the resistivity in ohm-cm.

The Hall mobility of fast-neutron-irradiated *n*-type germanium has been plotted as a function of the temperature in Fig. 5. The negative temperature coefficient of the original curve is characteristic of charge carrier scattering by thermal vibrations of the lattice.[3] Irradiation introduces additional scattering centers which scatter carriers more effectively as the temperature is lowered. Curve VIII of Fig. 5, after a total exposure of $\sim 10^{16}$ fast neutrons, indicates the onset of a low-temperature behavior which seriously complicates the analysis of the data obtained. Minority-carrier traps have previously been observed in irradiated *n*-type germanium, and the radioactive decay of transmuted germanium atoms provides a flux of ionizing radiation. Upon cooling to ~100°K, the minority-carrier traps evidently act as additional scattering centers that further decrease the mobility. The ionizing radiation, however, evidently alters the minority-carrier traps, decreasing their charge center scattering, and the resultant mobility slowly increases to that of the upper portion of the curve. The actual measurement of the mobility is thus a sensitive function of the time, temperature cycle, and background radiation, and as such prevents any detailed analysis of the results.

The Hall mobility of gamma-irradiated *n*-type germanium has been plotted as a function of the temperature in Fig. 6. The negative temperature coefficient resulting from charge carrier scattering by thermal vibrations of the lattice is altered by additional scattering centers which are more effective at lower temperatures. Curves VII, VIII, and IX of Fig. 6 exhibit the onset of an evident change in minority-carrier trap occupation or ionization change that is a sensitive function of the temperature. The sharp decrease in mobility of curve IX as the temperature is raised above ~70°K might presumably be caused by the sudden increase in charge carrier scattering expected if an occupied state was vacated or an uncharged interstitial atom suddenly ionized.

Further experimentation, a detailed examination of the data, and a comparison with existing theories of scattering are being continued.

---

[1] Summer research participant from North Texas State College.

[2] D. K. Stevens, *Solid State Quar. Prog. Rep. Aug. 10, 1952*, ORNL-1359, p 39.

[3] J. W. Cleland, J. H. Crawford, Jr., and J. C. Pigg, *Solid State Semiann. Prog. Rep. Feb. 28, 1955*, ORNL-1852, p 15.

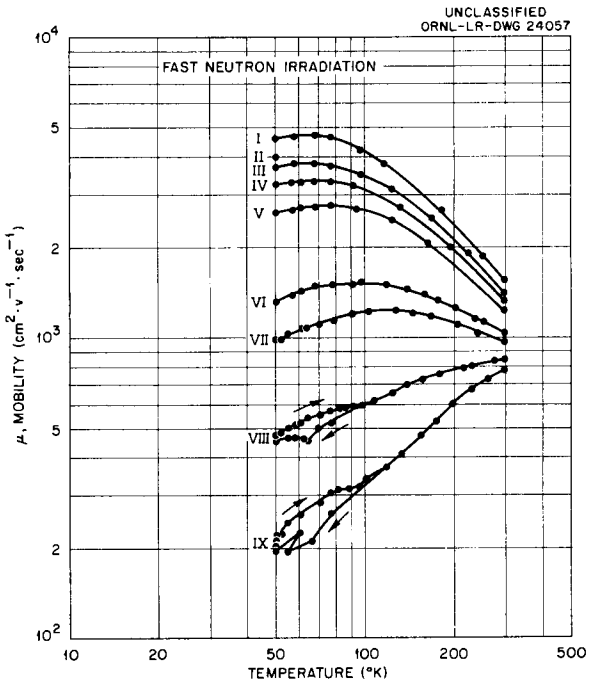

Fig. 5. *n*-Type Germanium Hall Mobility vs Temperature After Fast-Neutron Irradiations.

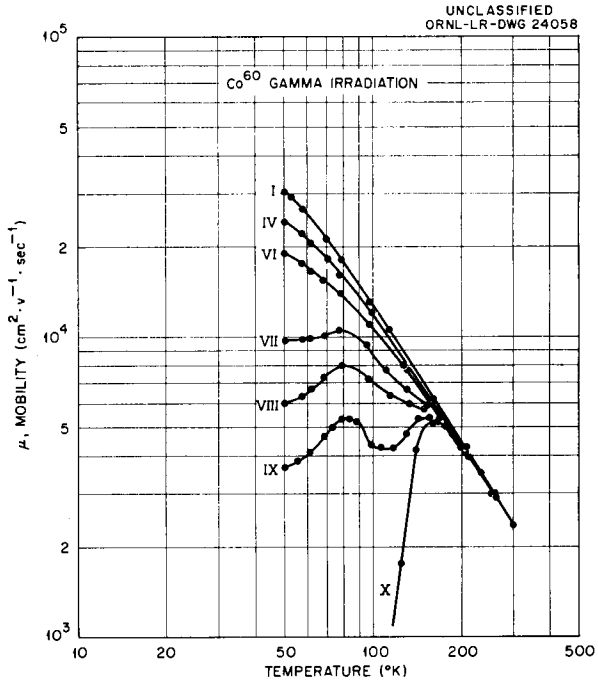

Fig. 6. *n*-Type Germanium Hall Mobility vs Temperature After Co^{60} Gamma-Ray Irradiations.

ANNEALING STUDIES OF IRRADIATED GERMANIUM

J. C. Pigg

Alterations in radiation-induced property changes have been noted previously when germanium irradiated at temperatures in the vicinity of 100°K was warmed to room temperature.[1] More recent work[2] shows definite annealing peaks at about 135 and 165°K. In addition, annealing at various temperatures in the range 0 to 100°C showed that a complicated annealing was occurring. It was not possible at that time to completely analyze the data, since only changes in conductivity had been measured. It was recognized that both the carrier concentration and the carrier mobility could be changing, and that the Hall effect as well as the conductivity would have to be studied.

In order to monitor both conductivity and Hall constant continuously during the prolonged annealing cycle, it is necessary to measure and record these parameters automatically. Consequently, such a circuit has been developed (Fig. 7).

The basic circuit used for measuring the Hall coefficient is shown in Fig. 8*a*. If the Hall voltage E_H is measured and the potentiometer is adjusted until the voltage output equals E_H, then

$$E_H = A_1 I r_1 \ , \tag{1}$$

$$\frac{E_H}{I} = A_1 r_1 = K_1 R \ ,$$

where R is the Hall constant, and K_1 is a constant which involves the magnetic field strength and the dimensions of the sample. Thus

$$R = \frac{A_1 r_1}{K_1} \ , \tag{2}$$

where R is determined in terms of constants and the position of the sliding contact of the potentiometer.

[1] J. W. Cleland, J. H. Crawford, Jr., and J. C. Pigg, *Solid State Semiann. Prog. Rep. Aug. 31, 1953*, ORNL-1606, Figs. 57 and 58, p 67.

[2] J. W. Cleland, J. H. Crawford, Jr., and J. C. Pigg, *Solid State Semiann. Prog. Rep. Feb. 28, 1955*, ORNL-1852, p 15–17.

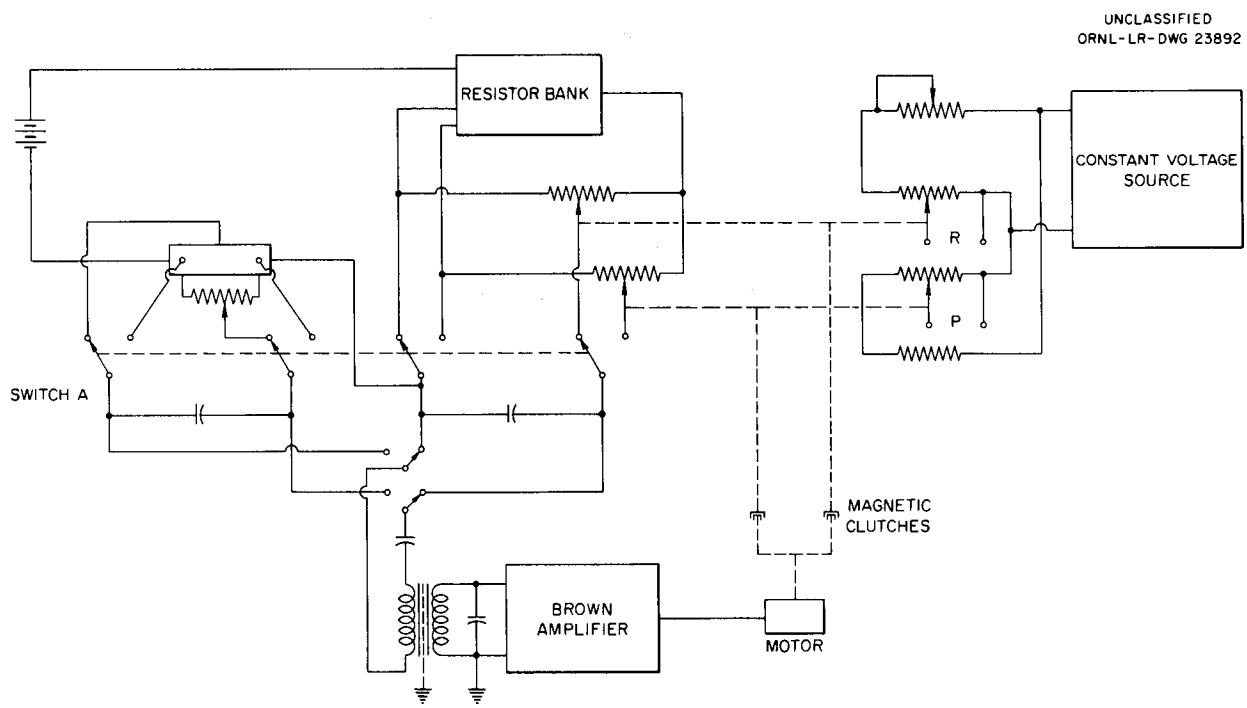

Fig. 7. Circuit for Automatic Measurement of Hall Constant and Resistivity.

The resistivity is obtained from the circuit shown in Fig. 8*b*:

(3) $$J = E_\rho \sigma ,$$

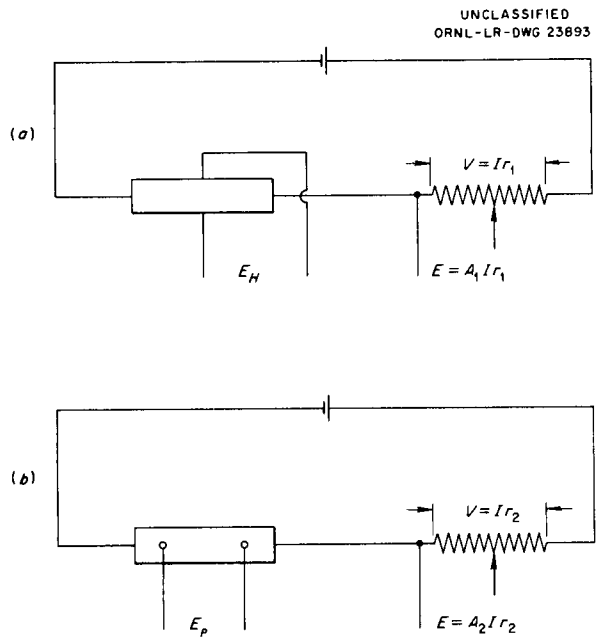

Fig. 8. Principle of Operation of Hall and Resistivity Measuring Circuit.

(4) $$\frac{I}{K_2} = \frac{E_\rho}{\rho} ,$$

(5) $$E_\rho = \frac{I_\rho}{K_2} = A_2 I r_2 ,$$

(6) $$\rho = A_2 r_2 K_2 ,$$

where K_2 is a constant determined by the dimensions of the specimen. Hence ρ is determined in terms of constants and the position of the sliding contact of the potentiometer.

The circuit shown in block diagram in Fig. 7 combines the circuits of Fig. 8 and provides readout voltages corresponding to the position of the sliding contacts on the respective potentiometer. Whenever the reading on the recorder is near either limit, limit switches actuate relays which change the range of the measuring circuit by switching to the appropriate resistor in the resistor bank. The position of the respective selector switch, hence the scale, is indicated on the recorder.

The device can measure the Hall constant and the resistivity with an accuracy of ±0.5%, providing the physical dimensions of the sample are known with a corresponding accuracy. Changes in Hall constant and resistivity of 0.2% can be measured.

OPTICAL ABSORPTION IN GERMANIUM

H. C. Schweinler C. H. Edwards [1]

In preparation for a study of the effect of fast-neutron bombardment on the absorption edge in high-purity germanium, the bulk absorption coefficient for light in the near-infrared region of the spectrum has been measured. A theoretical interpretation of these measurements is given here.

The valence-band structure of germanium is now quite well known. It has a maximum at $k = 0$, with two bands ($E_{v\mathrm{I}}$ and $E_{v\mathrm{II}}$) touching at that point. The equations for these energy surfaces are

$$E_{v\mathrm{I,II}} = E_v^0 + \frac{\hbar^2}{2m_0} \times \left[Ak^2 + \sqrt{B^2k^4 + C^2(k_x^2k_y^2 + k_y^2k_z^2 + k_z^2k_x^2)} \right],$$

with $A = -13.0$, $B^2 = (8.9)^2$, and $C^2 = (10.3)^2$. Band II is quite accurately spherical as a function of the wave propagation vector $\vec{k}$; band I differs somewhat from a sphere in shape and will be replaced by an appropriate spherical average in the work which follows. (The deviation from spherical form is perhaps 30% in the ratio of extreme diameters.)

The optical absorption treated here will be the "direct transitions" from valence bands to conduction band under the influence of the light wave, with no appreciable change in the propagation vector of the electron making the transition. The conduction band has a relative minimum near $\vec{k} = \vec{0}$, and is given by

$$E_c = E_c^0 + \frac{\hbar^2k^2}{2m_c},$$

where

$m_c = 0.034$ (Dresselhaus, Kip, and Kittel[2])
$= 0.042$ (Zwerdling and Lax[3])
$= 0.037$ (Dumke[4]).

This conduction band (named Γ_2^-) is known from group theory to have the symmetry of the octahedron and to be nondegenerate (except for the Kramers spin degeneracy). Therefore it is probably a good assumption to take the energy surfaces to be spherical. The energy surfaces are not necessarily quadratic in $\vec{k}$; however, one of the results of this analysis is that the quadratic approximation is a good one for at least 0.05 ev or so from the minimum.

For photons of energy $h\nu$ greater than $E_c^0 - E_v^0$, the absorptions are allowed, that is, are subject to no selection rule which decreases the strength of the absorption. The bulk absorption coefficient can be thrown into the following form:

$$(137a_{\mathrm{H}}\mu_n)^2 = 8\left[\frac{f_{c\leftarrow \mathrm{I}}^{(y)}}{(m_0/m_c + m_0/m_{v\mathrm{I}})^{3/2}} + \frac{f_{c\leftarrow \mathrm{II}}^{(y)}}{(m_0/m_c + m_0/m_{v\mathrm{II}})^{3/2}}\right]^2 \frac{h(\nu - \nu_t)}{e^2/a_{\mathrm{H}}},$$

in which "137" is $\hbar c/e^2$, the reciprocal of the fine-structure constant; $a_{\mathrm{H}} = 0.53 \times 10^{-8}$ cm is the radius of the first Bohr orbit for hydrogen; μ is the observed absorption coefficient; n is the index of refraction of germanium for the wavelength in question; the f's are oscillator strengths, for example,

$$f_{c\leftarrow \mathrm{I}}^{(y)} = \frac{2\,|\langle c\,|\,(\hbar/i)\,\partial/\partial y\,|\,v\mathrm{I}\rangle|^2}{m_0(E_c - E_{v\mathrm{I}})};$$

the m's are effective masses for the conduction and the valence bands (the latter, as mentioned above, are a spherical average of the more nearly correct function); $h\nu$ is the photon energy; $h\nu_t = E_c^0 - E_v^0$ is the threshold energy; and $e^2/a_{\mathrm{H}} = 27.2$ ev is twice the binding energy of the hydrogen atom.

[1] Summer employee from University of Tennessee.

[2] G. Dresselhaus, A. F. Kip, and C. Kittel, *Phys. Rev.* 98, 368 (1955).

[3] S. Zwerdling and B. Lax, *Phys. Rev.* 106, 51 (1957).

[4] W. P. Dumke, *Phys. Rev.* 105, 139 (1957).

From the above equation it is evident that the absorption coefficient squared is linear in photon energy, or in the reciprocal of the photon wavelength. Such a graph, based on Edwards' data, is presented in Fig. 9. It is clear that two straight lines suffice to represent the data over the energy range given here. The higher energy region is believed to be the direct optical transition; the lower energy region is not well understood at present, but may be due to surface absorption.

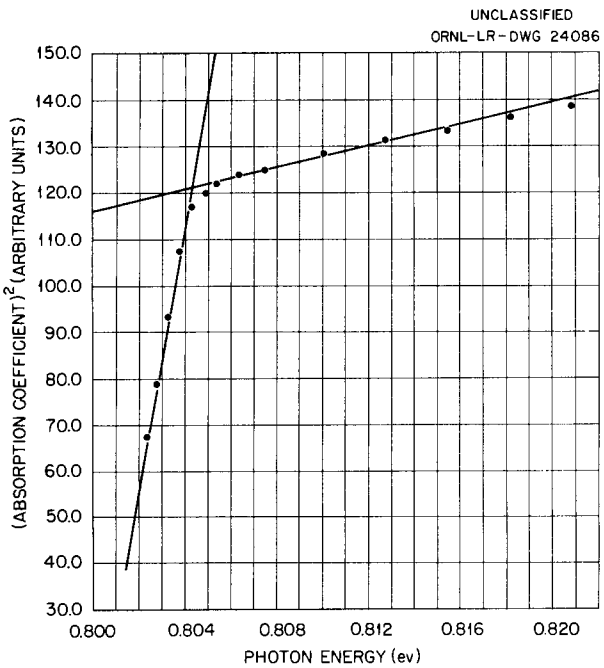

Fig. 9. Optical Absorption Coefficient of Germanium.

The coefficient of $h(\nu - \nu_t) \div (e^2/a_H)$ can be evaluated from Dresselhaus, Kip, and Kittel's[2] estimate of oscillator strengths. The spin of the electrons has been included in this treatment. The resulting average oscillator strengths are one-third of the above values[2] for each of three bands, but one of the bands is inactive for the photon energies used here. The parameters used were $m_0/m_c = 23.8$, $m_0/m_{vI} = 3.5$, $m_0/m_{vII} = 23.0$, $f_{c\leftarrow vI} = f_{c\leftarrow vII} = 7.6$. These values give 0.047 for the coefficient of $h(\nu - \nu_t) \div (e^2/a_H)$. Edwards found values of 0.032 and 0.030 in two separate experiments on two separate specimens. The threshold energy $h\nu_t$ was found to be 0.801 and 0.804 ev in the two specimens. Zwerdling and Lax[3] found a value of 0.803 ± 0.001 ev from measurements of the oscillatory magnetoabsorption effect. The agreement is, in part, fortuitous, for the specimen thicknesses are not well known. Nevertheless, the agreement in order of magnitude of the observed and computed coefficients indicates rather strongly that the basic interpretation is correct.

Work is continuing on the interpretation of the absorption coefficient for photon energies less than the threshold energy $h\nu_t$, and these studies will be extended to neutron-bombarded specimens.

ACTIVATION ENERGIES AND TOTAL ENERGIES OF LOCALIZED STATES IN SEMICONDUCTORS

H. C. Schweinler

Experiments performed in this laboratory have demonstrated a strong dependence of the lifetime of injected holes in n-type germanium[1] on neutron or gamma-ray irradiation.

Before the process of recombination of holes and electrons can be set forth in more detail, some properties of localized states of a crystal must be described, in a way which is rather general. In the following, the localized state may be vacancies or interstitial atoms; the example of substitutional impurities is taken only because there is a considerable quantity of experimental data available for these cases. From quantum statistical mechanics,[2] the probability of finding a localized system of the crystal in any of the g_m^i degenerate states $\psi_m^{i\kappa}$, of energy E_m^i, is

$$P_m^i = \frac{g_m^i \exp\left[-(E_m^i - m\zeta)/kT\right]}{Z(T,\zeta)} .$$

Here $\zeta(T)$ is the Fermi energy; $Z(T,\zeta)$ is the partition function

$$Z(T,\zeta) = \sum_{m,i} g_m^i \exp\left(-\frac{E_m^i - m\zeta}{kT}\right) ;$$

and T is the absolute temperature. In $\psi_m^{i\kappa}$, m denotes the number of electrons, i denotes the different energies E_m^i, and κ denotes which of the g_m^i degenerate states $\psi_m^{i\kappa}$ is involved.

The partition function Z can be written in the form

$$Z(T,\zeta) = \sum_m g_m(T) \exp\left(-\frac{E_m^0 - m\zeta}{kT}\right) ,$$

$$g_m(T) = \sum_i g_m^i \exp\left(-\frac{E_m^i - E_m^0}{kT}\right) .$$

Here E_m^0 is the total energy of a ground state of the m-electron configuration, and $g_m(T)$ is a sort of "effective degeneracy" of a single m-electron system of energy E_m^0. As the notation suggests, $g_m(T)$ is a function of temperature and of the relative spacing and degeneracies of the energy levels of the various m-electron states.

In the above equations the energies E_m^i or E_m^0 referred to the total energy of the localized m-electron atom or ion. These energies are almost always unknown in crystal problems. However, the difference between two such energies, say for an m-electron and an $(m-1)$-electron ion, is sometimes obtainable, at least approximately. Furthermore, this energy difference is actually the quantity needed for much semiconductor work, and is closely related to the "activation energy" which is commonly measured in many experiments. It is therefore necessary to consider this difference – the electron ionization or attachment energy – more closely.

The m-electron ion will be described, in the formulas which follow, in terms of its ground-state energy E_m^0, with all details of its excited states assimilated in the degeneracy factor $g_m(T)$. When an electron is removed from an m-electron ion, which is then left as an $(m-1)$-electron ion, there will be two important reference energies for the removed electrons: the lowest energy of the conduction band (E_c), and the highest energy of the valence band (E_v). The former will usually be taken as the reference energy when the Fermi level is high, and the latter when the Fermi energy is low. Formulas will be presented for both cases. When the defect is a substitutional atom of nuclear charge close to that of the host crystal, m will be the number of valence electrons outside the core (e.g., $m = 4$ for As^+ or Ga^- in Ge, and $m = 2$ for Zn^0 in Ge).

[1] O. L. Curtis, Jr., J. W. Cleland, J. H. Crawford, Jr., and J. C. Pigg (to be published).

[2] H. M. James, *Semiconductor Research Third Quar. Prog. Rep. Jan. 1 to March 31, 1952*, Purdue University Physics Dept., p 8.

When the Fermi level is high, as for an excess of donor atoms, the equation for the partition function has the form

$$Z(T,\zeta) = \exp\left(-\frac{E_4^0 - 4\zeta}{kT}\right)\left\{g_4(T) + xg_5(T)\exp\left(-\frac{E_5^0 - E_4^0 - E_c}{kT}\right) + \right.$$

$$\left. + x^2 g_6(T)\exp\left(-\frac{E_6^0 - E_5^0 - E_c}{kT}\right)\exp\left(-\frac{E_5^0 - E_4^0 - E_c}{kT}\right) + \cdots\right\},$$

with $x = \exp[-(E_c - \zeta)/kT]$. Here the largest neglected term in the braces is

$$g_3(T)\exp\left(-\frac{E_3^0 + E_v - E_4^0}{kT}\right)\exp\left(\frac{E_v - \zeta}{kT}\right),$$

and this is very small, because $(\zeta - E_v)/kT$ is a large number when the Fermi level is high (near E_c), while the other two factors are close to unity. For the familar case of the ionized-donor–neutral-donor equilibrium, as for As in Ge, the equilibrium distribution is

$$\frac{[\text{zero electrons}]}{[\text{one electron}]} = \frac{g_4(T)}{g_5(T)}\exp\frac{E_c - I - \zeta}{kT},$$

where I is the ionization energy of a neutral donor, $I = E_4^0 + E_c - E_5^0$. This can be thrown into a form like that of the Fermi-Dirac distribution in the usual way. The equilibrium between neutral and negatively charged donors can be expressed similarly, and can be expected to be important when the Fermi level is high. (This term has commonly been neglected, but there is no real justification for its neglect. For donors like As, $g_6(T)$ is probably considerably greater than $g_5(T)$, since the spacing of energy levels is smaller in As^- than in As^0; and the electron attachment energy $E_6^0 - E_5^0 - E_c$ is probably very small but positive. For $x \simeq 1$, the number of As^- ions is therefore comparable with the number of As^0 atoms.)

When the Fermi level is low, as for an excess of acceptor atoms, the equation for the partition function has the form

$$Z(T,\zeta) = \exp\left(-\frac{E_4^0 - 4\zeta}{kT}\right)\left\{g_4(T) + yg_3(T)\exp\left(-\frac{E_3^0 + E_v - E_4^0}{kT}\right) + \right.$$

$$\left. + y^2 g_2(T)\exp\left(-\frac{E_2^0 + E_v - E_3^0}{kT}\right)\exp\left(-\frac{E_3^0 + E_v - E_4^0}{kT}\right) + \cdots\right\},$$

with $y = \exp[(E_v - \zeta)/kT]$. Here the largest neglected term in the braces is

$$g_5(T)\exp\left(-\frac{E_5^0 - E_4^0 - E_c}{kT}\right)\exp\left(-\frac{E_c - \zeta}{kT}\right),$$

and this is very small, because $(E_c - \zeta)/kT$ is a large number when the Fermi level is low (near E_v), while the other two factors are close to unity. For the case of an ionized-acceptor–neutral-acceptor equilibrium, as for Ga in Ge, the equilibrium distribution is

$$\frac{[\text{zero holes}]}{[\text{one hole}]} = \frac{g_4(T)}{g_3(T)}\exp\frac{\zeta - E_v - A}{kT},$$

where A is the "attachment energy of a hole" to an acceptor atom with filled valence-band structure, $A = E_4^0 - E_3^0 - E_v$.

In a similar fashion it is found that

$$\frac{[\text{one hole}]}{[\text{two hole}]} = \frac{g_3(T)}{g_2(T)} \exp \frac{\zeta - E_v - A'}{kT},$$

where $A' = E_3^0 - E_2^0 - E_v$. These ratios can be thrown into a form resembling the Fermi-Dirac distribution function. For example, for the one-hole–two-hole equilibrium,

$$\frac{\Pr(\text{two holes})}{\Pr(\text{two holes}) + \Pr(\text{one hole})} = \frac{1}{1 + \gamma \exp[(\zeta - \epsilon)/kT]},$$

where "Pr( )" denotes "the probability of ( )", $\gamma = g_3(T)/g_2(T)$, and $\epsilon = E_v + A'$.

It is, fortunately, possible to illustrate many of these equations for the case of substitutional impurities in germanium. The excellently conceived experiments of Tyler and Woodbury have contributed most to an understanding of this problem. The activation energies are given in Table 1 and are illustrated graphically in Fig. 10.

In constructing Fig. 10, the energy gap $E_c - E_v$ was taken[3] to be 0.66 ev, and the energy differences were taken to be the experimental activation energies. This latter assumption is not strictly accurate, for the "effective statistical weight" factors $g_m(T)$ are not constant, having, in fact, a fairly strong temperature dependence in the case of a negative ion, for which the energy levels are

[3]See references in H. Brooks, *Advances in Electronics and Electron Phys.* 7, 110 (1955).

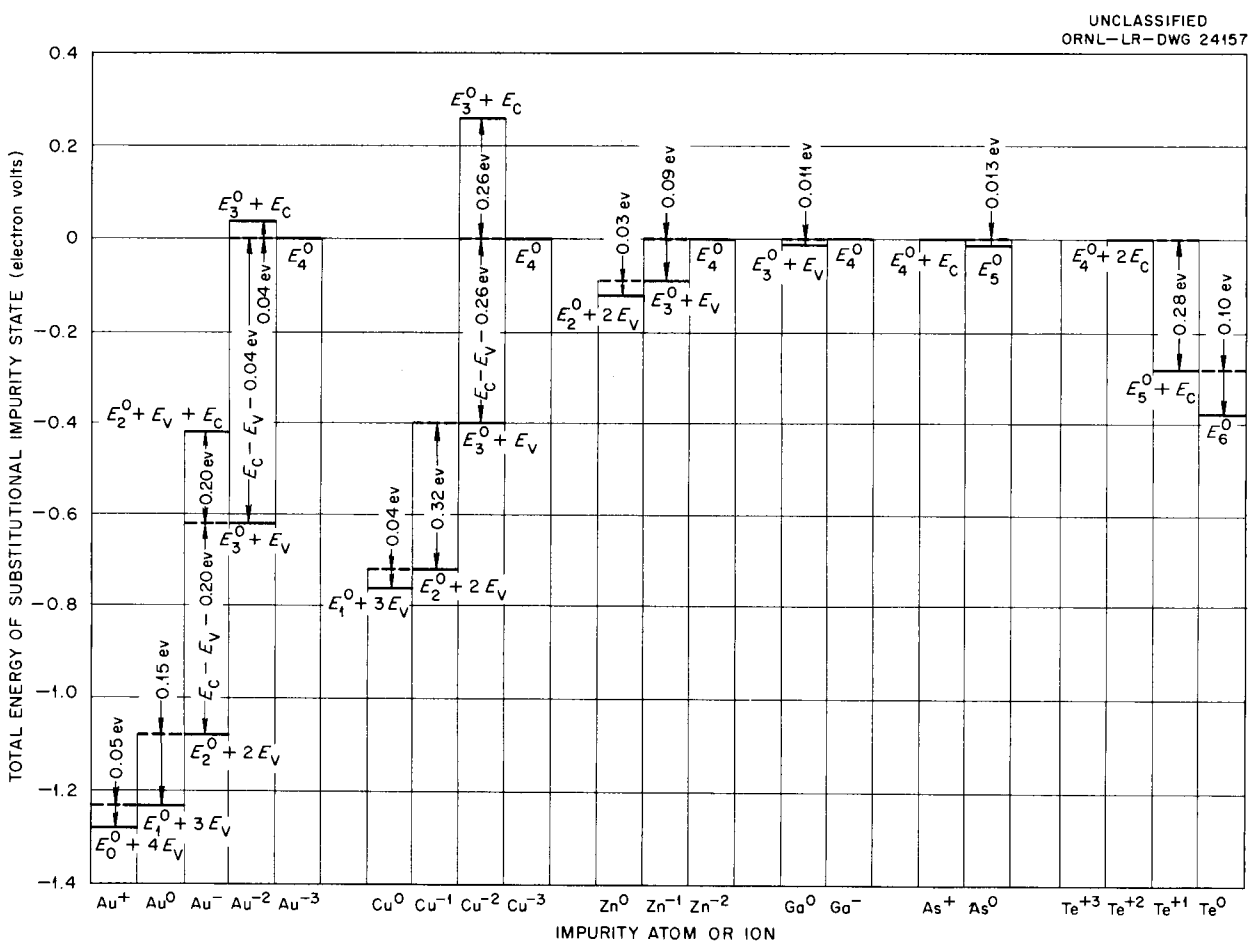

Fig. 10. Total Energies of Substitutional Impurities in Germanium.

closely spaced. This lack of constancy of $g_m(T)$, or, rather, of the ratio $g_m(T)/g_{m-1}(T)$, leads to an apparent activation energy which is not the true energy difference

$$E_m^0 - E_{m-1}^0 - E_v$$

or

$$E_{m-1}^0 + E_c - E_m^0 ,$$

but which differs from it by an amount of the order of kT. This difference cannot be estimated very accurately at the present time.

Table 1. Activation Energies of Substitutional Impurities in Germanium

Impurity	Equation	Reference
Te[a]	$E_5^0 + E_c - E_6^0 = 0.10$ ev	b
	$E_4^0 + E_c - E_5^0 = 0.28$ ev	b
As	$E_4^0 + E_c - E_5^0 = 0.0127$ ev	c
Ga	$E_4^0 - E_3^0 - E_v = 0.0108$ ev	c
Zn	$E_3^0 - E_2^0 - E_v = 0.030$ ev	d
	$E_4^0 - E_3^0 - E_v = 0.090$ ev	d
Cu	$E_2^0 - E_1^0 - E_v = 0.04$ ev	e
	$E_3^0 - E_2^0 - E_v = 0.32$ ev	e
	$\begin{cases} E_4^0 - E_3^0 - E_v = (E_c - E_v) - 0.26 \text{ ev} \\ E_3^0 + E_c - E_4^0 = 0.26 \text{ ev} \end{cases}$	e
Au	$E_1^0 - E_0^0 - E_v = 0.05$ ev	e
	$E_2^0 - E_1^0 - E_v = 0.15$ ev	e
	$\begin{cases} E_3^0 - E_2^0 - E_v = (E_c - E_v) - 0.20 \text{ ev} \\ E_2^0 + E_c - E_3^0 = 0.20 \text{ ev} \end{cases}$	e
	$\begin{cases} E_4^0 - E_3^0 - E_v = (E_c - E_v) - 0.04 \text{ ev} \\ E_3^0 + E_c - E_4^0 = 0.04 \text{ ev} \end{cases}$	e

[a]Te is isoelectronic with Se.

[b]J. A. Armstrong, W. W. Tyler, and H. H. Woodbury, *Bull. Am. Phys. Soc.* Series II **2**, 265 (1957).

[c]See references given by H. Brooks, *Advances in Electronics and Electron Phys.* **7**, 110 (1955).

[d]W. W. Tyler and H. H. Woodbury, *Phys. Rev.* **102**, 647 (1956).

[e]H. H. Woodbury and W. W. Tyler, *Phys. Rev.* **105**, 84 (1957).

MAGNETIC PROPERTIES OF ARSENIC-DOPED SILICON

E. Sonder D. K. Stevens
L. C. Templeton

Temperature Dependence of Magnetic Susceptibility

Measurements of the magnetic susceptibility reported last year for silicon were extended to liquid-helium temperatures and to a number of additional n-type samples in the 10^{17} cm^{-3} range of impurity. The data are reproduced in Fig. 11. It should be pointed out that the dashed line shown for the "pure" specimen (No. 26-76-6; $n_p = 4 \times 10^{14}$) is an extrapolation of measurements made above 60°K. The extrapolation is based on theoretical grounds and on the expected similarity between pure silicon and germanium, the latter having been measured by Bowers[1] and by Van Itterbeek and Duchateau.[2] In both cases χ was practically independent of temperature below 60°K.

[1]R. Bowers, Westinghouse Research Laboratories Scientific Paper 8-1038-P25.

[2]A. Van Itterbeek and W. Duchateau, *Physica* 22, 649 (1956).

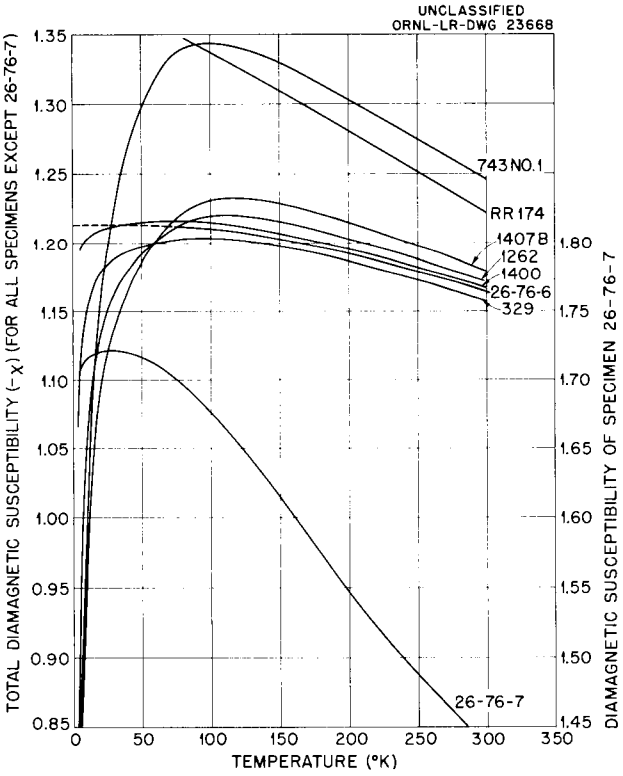

Fig. 11. Magnetic Susceptibility of Arsenic-Doped Silicon as a Function of Temperature.

The values for all the specimens shown have been corrected for the small contribution to the susceptibility made by the molybdenum suspension wire, which was calculated from the latest reported[3] value of the room-temperature susceptibility of molybdenum and from the authors' measurements of its variation with T. In the case of the smallest sample, RR176, the correction was 1.2%; in the case of the largest samples it was as little as 0.1%.

Hall Effect and Carrier Concentration of Silicon Samples

The Hall coefficient has been measured as a function of temperature for a number of samples originating from the same ingots as the samples discussed above. For sample 329, where a composition gradient was expected, a Hall plate was cut from portions adjacent to the susceptibility specimen on both the high- and low-concentration side.

Figure 12 shows the Hall data obtained to date, and Table 2 lists the samples and their donor concentrations as obtained from measurements of the Hall coefficient R by the following formulas:[4,5]

[3]C. J. Kriessman, *Revs. Modern Phys.* 25, 122 (1953).

[4]B. Abeles and S. Maiboom, *Phys. Rev.* 95, 31 (1954).

[5]C. Herring, *Bell System Tech. J.* 34, 237 (1955).

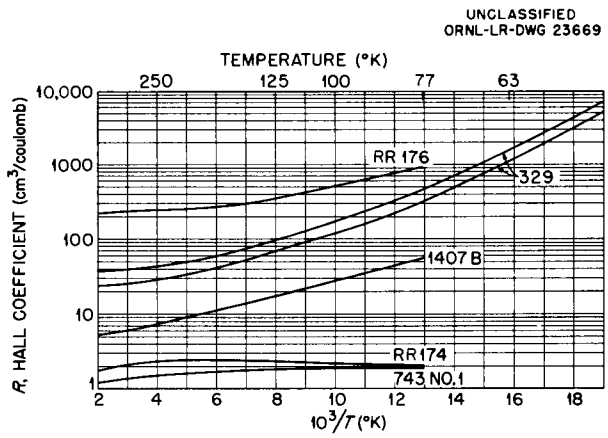

Fig. 12. Hall Effect of Arsenic-Doped Silicon as a Function of Reciprocal Temperature.

$$(1a) \qquad n = \frac{1.02}{Rec} = \frac{6.26 \times 10^{18}}{R},$$

when scattering is due mainly to thermal vibrations and all donors are ionized, as is the case just above room temperature; and

$$(1b) \qquad n = \frac{1.67}{Rec} = \frac{10.26 \times 10^{18}}{R},$$

when scattering is due mainly to charged impurity ions and most donors are ionized, as is the case for highly impure samples near 100°K. It may be pointed out that these measurements have verified the suspected lack of reliability of the values for n reported by those who supplied[6] the silicon.

Banding of Donor Levels

A complete analysis of the magnetic properties of donors in silicon must await completion of measurements of the Hall effect. However, from the data available thus far, a fairly accurate qualitative picture can be obtained.

[6]The samples measured were donated by the Bell Telephone Laboratories, the General Electric Research Laboratories, and Texas Instruments, Inc.

Two kinds of evidence for impurity banding may be found in the present data. One comes from the temperature dependence of the low-temperature susceptibility, the other from a comparison of the number of excess donors obtained from Hall and from susceptibility measurements. Both would be difficult to explain if resort were not made to interactions between the donor electrons, that is, banding. If noninteracting hydrogen-like donor centers are assumed, then it follows that the magnetic susceptibility χ_I obeys a Curie law of the form

$$(2) \qquad \chi_I = \frac{n\beta^2}{\rho kT},$$

where

n = the concentration of electrons at donor sites,
β = the Bohr magneton,
ρ = the specimen density,
k = the Boltzmann constant,
T = the absolute temperature.

Below about 30°K none of the donors are ionized, and n is equal to N, the number of excess donors. Also, since there are no electrons in the conduction band, the only other contribution to the total susceptibility is the lattice susceptibility.

Table 2. Donor Concentration of Magnetic Susceptibility Samples

Source	Sample No.	Resistivity (ohm-cm)	Room-Temperature Net Donor Concentration (Donors per cm^3)		
			As Reported by Supplier	From Hall Measurements	From Slope of Low-Temperature Susceptibility
Bell	26-76-7	0.003*	10^{19}		
Bell	743	0.0084	3×10^{18}	6.0×10^{18}	7.3×10^{17}
GE	RR174	0.013	2×10^{18}	3.8×10^{18}	
Bell	1407B	0.017	3×10^{18}	1.2×10^{18}	9.5×10^{17}
Bell	1262	0.04*	6×10^{17}		6.1×10^{17}
Texas Instruments	329	0.046		2.7×10^{17}	2.0×10^{17}
		0.059		1.6×10^{17}	
Bell	1400	0.13*	1×10^{17}		4.5×10^{16}
GE	RR176	0.26	7×10^{17}	2.8×10^{16}	

*Reported by supplier.

As a result the difference between the total susceptibility and the lattice susceptibility follows a straight line when plotted vs $1/T$. From the slope, since the various constants in Eq. 2 are known, the number of donor atoms can be found.

Figure 13 shows the difference between the the susceptibility of a pure silicon specimen (26-76-6) and that of n-type samples of various doping levels, plotted vs $1/T$. At low temperatures

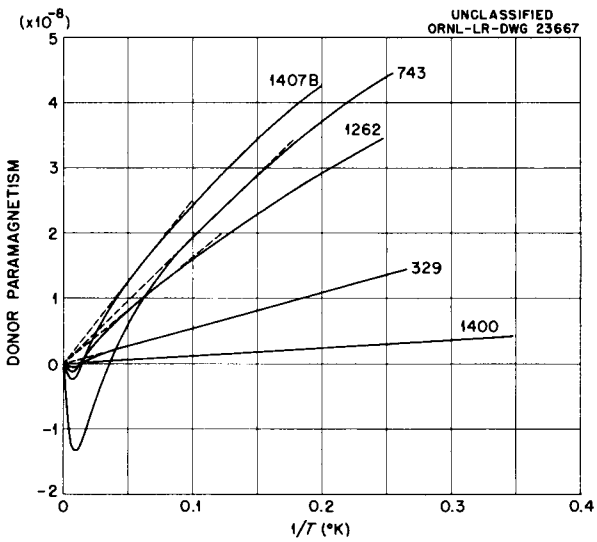

Fig. 13. Donor Electron Paramagnetism as a Function of Reciprocal Temperature.

the electrons are trapped by the donor atoms, and this difference is the donor contribution. At high temperatures, when the electrons enter the conduction band, "free" electron diamagnetism appears as well. It is immediately evident that the points for samples 1400 and 329, which were doped with less than 2×10^{17} arsenic atoms per cubic centimeter, form straight lines below about 40°K. The straight lines go through the origin, as would be expected from Eq. 2. Moreover, when the number of donors as obtained from the slope is compared with the Hall effect value (see Table 2) for sample 329, reasonably good agreement is obtained. However, the more heavily doped samples show definite deviations from a straight line below 15°K. Besides, the donor density obtained from the maximum slopes is less than that obtained from the Hall measurements, the discrepancy for the very heavily doped specimen 743 being much greater than for the less heavily doped sample 1407B.

It can be concluded from this analysis that there is little interaction when the donor density is below 2×10^{17} cm^{-3} but that it becomes appreciable in the 10^{18} cm^{-3} range. Furthermore, as is shown by measurements on specimen 26-76-7 (see Fig. 11), when the donor density is 10^{19} cm^{-3}, the impurity band has probably become so broad as to eliminate the energy gap between the impurity levels and the conduction band, causing the susceptibility to remain negative throughout the temperature range 4 to 300°K.

The 2×10^{17} cm^{-3} limit for impurity banding reported here should be considered as an upper limit. The agreement between the number of donors obtained from Hall and susceptibility data is at best approximate, and is based upon a value of 1.02 for the factor $\gamma = \mu_H/\mu_c$ which appears in the Hall expression $R = \gamma/nec$. This value is based upon Herring's[5] calculations for thermal scattering by use of a many-valley model. An admixture of impurity scattering would increase γ appreciably. Moreover, there is evidence from spin resonance measurements[7] on samples containing about 10^{17} phosphorus donors per cubic centimeter that some interaction may exist at these impurity densities.

Conduction Electron Properties

Electrons free to move in the conduction band contribute a Landau diamagnetism[8] as well as their spin paramagnetism, giving for their susceptibility

$$\chi_c = \frac{\beta^2}{3\rho kt} n(3 - f^2) \ . \tag{3}$$

The quantity f is called the "freedom number." The value of f^2 depends upon the details of the conduction band structure, and for silicon should be of the order of 13. It is possible to calculate f^2 from the total electron susceptibility, if the assumption is made that the spin magnetism of all electrons is present irrespective of whether the electrons are trapped at the donor sites or not, and if N and $n(T)$, the number of excess donors and the number of electrons in the conduction band, respectively, are obtained from

[7] G. Feher, R. C. Fletcher, and E. A. Gere, *Phys. Rev.* 100, 1784 (1955).

[8] L. Landau, *Z. Physik* 64, 629 (1930).

Hall measurements. The equation used has the form

$$(4)\quad \chi_c + \chi_I = \frac{\beta^2}{3\rho kT}(3N - nf^2)$$

$$= \chi(\text{measured}) - \chi(\text{pure Si}) .$$

The results of such a calculation for three of the silicon samples are given in Table 3. The use in Eq. 4 of the difference between two separate measurements, $\chi - \chi$(pure Si), introduces the relatively large (½%) error inherent in the determination of the absolute value of the susceptibility. For specimen 1407B this makes the analysis good to about 25%. For the purer specimen 329 it may introduce an uncertainty close to 100% in $\chi - \chi$(pure Si); however, this error, irrespective of its magnitude, is the same at all temperatures, so that it can be compensated for by the addition of a factor δ to the difference in the χ's. When the analysis was carried through for various temperature-independent values of δ, no reasonable results essentially different from those shown in Table 3 were obtained. It should also be kept in mind that N and n are obtained from the Hall effect, where the analysis depends upon the poorly understood scattering processes, and may therefore be in error by as much as 50%.

Table 3. Values* of the Square of the "Freedom Number" f

Specimen	Absolute Temperature (°K)	Carrier Diamagnetism (emu)	Carrier Density (cm^{-3})	f^2
		$\times 10^{-10}$	$\times 10^{17}$	
329	295	3.0	2.0	8.0
	247	3.1	1.7	8.8
	166	4.5	1.24	11
	119	4.4	0.70	17
	81	1.1	0.20	36
	62	−2.7	0.06	74
		$\times 10^{-9}$	$\times 10^{18}$	
1407B	289	1.61	1.10	9.5
	245	1.82	0.83	10
	204	2.36	0.70	13
	155	2.54	0.61	13
	118	2.52	0.57	12
	105	2.11	0.25	24
	77	0.74	0.114	37
		$\times 10^{-8}$	$\times 10^{18}$	
743	296	0.83	6.0	7.6
	232	1.02	6.0	7.4
	197	1.13	5.9	7.3
	155	1.25	5.8	6.8
	118	1.33	5.7	6.3
	95	1.31	5.6	5.7
	87	1.31	5.6	5.5
	78	1.23	5.5	5.2

*Calculated from the formula: $f^2 = \frac{1}{n}\left[\frac{3\rho kT}{\beta^2}(-\Delta\chi) + 3N\right]$.

However, if consideration is given to the possibility that a transition from pure thermal scattering to impurity scattering may occur in the range of the measurements, as has been done, the conclusions drawn from Table 3 are not changed.

The results in Table 3 are unexpected in two ways. First, it is evident that, for all three samples, f^2 at room temperature is nearer 8 than the value 13 expected from cyclotron resonance[9] determinations of the effective masses in high-purity silicon. Second, for the two purer samples, 1407B and 329, f^2 seems to increase fairly rapidly as the temperature decreases, mainly because the change with temperature of the Hall coefficient is much faster than that of the susceptibility difference. For specimen 743, where the Hall effect shows no decrease of the carrier concentration down to 77°K, the large variation of f^2 is absent.

Evidently, as the carriers freeze out of the conduction band they do not change their contribution from the full diamagnetism attributed to them in Eq. 3 to the paramagnetism attributed to them in Eq. 2. Possibly there exists, even at a doping level of 10^{17} cm^{-3}, enough impurity banding to prevent the trapped electrons from contributing all their spin paramagnetism. In fact, the electrons in the impurity band may well contribute a diamagnetism analogous to that of electrons in a conduction band.

A real variation with temperature of f^2 cannot, of course, be ruled out, especially since the work was done with fairly heavily doped material, for which the bottom of the conduction band may actually be extended by an impurity band of hydrogen-like donor states with principal quantum number greater than 1. Unfortunately, due to the large uncertainties discussed above, the kind of stringent analysis inherent in calculating f^2 must not be carried too far. Nevertheless, it is safe to say that the simple ideas of independent, noninteracting trapped donors at low temperatures and of quasi-free electrons with temperature-independent effective masses equal to those obtained by cyclotron measurement at high temperatures do not apply without modification to the materials that have been measured.

[9] R. N. Dexter, B. Lax, A. F. Kip, and G. Dresselhaus, *Phys. Rev.* 96, 22 (1954).

Density of Silicon

The density of the silicon specimens, ρ, enters into the formula used to determine the room-temperature value of the susceptibility,

$$\chi = \frac{k(O_2)}{\rho(Si)} F(I) ,$$

where $k(O_2)$ is the volume susceptibility of the oxygen ambient, and $F(I)$ is a function of the balance currents.[10] Since the specimens came from different sources[6] and had different histories and since the variation in room-temperature values of χ for various "pure" samples seemed to differ by more than the expected ½% (this was observed prior to the use of a correction for the molybdenum wire suspensions), it was felt that a search for differences in density of the various samples would be useful. Table 4 is a summary of the results obtained at 21.8°C by an immersion technique using CCl_4. It is evident that any variations are barely detectable and are surely insignificant as far as errors in the room-temperature value of χ are concerned.

[10] D. K. Stevens, *Magnetic Susceptibility of Annealed and Fast-Neutron Bombarded Germanium*, ORNL-1599 (Feb. 17, 1954).

Table 4. Density of Silicon Specimens

Source	Specimen	Donor Density (cm^{-3})	Density (g/cm^3)
GE	RR176	3×10^{16}	2.326
GE	RR176F		2.3246
Bell	1400	3×10^{16}	2.3276
GE	RR174	4×10^{18}	2.3248
GE	RR174A		2.3249
Bell	743	5×10^{18}	2.3272
Bell	26-76-7	3×10^{19}	2.330

MAGNETIC SUSCEPTIBILITY OF MOLYBDENUM

E. Sonder L. C. Templeton

Since the molybdenum suspension wire can contribute as much as 1.2% to the measured susceptibility of some of the silicon samples and since a precision of 0.1% is possible in the temperature dependence of χ, it was felt advisable to measure the temperature dependence of the susceptibility of the molybdenum wire. The results, normalized to the presently accepted room-temperature value, are shown in Fig. 14. Also shown are De Haas and Van Alphen's[1] results, obtained in 1933. An increase in the paramagnetism at low temperature, observed by the Dutch researchers, also appears in the present results, but to a much smaller extent. Perhaps this temperature-dependent term is due to impurities, in which case the discrepancy is not too surprising in view of the greater purity of the materials now available.

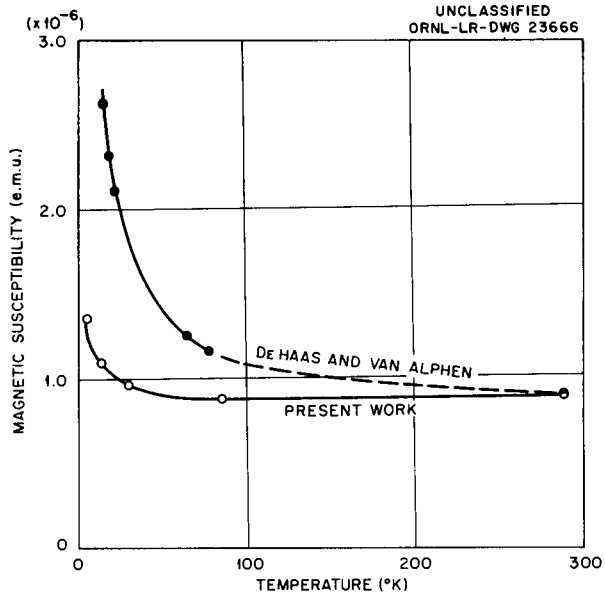

Fig. 14. Magnetic Susceptibility of Molybdenum as a Function of Temperature.

[1]W. J. de Haas and P. M. van Alphen, *Koninkl. Ned. Akad. Wetenschap. Proc.* 36, 263 (1933).

INSTRUMENTATION FOR SUSCEPTIBILITY STUDIES

D. K. Stevens E. Sonder

Liquid-Helium Cryostat

Magnetic susceptibility measurements of some n-type silicon samples between liquid-nitrogen and room temperatures[1] have indicated that freezing-out of carriers may be observed below nitrogen temperatures. Such data may be very useful in constructing models for the imperfection (donor in this case) and in interpreting impurity banding phenomena. Consequently, a helium cryostat, which had been designed earlier, was put into operation (a diagram of the cryostat is shown in Fig. 15). In principle its operation is identical with that of the previous liquid-nitrogen cryostat in that a heater and a heat leak between the specimen thimble and the liquid reservoir permit operation above the liquid boiling temperature. Thus the temperature ranges 4.2 to 38°K and 78°K to room temperature can be covered with helium and nitrogen, respectively. Pumping permits the achievement of temperatures below the respective boiling points so that, with the exception of a small range between 38 and 51°K, the whole temperature range from 3 to 350°K can be covered with little difficulty.

Temperature measurement at present is accomplished with two copper-constantan thermocouples, calibrated in the cryostat with a standardized platinum resistance thermometer, and with four 2-mm germanium cube resistance thermometers. The latter were designed for temperatures below 20°K, where the thermocouples lose sensitivity. Unfortunately it was found that the resistance of the germanium cubes, when measured in a simple series circuit, was not very reproducible, making it necessary in practice to use the thermocouples down to 10°K and to calibrate the germanium elements during each run. This was done by condensing helium in the specimen thimble immediately after the susceptibility measurements in the helium range had been completed and comparing the resistances of the germanium thermometers with the temperature obtained from the vapor pressure of the condensed helium. This method gave temperatures accurate to about ½°K.

[1] D. K. Stevens, W. J. Sturm, and J. H. Crawford, Jr., *Solid State Semiann. Prog. Rep. Aug. 30, 1956*, ORNL-2188, p 7.

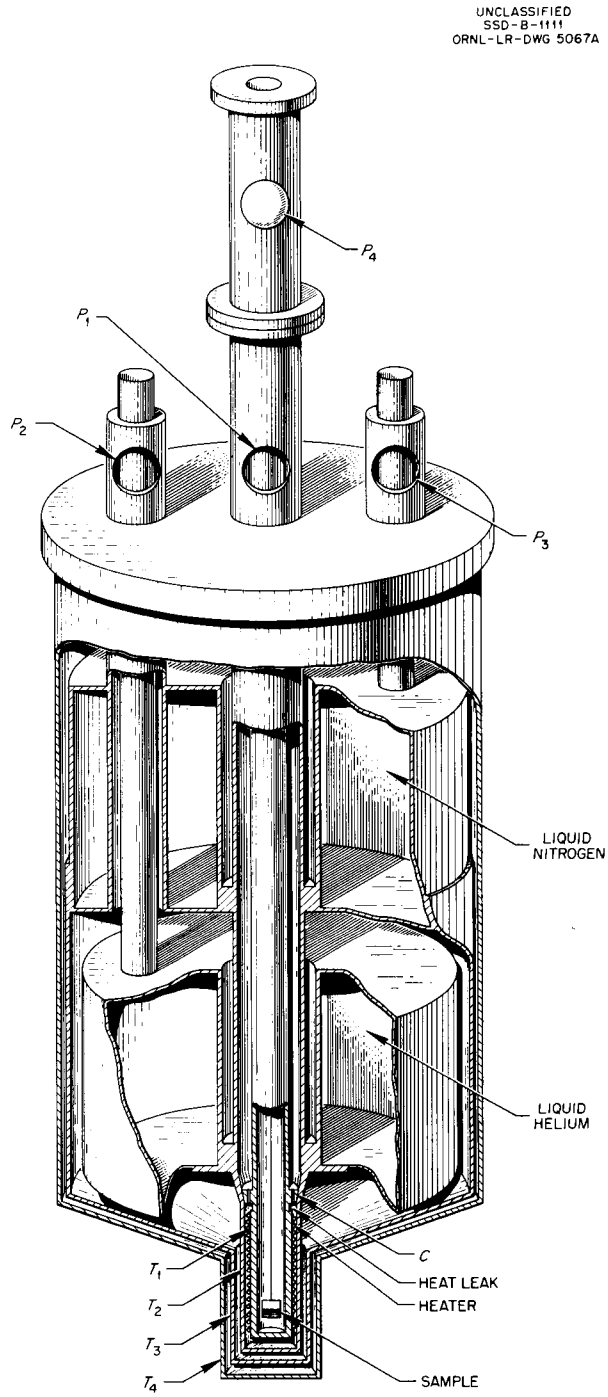

Fig. 15. Liquid-Helium Cryostat Used for Low-Temperature Susceptibility Measurements.

It is hoped that the precision of temperature measurements in the helium range can be improved by use of small germanium bridges and a four-wire system for measuring their resistance. Evidently reproducibilities to within 0.001°K can be obtained[2] by this means.

Magnet Isolation and New Installation

In the past, measurements have occasionally had to be discontinued in the middle of a run because of building vibrations. Since with liquid helium such interruptions can be very costly in time and since a move of the magnet to a larger laboratory was already planned, it was decided to build an isolation system for the magnet in its new location. The system consists of a 5-ton concrete slab, located on critically loaded rubber shear mounts in a pit in the new magnet room. The magnet is bolted to the top of the slab, and all connections to the magnet are through flexible couplings.

[2] J. E. Kunzler, T. H. Geballe, and G. W. Hull, *Rev. Sci. Instr.* 28, 96 (1957).

The auxiliary equipment, consisting of heat exchanger, coolant pump, and motor-generator set for the magnet, and a high-speed vacuum pump for pumping on the helium, is located in the sub-basement. Thus the magnet with its delicate equipment is isolated from the noise and vibration of the heavy machinery.

Magnet Control

In order to minimize heating of the cryostat by eddy currents resulting from the change in the magnetic field as the magnet is turned on and off, the controlled magnet-exitation power supply has been modified to permit the magnetic field to be turned on and off slowly. A potentiometer, driven by a 1-rpm motor, in the bias supply of the control tubes accomplishes this purpose. It is now planned to add three cams and micro-switches to the same shaft in order to simplify exitation of the magnet. Previously three switches had to be turned on manually in a given timed sequence. A single toggle switch should initiate automatic sequencing in the future.

MAGNETIC DEFECTS IN COVALENT AND IONIC CRYSTAL SYSTEMS

R. A. Weeks R. H. Silsbee

In the production of defects in solids by irradiation with energetic particles a variety of processes can be expected, the most obvious being the formation of atomic displacements and, in covalently bonded materials, such as the silicas, of broken bonds. There will, in general, be a variety of ionization states available to such defects, and some of them may be expected to have an odd number of electrons and hence be paramagnetic. It should be possible to use magnetic techniques to study some of the defects formed during irradiation. The power of the paramagnetic resonance technique is well illustrated by the work on F centers[1] and V centers[2] in the alkali halides.

Some progress has been made in identifying the magnetic defects in the quartz system produced by irradiation. Two of the magnetic defects have been tentatively related to two optical absorption bands. By consideration of the resonance, optical, and x-ray data some preliminary deductions with respect to the radiation damage behavior are made. These results are described later in this section.

One of the defects produced by neutron irradiation of magnesium oxide, as described in the last report,[3] has been positively identified (by Wertz and Auzins[4]) as an F center. An abstract of a paper on this work is given below. In this paper, the values of the observed hyperfine interaction are compared with those calculated from theoretical F-center wave functions. The anisotropic hyperfine interaction calculated with these wave functions was one-half the observed value. The reason for the disagreement is discussed in the paper.

Electron Spin Resonance of F Centers in Magnesium Oxide: Confirmation of the Spin of Magnesium-25.[4] J. E. Wertz, P. Auzins, R. A. Weeks, and R. H. Silsbee. – An electron spin resonance (ESR) spectrum induced in magnesium oxide by pile irradiation has been interpreted as arising from F centers. After an oxide ion is displaced from its normal position by neutrons, an electron donated by ever-present divalent impurities may become trapped at the vacancy. Those centers having only Mg^{24} and Mg^{26} neighbors give a single ESR line with $g = 2.0023$, while those with one or more Mg^{25} neighbors give hyperfine patterns corresponding to the nuclear spin value of 5/2. The magnitudes of the isotropic and anisotropic parts of the hyperfine interaction show strong localization of the electron in the vacancy.

A superheterodyne spectrometer has been put into operation, and its sensitivity, based on some preliminary measurements, is greater, by a factor of 100, than that of the previous system. On the basis of the measurements that have been made, it is estimated that a signal-to-noise ratio of 1 will be produced by 2×10^{13} spins in the narrow resonance group of the quartz system. The data reported below were taken with the old spectrometer at room temperature. The new spectrometer should permit a more extensive analysis of the resonance data on the quartz system.

Standard microwave techniques have been used in studies of electron spin resonance in quartz and fused silica. The results quoted here were made with a spectrometer with a sensitivity of 10^{15} hydrazyl spins at room temperature. All the following results were obtained from measurements at room temperature.

No resonances were observed in any of the samples examined before irradiation. The high saturation density of centers produced by heavy neutron irradiation and the absence of any correlation of the resonances with impurity content showed that impurities were not responsible for the principal lines observed.[5]

Figure 16 illustrates the resonance spectrum observed in neutron-irradiated fused silica. The narrow line has a g value of 2.0011 and a width

[1] A. F. Kip *et al.*, *Phys. Rev.* **91**, 1066 (1953); G. Feher, *Phys. Rev.* **105**, 1122 (1957).

[2] W. Känzig, *Phys. Rev.* **99**, 1890 (1955).

[3] R. A. Weeks and R. H. Silsbee, *Solid State Semiann. Prog. Rep. Aug. 30, 1956*, ORNL-2188, p 102.

[4] J. E. Wertz, P. Auzins, R. A. Weeks, and R. H. Silsbee, "Electron Spin Resonance of F Centers in Magnesium Oxide: Confirmation of the Spin of Magnesium-25," to be published in *Phys. Rev.*

[5] R. A. Weeks, *J. Appl. Phy.* **27**, 1376–1381 (1956).

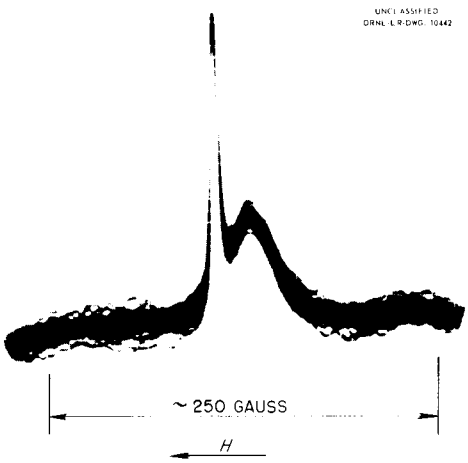

Fig. 16. Paramagnetic Resonance in Neutron-Irradiated Fused Silica.

of 2 gauss, while the broader line has a g value of 2.0090 and a 50-gauss line width.

Figures 17 and 18 compare the broad and narrow resonances produced by neutron bombardment in the fused material and in crystalline quartz. In both resonances there is a complex line structure in the crystalline samples which extends over a range in field corresponding to the line width of the corresponding line in the silica. In the case of the narrow resonance it has been shown (see Fig. 18) that an average over all crystal orientations of the crystal resonance gives a line shape identical with that in the fused material. The same averaging for the lines in the crystal that are associated with the broad resonance in the silica has not been performed experimentally. Observation of this group of lines for several different orientations of the crystalline axis (relative to the fixed magnetic field) suggests that they are a major contributor to the broad line in the silica. In Fig. 17 the Corning silica shows two additional resonances, on each side of and displaced 35 gauss from the center of the narrow resonance. These lines are not observed in the G-E synthetic crystal or in the natural crystals, but are found in Amersil. The origin of these two lines is unknown at present.

Gamma irradiation of crystalline quartz to doses of 5×10^8 r gives both resonances, although with small concentration. The narrow line (very small concentration) was observed in one sample of Amersil fused silica after Co^{60} gamma-ray exposure. Very little work has been done on

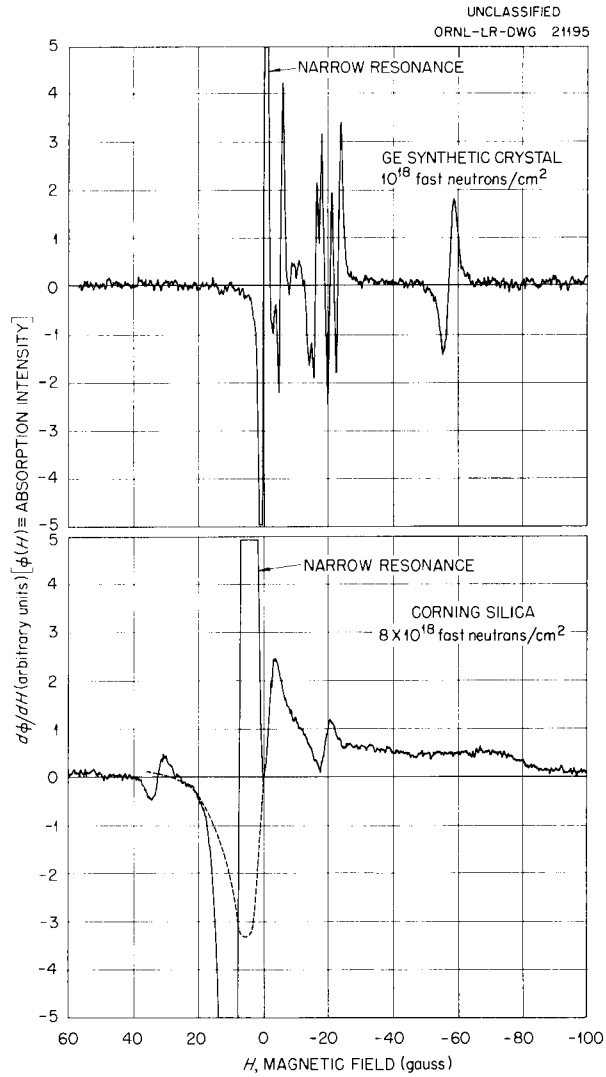

Fig. 17. Broad Resonance in Crystalline and in Fused Quartz.

gamma-irradiated samples, and these results will not be discussed.

The similarity of the results in the fused and crystalline silica suggests that the defects produced in both are essentially the same and that the local environment of these defects is similar. An analysis of the resonance structure for the crystal, then, should give useful information about the defects produced in both materials.

The variation with orientation of the line positions of the narrow resonance fits satisfactorily to a model of a defect with spin ½ and an anisotropic

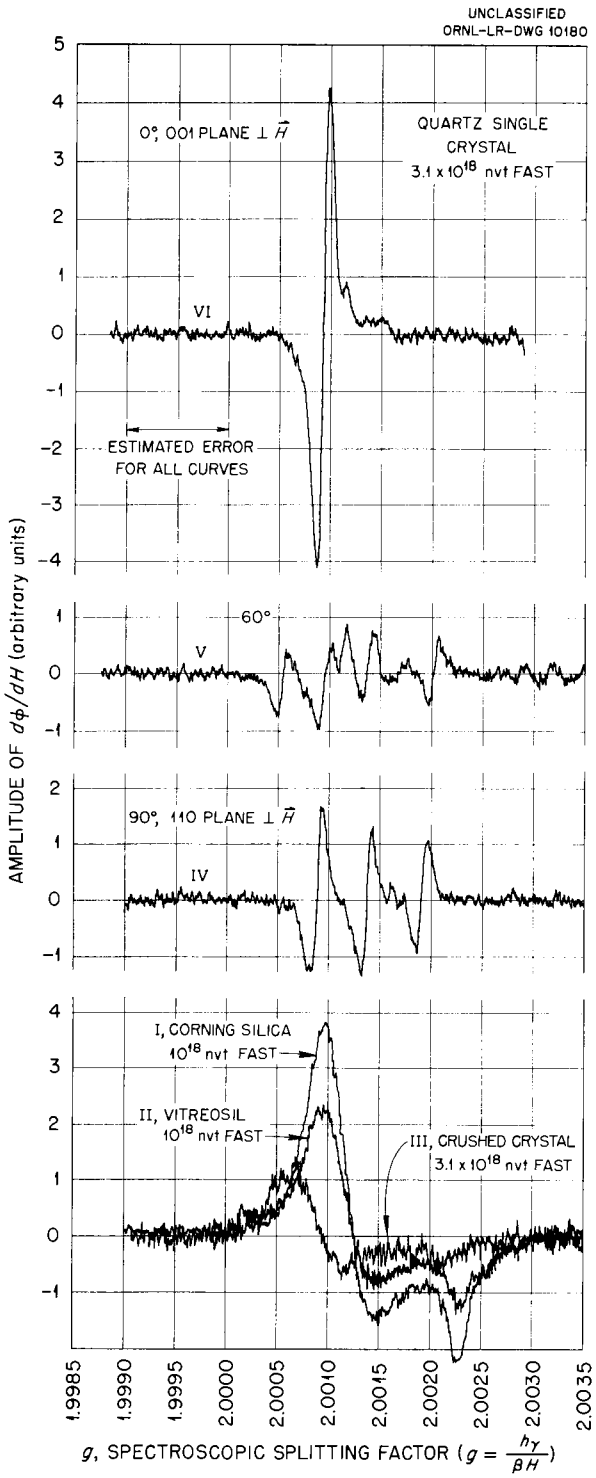

Fig. 18. Paramagnetic Resonance Absorption (Narrow Lines) in Irradiated Fused and Crystalline Quartz.

g tensor with nearly axial symmetry.[6] Unfortunately, this information is by no means sufficient for identification of the defect. The orientation of the g tensor does not fit in with the crystalline field symmetry at either a silicon or an oxygen vacancy. If the defect is a vacancy, there must be considerable relaxation of the neighbors of the vacancy. The possible positions of interstitials in the unit cell are sufficiently numerous that little can be said about the interstitial model on the basis of the present results.

A hyperfine interaction with the 4.7%-abundant Si^{29} nucleus (nuclear spin of $\frac{1}{2}$) has been observed in the narrow resonance, and with the new spectrometer an analysis of the orientation dependence of this structure is feasible. Such an analysis should give much more information about the defect, since it can give a reasonable measure of the values of the S and P parts of the defect wave function at the silicon nuclei.

No attempt has been made to analyze the data for the broad resonance, but again it is hoped that the new spectrometer will make such an analysis possible.

Although absolute intensity measurements are difficult to obtain in resonance experiments, relative intensity estimates are somewhat easier. The ratio of the relative number of centers in narrow and broad resonances in the same specimens is shown as a function of neutron dose in Fig. 19. At doses of 10^{18} and greater the center

[6] R. H. Silsbee and R. A. Weeks, *Solid State Semiann. Prog. Rep. Aug. 30, 1956*, ORNL-2188, p 105–106.

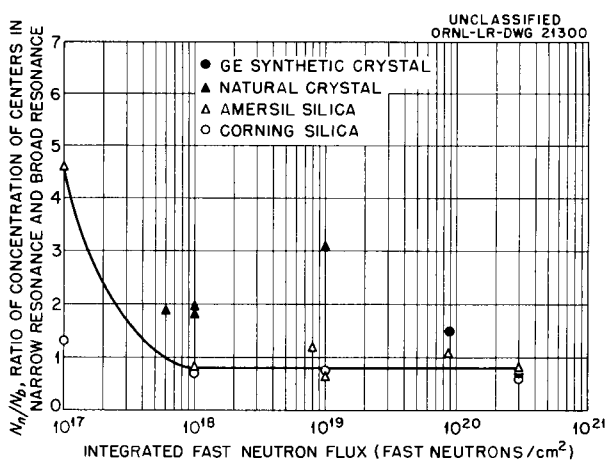

Fig. 19. Ratio of Intensities of the Narrow and Broad Resonances.

densities are roughly equal in the fused material. The large value of the ratio of the narrow to the broad resonance intensities for Amersil at 10^{17} neutrons/cm^2 may be related to the high initial colorability of that material in contrast to Corning silica. In the crystalline quartz the ratio drops from 2 at low doses to about 1 at high doses with an apparent peaking at about 10^{19} neutrons/cm^2. The accuracy of the ratio is considerably less in the crystals as a result of the complex line structure.

Finally, qualitative observations have been made on the line structure of the narrow resonance in the crystal and in silica as a function of dose. In the crystal at low neutron doses the lines comprising the narrow resonance group are quite narrow, of the order of 0.1 gauss at doses of less than 5×10^{18} fast neutrons/cm^2, the width probably being due to inhomogeneous broadening. At neutron doses greater than 5×10^{18} the lines begin to broaden, and at a dose of 7×10^{19} the structure has disappeared. There is also a change in the shape of the narrow resonance in the silica after 10^{19} fast neutrons/cm^2. For neutron doses greater than 10^{20} fast neutrons/cm^2 the line shape is the same in the crystal and the silica. This broadening is interpreted as a breakdown of the crystal structure as a result of which the the defect orientation becomes essentially random at high neutron doses. The broadening and alteration of the shape of the resonance curve, which occur in the fused silica as well, suggest some change in the immediate surroundings of the defect, perhaps a distortion of the normal bond distances.

A specimen of Corning silica which had been given a neutron dose of 8×10^{18} fast neutrons/cm^2 was successively annealed for 30 min at various temperatures up to 550°C. Measurements made after a 500°C anneal showed that the narrow resonance was still present. Before annealing, the ratio of the concentration of centers in the narrow resonance to the concentration in the broad resonance was 0.6, whereas after the anneal the ratio decreased to 0.04. No appreciable change in the concentration of centers in the broad resonance was observed. After the 550°C anneal, the narrow resonance could no longer be detected and the ratio was essentially zero. The concentration of centers in the broad resonance decreased by a factor of approximately 2.

At 550°C all optical absorption bands above 1850 Å, except a very weak one at 2350 Å, completely disappeared.[7] Mitchell and Paige[8] report that after an anneal at 520°C the *E* band (1650 Å) in fused quartz is still quite strong, whereas the bands at longer wavelengths have apparently disappeared. At longer wavelengths (1850 Å and up) similar results have been obtained on Corning silica.[6]

In comparing the annealing data on the optical absorption bands with those on the resonance centers, a highly probably conclusion is that both a major component of the broad resonance and the *E* band arise from the same center. The conclusion is restricted to a "major component" of the broad resonance because of an alteration of the shape of the broad resonance curve after the 550°C anneal. At the present time there is no evidence to show that the broad resonance is due to only one type of defect.

Although the results of this investigation are still preliminary, a few conclusions have become evident. Below doses of a few times 10^{19} fast neutrons/cm^2 the damage behavior is relatively simple. The similarity of the resonances in the fused and crystalline quartz shows that at least one and probably two of the defects produced are essentially the same in both materials. The line structure in the crystalline material and its variation with the direction of the magnetic field show that the orientation of the macroscopic crystal determines the defect orientation. This could not be the case for defects in vitreous regions or regions of high disorder. Hence these results show that, although vitreous regions may be present, a major portion of the damage is present as point defects in an environment of essentially perfect crystal.

In this low dose region the lattice expansion is small[9] and the defect density increases linearly as expected. At doses greater than a few times 10^{19} fast neutrons/cm^2, there is a rapid increase

---

[7] C. M. Nelson, private communication.

[8] E. W. J. Mitchell and E. G. S. Paige, *Phil. Mag.* 1, Series 8, 1085 (1956).

[9] M. C. Wittels and F. A. Sherrill (to be published).

in the lattice expansion (Fig. 20). At about this dose there is a rapid broadening of the x-ray reflections and of the lines observed in the paramagnetic resonance, all suggesting a rapid loss of the crystalline structure at these doses.

At these same doses there is a decrease in the density of paramagnetic centers, as revealed by magnetic susceptibility measurements, and at slightly higher doses there is a decrease in the intensity of the 2150-Å absorption band. It is in this region, too, that the ratio of the narrow to broad resonances goes to a maximum. These results suggest that, as the crystal structure begins to break down, the crystal cannot support a high density of unpaired spins and that the crystal deforms microscopically to allow the formation of new bonds from the unpaired electrons with the consequent loss of crystalline structure and magnetic center density.

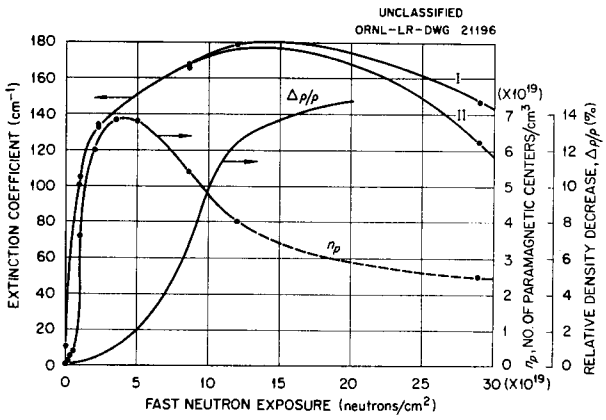

Fig. 20. Summary of the Optical Absorption (215 mμ), Static Magnetic Susceptibility, and Density Change of Crystalline Quartz as a Function of Fast-Neutron Irradiation.

SUPERHETERODYNE ELECTRON-SPIN-RESONANCE SPECTROMETER

R. A. Weeks

In nonconducting solids the concentration of magnetic defects produced by irradiation with energetic particles has a range of values dependent upon the integrated flux. In order to study the detailed structure of irradiation-produced magnetic defects by electron-spin-resonance techniques, it is often desirable that the total magnetic-defect concentration be $\lesssim 10^{18}$ centers per cubic centimeter. At this concentration, interaction of the defects with each other is avoided. Specimen size requirements then place an upper limit on the total number of defects of $\lesssim 10^{17}$. In some cases this upper limit may be 10^{16}. Since the total concentration of magnetic defects should not exceed 10^{18} cm^{-3}, the concentration of defects of one species may be considerably less than 10^{18}.

If these values are applied to a particular system, in this case single crystals of quartz, then one species produced is present in concentrations of $\sim 5 \times 10^{17}$ centers per cubic centimeter for a total concentration of magnetic defects of 10^{18} cm^{-3}. Specimen size requirements for a study of crystalline-field orientation effects reduce the number of spins of this type of defect to $\lesssim 10^{16}$. The hyperfine interaction of this defect with the Si^{29} isotope is of great importance in establishing its characteristics. Since the natural abundance of Si^{29} is 4.7%, the number of defects of this type interacting with Si^{29} can be no more than 5×10^{14}. In order to gather adequate experimental data on this hyperfine interaction, the sensitivity of the electron-spin-resonance spectrometer should be such that the signal-to-noise ratio for the hyperfine lines is 5. But since the concentration may be less than the maximum given above, an even greater sensitivity is desirable. As an approximation to the desired sensitivity, a signal-to-noise ratio of 1 for 5×10^{13} centers of the above type seems necessary.

These numbers are all related to a particular defect in quartz whose relaxation time is quite long compared with that of diphenylpicrylhydrazyl, for instance. Hence the power level at which measurements can be made, avoiding saturation effects, is of the order of microwatts. In this particular example, where such low power levels are required, it has been shown that the superheterodyne method of detection is approximately 100 times more sensitive than other methods.[1]

A block diagram of the 30-megacycle intermediate-frequency superheterodyne system[2] that has been built is given in Fig. 21. The specimen cavity is a reflection type placed on one arm of a "magic-tee" junction. A tuning stub is also placed in this arm for balancing the tee. The magic tee was fabricated from solid brass block and matched at a suitable frequency. A balanced mixer is used to eliminate noise from the local oscillator. The signal oscillator frequency is controlled by the specimen cavity through a Pound stabilizer,[3] the lock-in mixer being placed between the output of the klystron reflector supply and the klystron. The reference signal for the lock-in mixer is derived from a mixer crystal in a separate channel. The output of the mixer crystal is fed to an intermediate-frequency reference amplifier whose output is split, one channel giving the reference signal for the lock-in mixer and the other channel providing a signal to an automatic frequency control (AFC) circuit. The output of the AFC circuit is amplified by a d-c amplifier and is then applied to the reflector supply of the local oscillator, maintaining a 30-megacycle difference in frequency between the local oscillator and the signal oscillator. The other output channel of the reference amplifier furnishes a reference signal to the lock-in mixer controlling the signal klystron.

The operation of the system is quite reliable. One difficulty that has been found is that the microwave flange joints leak. The r.f. power is then reflected back into the system giving rise to power fluctuations at the detector. In an effort to eliminate this difficulty, microwave absorbent material has been obtained and all the joints have been wrapped.

By comparing a known weight of diphenylpicrylhydrazyl with an irradiated quartz crystal, the number of centers in the narrow-resonance group was estimated (see section on "Magnetic Defects in Covalent and Ionic Crystal Systems"). The quartz specimen was oriented with the *c* axis parallel to the magnetic field.

---

[1] G. Feher, *Bell Sys. Tech. J.* 36, 449, esp 474 (1957).

[2] J. M. Hirshon and G. K. Fraenkel, *Rev. Sci. Instr.* 26, 34 (1955).

[3] R. V. Pound, *Proc. I.R.E. (Inst. Radio Engrs.)* 35, 1405 (1947).

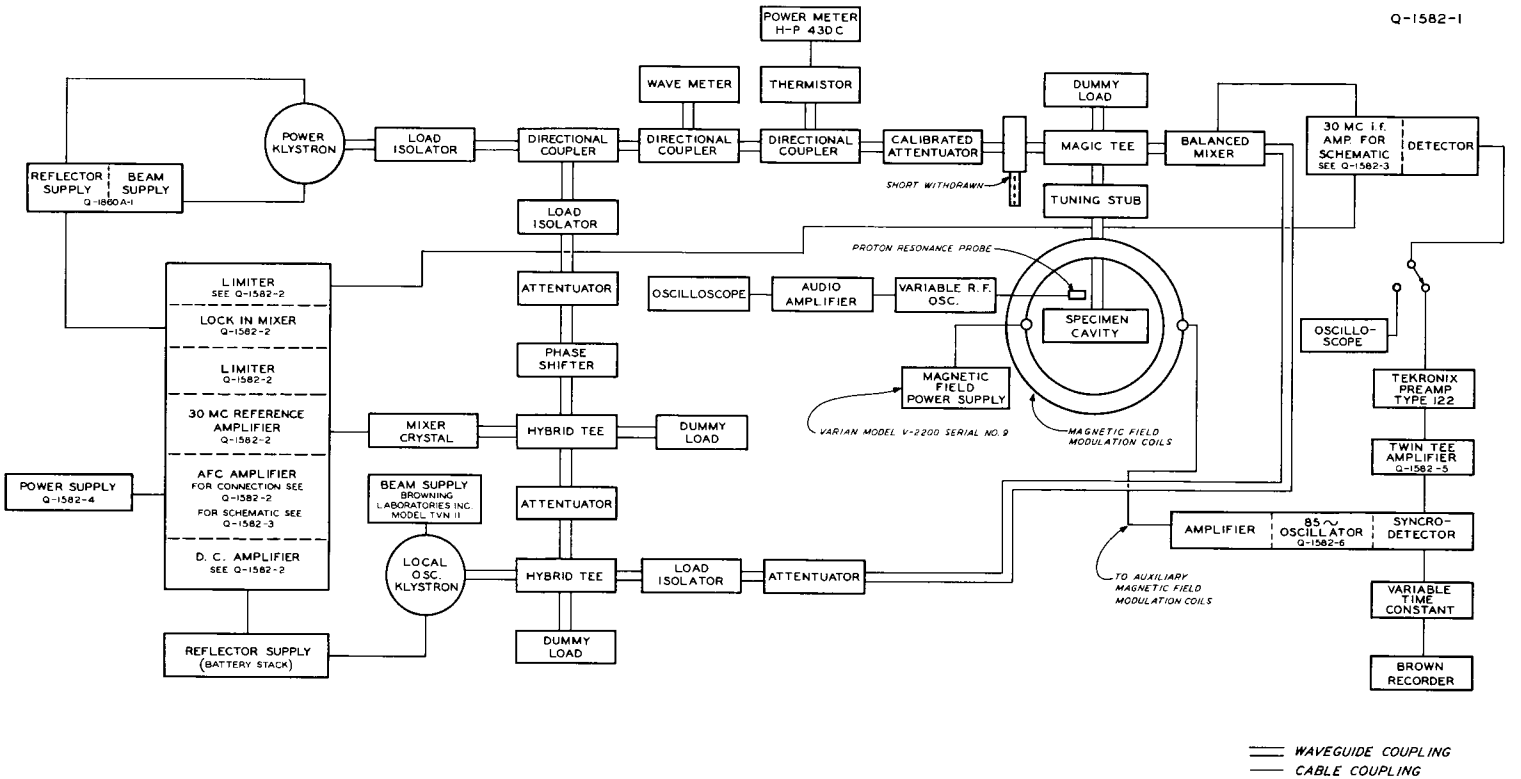

Fig. 21. Block Diagram of Superheterodyne Electron-Spin-Resonance Spectrometer.

The signal-to-noise ratio of the hyperfine lines arising from an interaction of this defect with the 4.7%-abundant Si^{29} nucleus ($I = \frac{1}{2}$) was then measured. This signal-to-noise ratio can be considered as an effective measure of the sensitivity of the spectrometer. The number of centers contributing to the single line observed for the c axis orientation was estimated to be $\sim 5 \times 10^{15}$. The intensity of one of the hyperfine lines is ~2% of the intensity of the central line, and therefore the number of centers contributing to the hyperfine line is 10^{14}. The signal-to-noise ratio was observed to be ~5. A signal-to-noise ratio of 1 should be observed for $\sim 2 \times 10^{13}$ centers of this defect. The power input to the cavity was of the order of 10 microwatts, and the magnetic field modulation was approximately equal to the half width of the line, which is 0.1 gauss. The signal was fed into a synchronous detector (pass band = 0.5 cps) and then recorded on a chart. The loaded cavity Q was ~1500.

The observed sensitivity is reasonable for a superheterodyne spectrometer operating at a 10-microwatt power level and for a magnetic center with the characteristics of the one in the quartz system. Some increase in sensitivity may be expected when leakage from the wave-guide system is eliminated and when the feedback loops are adjusted for optimum control.

OPTICAL ABSORPTION STUDIES OF IRRADIATED SOLIDS

C. M. Nelson

During the past year most of the effort has been spent on studying the nature of the defects in irradiated silica, both crystalline and vitreous, which give rise to optical absorption. Much information concerning the effect of neutron and gamma irradiation on these materials has been collected. By performing thermal annealing and optical bleaching experiments, interrelationships and stability of the different defects could be be studied. A comprehensive review of this work has been written for publication.[1]

As mentioned in the previous report,[2] a comprehensive series of fast-neutron bombardments was carried out in a partial fuel element in the lattice of the LITR. These samples of natural and synthetic (General Electric, Ltd., of England) crystalline quartz and three sources of fused silica (Corning No. 7940, General Electric type III, and Amersil optical-grade No. 2) have now been measured and analyzed. Optical absorption measurements were made with a Cary model 14 spectrophotometer.

The optical absorption spectra of three types of silica after a small dose of reactor radiation ($\sim 10^{17}$ fast neutrons/cm^2) are shown in Fig. 22, in which the extinction coefficient (per centimeter) E is plotted against wavelength over the range from 1850 to 4000 Å. Corning silica is the most resistant to coloration and Amersil optical-grade No. 2 is the least. While both varieties of fused silica show the familiar 2150-Å absorption peak of the C band, their absorption at this wavelength differs by a factor of 10. Quartz gives an intermediate absorption in this region. In all samples there is a continuous "background" absorption which rises rapidly toward shorter wavelengths. This may be the tail of one of the vacuum-ultraviolet bands observed by Mitchell and Paige.[3]

After prolonged neutron bombardment ($>10^{20}$ fast neutrons/cm^2) the introduced damage outweighs previous specimen history, and the spectra become quite similar. Spectra of the same three types of silica after exposure to 2.9×10^{20} fast neutrons/cm^2 are shown in Fig. 23. The predominant feature is the 2150-Å peak (C band), which now falls at the same position for both the quartz and the fused silica. Faintly evident is the band near 2500 Å, the B_2 band in the nomenclature of Mitchell and Paige. Both these bands are superimposed on a background absorption which is presumably the tail of the E band (1620 Å) observed by Mitchell and Paige. The conversion of the quartz spectrum to one almost identical to that of the glasses is to be expected on the basis of structure studies, since the x-ray diffraction patterns of heavily irradiated quartz ($>10^{20}$ fast neutrons/cm^2) indicate that all long-range order has been destroyed, and since the density of both fused and crystalline material approaches the same saturation value.

The intensity of coloration as a function of neutron dose is shown in Fig. 24, where E at 2150 Å is plotted against integrated fast-neutron flux. It will be noted that all specimens tend to

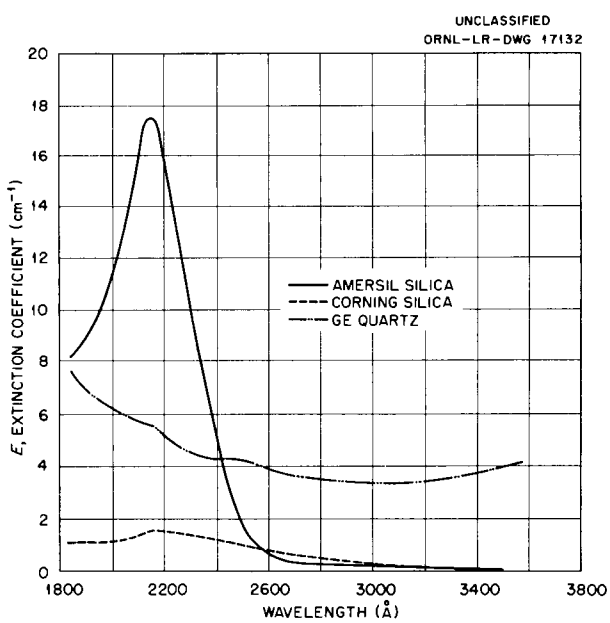

Fig. 22. Absorption Spectra of Irradiated SiO_2 Samples (1×10^{17} Fast Neutrons/cm^2).

[1] Based on *Symposium on Defect Structure of Quartz and Glassy Silica*, given at the Mellon Institute in May 1957, and to be published by Wiley.

[2] C. M. Nelson, *Solid State Semiann. Prog. Rep. Aug. 30, 1956*, ORNL-2188, p 23–25.

[3] E. W. J. Mitchell and E. G. S. Paige, *Phil. Mag.* 1, Ser. 8, 1085 (1956).

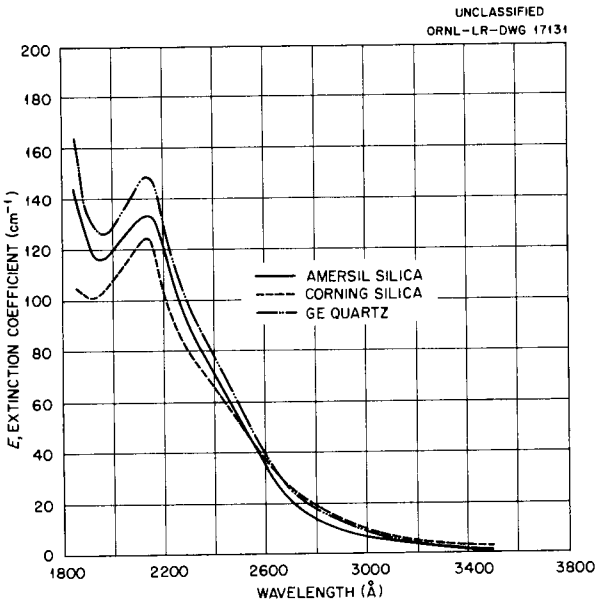

Fig. 23. Absorption Spectra of Irradiated SiO_2 Samples (2.9×10^{20} Fast Neutrons/cm^2).

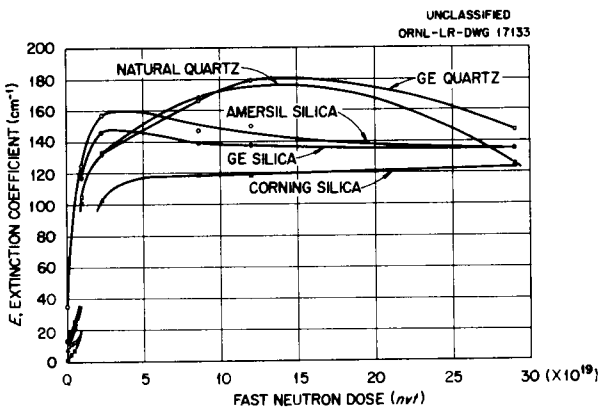

Fig. 24. Buildup of Coloration in SiO_2 Samples During Fast-Neutron Bombardment.

saturate near the same absorption and that the quartz samples pass through a maximum in the same region where there is a loss of crystallinity.

Irradiation of General Electric, Ltd., crystalline quartz with Co^{60} gamma rays produces spectra as shown in Fig. 25. The curve labeled "⊥ cut" refers to a crystal in which the *c* axis is perpendicular to the face of the plate, while the curve marked "|| cut" refers to a crystal cut parallel to the *c* axis. The most important feature of this spectrum is the apparent absence of any *C* band near 2150 to 2200 Å, even where the *A* bands in the visible region are fairly intense. Mitchell and

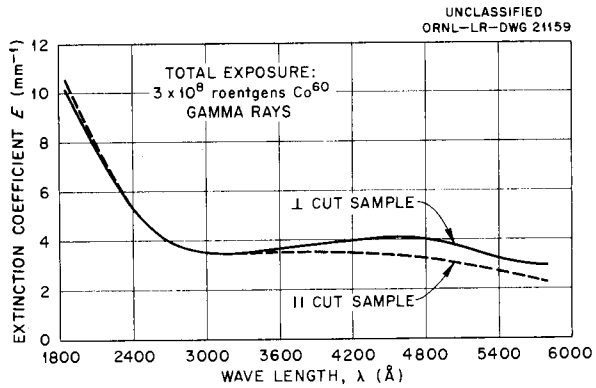

Fig. 25. Absorption Spectra of GE Synthetic Quartz After Gamma-Ray Irradiation.

Paige have suggested[3] that the *A* bands and the *C* band are coupled. If this is true, the oscillator strength of the *C* band is only about 1% of the value for the combined *A* bands. Consequently, their interpretation of the nature of the *C* band is questionable. Since the *A* band is accepted to be due to substitutional aluminum impurity, they assumed that the *C* band in quartz was produced by electrons, originating from the aluminum atoms, trapped at oxygen vacancies. Examination of their published data does not indicate conclusively that a band of appreciable amplitude exists at this position after x-ray exposure. The ranges of the two instruments which they used overlap in this range. Therefore, the apparent maximum that they observed was near the limit of the range on both instruments, and may have been distorted by instrumental limitations. The present data were obtained on a Cary model 14 spectrophotometer which covers the range from 1850 to 4000 Å continuously. It is interesting that this spectrum is quite similar to most of the spectra obtained on synthetic quartz after short reactor exposures ($<5 \times 10^{17}$ fast neutrons/cm^2).

A comparison between gamma-irradiated (5×10^8 r) and neutron-bombarded (1×10^{20} fast neutrons/cm^2) Corning silica is shown in Fig. 26, where the curves are normalized to coincide at 2150 Å. This comparison shows that neutron exposure results in (1) a greater development of the far-ultraviolet band, (2) a greater width of the 2150-Å band, and (3) less development of the 2550-Å band.

The rate of coloration of both quartz and fused silica during gamma-ray exposure, plotted in Fig. 27, shows some interesting features. An Amersil

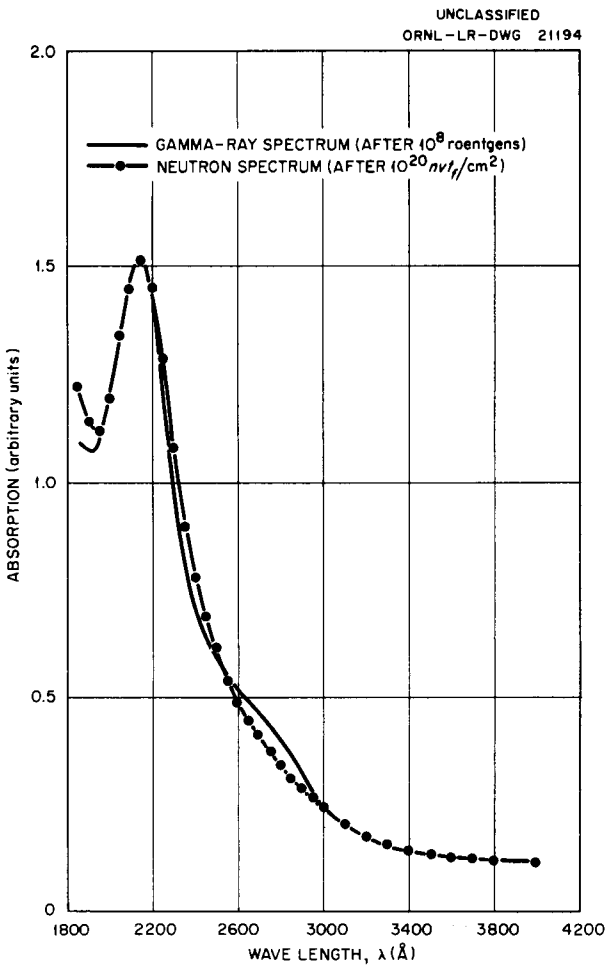

Fig. 26. Absorption Spectra of Corning Silica After Neutron and Gamma-Ray Irradiation.

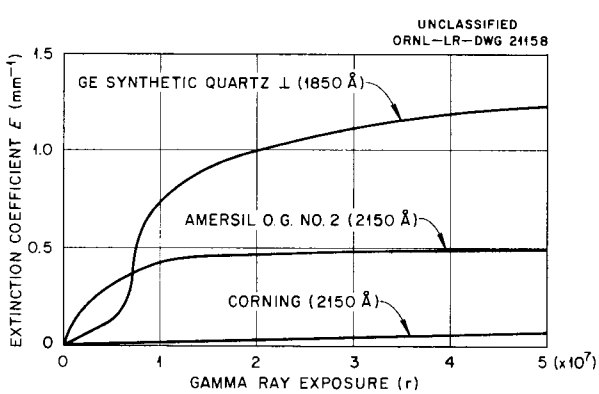

Fig. 27. Buildup of Coloration in SiO_2 During Gamma-Ray Exposure.

(optical-grade No. 2) specimen measured at 2150 Å shows a simple initial buildup to an early apparent saturation near 10^7 r. Continued exposure, however, causes a slow linear increase, and the slope of this portion of the curve is similar to that of the Corning specimen. Measurements of specimens exposed to 10^9 r reveal that this slow increase persists in the two types of silica examined. This slow linear increase appears to be due to the creation of defects by the gamma rays, presumably through the displacement of atoms by energetic Compton electrons. The Varley mechanism of bond rupture and displacement after multiple ionization of the electronegative constituent is also a possible explanation.

In the remaining curve shown in Fig. 27, a complex initial behavior is noted for the absorption of quartz at 1850 Å. The reason for the early sigmoid curvature is unknown. It appears that a certain induction period is required before the rate of coloration becomes appreciable.

Much of the coloration in irradiated quartz and silica can be bleached with light falling in the range from 2000 to 3000 Å. In gamma-irradiated quartz almost all the absorption above 1850 Å can be bleached with a 500-w mercury vapor lamp whose peak intensity falls in the 2537 Å range with appreciable intensity near 2000 Å. After successive periods of bleaching, little if any spectral selectivity can be observed, the bleaching being uniform from 1850 to 4000 Å. After neutron exposure, bleaching is more difficult than for gamma-irradiated specimens. Also, the longer the exposure the less the removal of coloration for a given bleaching period.

In comparison with quartz, gamma-irradiated fused silica is somewhat more resistant to optical decoloration. After long irradiations ($>5 \times 10^8$ r), the absorption at 2150 Å for Corning silica cannot be completely eliminated by ultraviolet light. However, for shorter irradiations, it seems that the coloration can be removed. A series of bleaching experiments were carried out at liquid-nitrogen temperature. The bleaching efficiency was considerably reduced in comparison with experiments at room temperature. This behavior suggests that the excited state of the absorbing center is a discrete state and does not lie in the ionization continuum.

It was observed that on optical bleaching at 77°K a pronounced change occurred in the shape

of the spectra. After bleaching with the 500-w lamp, there was a marked increase in absorption on the long-wavelength side of the 2150-Å peak, whereas a decrease was observed on the short-wavelength side. This suggests that a subsidiary band near 2200 Å was either developed or enhanced by a redistribution of electrons over various possible defects.

A change in the spectra has been observed at room temperature, as well. Use of a 2-w germicidal lamp (very little intensity below 2537 Å) causes a marked decrease in absorption at 2150 Å but affects the band near 2550 Å only slightly. If a neutron-bombarded Corning silica specimen (same material as used above) is exposed to the 500-w lamp, the absorption on the long-wavelength side of the 2150 Å maximum is increased even though the absorption at 2150 Å continues to decrease. It appears that electrons or holes may be excited from a band on the short-wavelength side of the maximum into a defect, leading to absorption between 2150 and 2600 Å, a behavior that is consistent with Levy's picture of the C-band complex.[4]

For gamma-irradiated quartz and silica specimens most of the absorption can be removed by heating to 350 to 400°C, whereas after a moderate neutron exposure ($>10^{18}$ *nvt*), higher temperatures (500°C) are required. Figure 28 shows the effects of thermal annealing on a synthetic quartz specimen after it was exposed to 3×10^8 r. The specimen was held at each anneal temperature for 1 hr. Since there is no 2150-Å band or other maxima in this material, the annealing process was followed at two arbitrary wavelengths, 2500 Å (upper curve) and 4000 Å (lower curve). The very sharp decoloration over the range from 200 to 300°C (Fig. 28) suggests that a singly activated process is responsible for the bleaching, which is consistent with the results of Mitchell and Paige.[3] They calculated an activation energy of 0.75 ev for the thermal bleaching process from an analysis of isothermal bleaching curves. It will be noticed that the two curves are not directly superimposable, the one at 4000 Å showing continued curvature at high temperatures. This suggests that the annealing rate for the *A* bands is different from that for the ultraviolet absorption bands.

[4]P. W. Levy, Color Center Symposium, Argonne National Laboratory, November 1956.

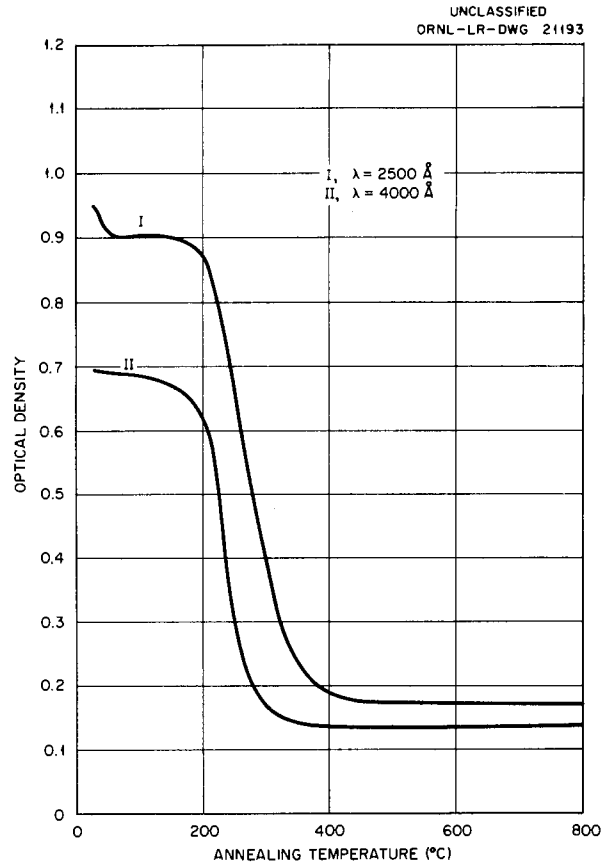

Fig. 28. Thermal Annealing of Coloration in Gamma-Irradiated Quartz.

Thermal annealing of neutron-irradiated quartz is more difficult and more complex than that for gamma-irradiated specimens. Heavily irradiated ($>10^{20}$ *nvt*) specimens behave in the same way as neutron-bombarded fused silica (see below). For small and moderate bombardments a complex change in the absorption spectrum is produced by heating. Figure 29 shows the absorption spectrum of a synthetic quartz specimen, which had been exposed to 5×10^{17} fast neutrons/cm^2, after successive heat treatments. Initially there appeared to be a slight indication of the 2200-Å *C* band and possibly a weak absorption at 2000 Å. Both were superimposed on a strong background absorption which rose continuously toward short wavelength. On heating successively at 60, 100, and 150°C for 1 hr and at 200°C for 30 min, the background absorption and the 2200-Å-region absorption were noticeably diminished, while there was a small enhancement in the 2000-Å band. After a 30-min

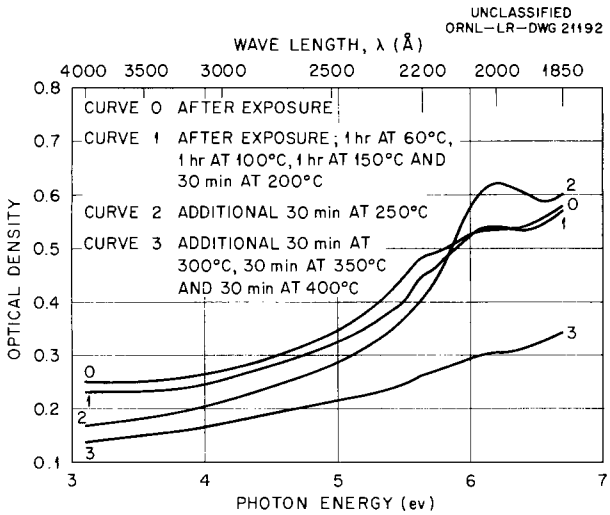

Fig. 29. Absorption Spectra of Quartz After Irradiation by 5 × 10^{17} Fast Neutrons/cm^2 and Thermal Annealing.

anneal at 250°C, the 2000-Å band was greatly enhanced. Higher temperatures removed all structure, leaving only a greatly diminished background absorption. The nature of the 2000-Å band is not known, but it may be related to the one postulated by Levy[4] to lie at 2000 Å in fused silica. It is significant, however, that after extensive bombardment, in which there is disordering of the quartz structure, enhancement of a 2000-Å band is not evident. It would seem, therefore, that if this band is produced by thermal treatment in heavily irradiated specimens, it is obscured by more intense absorption due to other centers; consequently, its production by bombardment is not nearly so efficient as that of the latter centers.

The thermal bleaching of a gamma-irradiated Corning silica specimen at 2150 Å is compared in Fig. 30 with that for a neutron-bombarded one. After gamma irradiation, rapid bleaching in the range from 200 to 350°C is observed. However, the form of the curve suggests that two processes rather than a single one are involved. After neutron bombardment two major annealing stages are again evident, although the stages are spread over a larger temperature range. Such a situation is usual for recovery of property changes after neutron bombardment. After heavy neutron exposures the annealing is spread over an even larger temperature range, and the behavior of quartz and silica becomes quite similar.

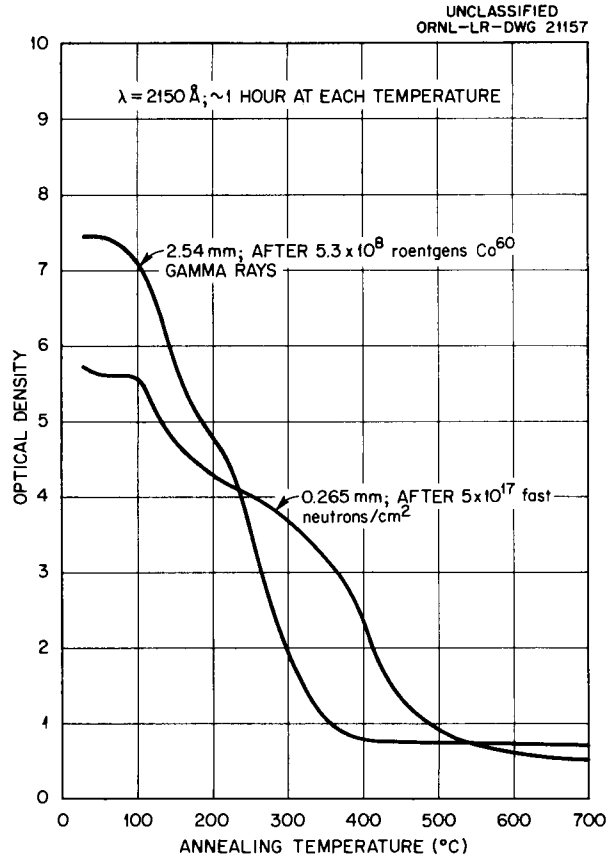

Fig. 30. Thermal Annealing of Coloration in Gamma- and Neutron-Irradiated Corning Silica.

The effect of previous neutron exposure on colorability by gamma rays has also been studied. Extensive disruption of the silicon-oxygen network would be expected to have an effect on the rate of growth of absorption and on its saturation value. Figure 31 shows this effect for a Corning silica specimen after being exposed to 5 × 10^{17} fast neutrons/cm^2 and then thermally annealed at 700°C. A marked increase in coloration rate and saturation absorption at 2150 Å is observed. Included in this figure are the curves for an unirradiated specimen and a previously gamma-irradiated specimen which was then annealed at 700°C. There is little difference between these two curves. Consequently, it appears that neutron-produced defects in the network are not completely annealed by heating at 700°C for 1 hr and that ionizing radiation will produce the optical absorption.

In contrast to that for fused silica, the coloration-vs-dose curve for quartz shows an appreciable

decrease after similar pretreatment by neutron bombardment and annealing. The reason for this result is obscure. A behavior similar to that of the fused silica would be expected.

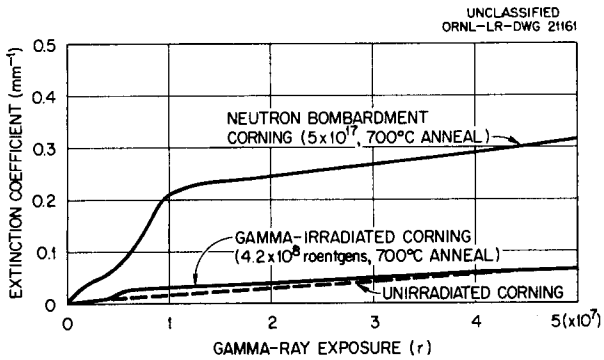

Fig. 31. Buildup of Coloration in Previously Irradiated and Annealed SiO_2.

Recoloration by short gamma-ray exposures after optical bleaching of neutron-irradiated crystalline and fused specimens has also been studied. As would be expected, the specimens recolored rapidly, but not completely back to the absorption value observed before bleaching.

A vacuum ultraviolet spectrophotometer is being constructed and should be completed within several months. This instrument will be very useful in covering the range 900 to 2200 Å, where Mitchell and Paige discovered several absorption bands important to the quartz structure. Correlation of these bands with the bands discussed above should aid considerably in understanding the nature of the defects giving rise to optical absorption in this system.

X-RAY DIFFRACTION STUDIES

M. C. Wittels F. A. Sherrill

Radiation-Induced Phase Transformations

Single crystals of tetragonal $BaTiO_3$ transform to the perovskite-type cubic structure when exposed to fast pile neutrons. The initial studies of this effect have been published,[1] and an abstract of the paper is given below.

Fast-Neutron Effects in Tetragonal Barium Titanate.[1] M. C. Wittels and F. S. Sherrill. – Tetragonal $BaTiO_3$ is transformed into cubic $BaTiO_3$ as a result of irradiation with fast neutrons at a temperature of approximately 100°C. Sufficient atomic displacements are produced by bombardment with an integrated fast neutron flux of 1.8×10^{20} neutrons/cm^2 so that tetragonal single crystals (c_0 = 4.0349 Å and a_0 = 3.9923 Å) expand anisotropically to form perovskite-type cubic single crystals with a_0 = 4.0824 Å. The irradiated material remains cubic to the lowest temperature of measurement, 78°K, showing none of the low temperature phase transitions of unirradiated $BaTiO_3$, and after annealing at 1000°C the crystal remains cubic but with a reduced lattice parameter. X-ray, thermal, and optical methods were employed in studying these effects.

Radiation-damage studies on $BaTiO_3$ and several other ferroelectric crystals are being made with x-ray, thermal, optical, and electrical methods in order to facilitate the understanding of the radiation-damage process in these materials.

A similar type of investigation is being pursued in the zirconium-oxygen system, in which an irradiation-induced phase transition has already been reported.[2] In that study, it was found that natural monoclinic ZrO_2 with small amounts of chemical impurities was transformed into a fluorite-type cubic phase after bombardment with 9.4×10^{19} neutrons/cm^2 and that the irradiated structure was stable on annealing to 800°C. The unique temperature-structure behavior in the zirconia system gives credence to the idea that thermal spikes contributed to this transition, and the particle sizes found in the transformed material lend support to that conclusion. Continued exposure of the transformed crystals to integrated fluxes of 3×10^{20} neutrons/cm^2 reveals that the transformed material is stable after prolonged exposure to fast-neutron flux. More recently it has been found that the type and concentration of impurities in zirconia are important factors in the irradiation-induced transformation, and their role is still not clearly understood. In an effort to clarify these matters this investigation is being pursued with zirconia of variable purity and with its isomorphs.

Expansions in Neutron-Irradiated Germanium and Silicon

Single crystals of germanium and silicon irradiated in the MTR with an estimated integrated neutron flux of 4×10^{20} neutrons/cm^2 were measured for lattice parameter shifts following storage at room temperature. An expansion[3] was reported in both cases, and the results of irradiation at two different temperatures indicated that the irradiation dose rate is a contributing factor to the freezing-in of lattice damage. These irradiation studies of germanium and silicon are continuing in an effort to determine the nature of the bombardment-induced imperfections and their effect upon the lattices of these semiconductors.

Irradiation Effects in Quartz

X-ray studies of reactor-irradiated single-crystal quartz have been made in the range where single-crystal reflections are still visible. The effects of prolonged neutron bombardment of polycrystalline coesite, a high-density silica, have also been observed. Some of these results have been presented for publication,[4] and the following is an abstract of the paper.

Structural Behavior of Neutron-Irradiated Quartz.[4] M. C. Wittels. – X-ray and density studies have been made on single crystals of quartz irradiated with fast pile neutrons at approximately 100°C. The structural effects of the irradiation follow at least two processes

[1] M. C. Wittels and F. A. Sherrill, *J. Appl. Phy.* 28, 606 (1957).

[2] M. C. Wittels and F. A. Sherrill, *J. Appl. Phy.* 27, 643 (1956).

[3] M. C. Wittels, *J. Appl. Phy.* 28, 921 (1957).

[4] M. C. Wittels, "Structural Behavior of Neutron-Irradiated Quartz," to be published in *Phil. Mag.*

with doses up to 1.2×10^{20} neutrons/cm^2. Crystals irradiated with less than 3×10^{19} neutrons/cm^2 expand anisotropically in a manner that is similar to the thermal expansion of unirradiated quartz. In this dosage range the volume increase is the same, as determined by x-ray and hydrostatic methods, and little or no distortion is observed in x-ray diffraction patterns. The model which seems to fit these results best consists of paint defects and slightly disordered regions which result in an elastic distention of the lattice.

After doses in excess of 3×10^{19} neutrons/cm^2 the damaging process is more complex since the volume change indicated by x-ray measurements of the host lattice becomes larger than the bulk volume change determined hydrostatically. After irradiation with 8×10^{19} neutrons/cm^2 an inhomogeneous shear strain is observed in the extreme skewing of the (22.0) reflection which is interpreted as being due to the crowding of oxygen ion interstitials into the open *c*-axis channels. Amorphous regions enmeshed in the host lattice are identified in crystals that still possess long range order after irradiation with 7×10^{19} neutrons/cm^2. The diffuse x-ray scattering halo associated with the amorphous material changes peak position, shape, and intensity with increasing dosages of irradiation. It is suggested that these changes result from a reorientation of disordered regions which is assisted by the increased expansion of the lattice and the presence of ruptured silicon-oxygen bonds. A second kind of diffuse scattering appears at these high doses which cannot be accounted for on the basis of a thermal origin but is probably related to scattering resulting from inhomogeneous lattice strains.

In a complementary study it was found that coesite, a high density crystalline silica, remained stable under neutron irradiation dosages which completely disorder quartz. These results indicate that the rate of damage in silica solids is structure dependent.

Twinning in Face-Centered Cubic Metals

Conjugate (111) deformation twins have been verified by x-ray studies[5,6] and an abstract of the report[6] follows.

X-Ray Determination of Conjugate Deformation Twins in Copper.[6] F. A. Sherrill, M. C. Wittels, and T. H. Blewitt. – Deformation twins related to two separate (111) orientations have been observed in a copper single crystal deformed by tensile extension at 4.2°K. The unambiguous determination of the twin relationships is accomplished by a unique x-ray technique which makes use of a single crystal adapter and Geiger counter methods. The adapter permits the detection and measurement of weakly diffracting reflections and the twin relationships are established by the unique application of geometrical data in a stereographic projection.

In cooperation with the Low Temperature Group these studies have been extended to silver and gold, and by the same technique the formation of (111) twinning has again been established as a result of tensile extension at 4.2°K.

Future Plans

A double-crystal spectrometer will soon be available for studying small changes in x-ray diffraction lines by employment of a narrow monochromatic beam and a rocking apparatus capable of small and accurate rotations (1 sec of arc). Plans are now in progress for the fabrication of a liquid-helium cryostat attachment to the G-E horizontal spectrometer, and it is hoped that this apparatus may be utilized for the study of defects frozen in during low-temperature reactor irradiation. It is also recognized that the annealing of many irradiation-induced lattice defects takes place at elevated temperatures, and it is therefore desirable to observe these phenomena by high-temperature x-ray methods. For this reason, much thought is being given to the development of a suitable high-temperature x-ray camera. It is also hoped that a microfocus x-ray source will become available for the investigation of irradiation effects upon substructures.

[5] F. A. Sherrill, M. C. Wittels, and T. H. Blewitt, *Solid State Semiann. Prog. Rep. Aug. 30, 1956*, ORNL-2188, p 83.

[6] F. A. Sherrill, M. C. Wittels, and T. H. Blewitt, *J. Appl. Phy.* 28, 526 (1957).

LOW-TEMPERATURE THERMAL CONDUCTIVITY OF POTASSIUM CHLORIDE CRYSTALS, INCLUDING THE EFFECTS OF STRAIN AND PARTICLE IRRADIATION

A. Foner Cohen L. C. Templeton

The thermal conductivity of nonmetallic crystals has been studied for more than 50 years, and it was first shown in 1905 that the conductivity increases with decreasing temperature.[1] Eucken,[2] in measuring the thermal conductivity of nonmetals from liquid-oxygen to room temperatures, found the thermal conductivity to vary as T^{-1}. In 1914, Debye[3] showed such a dependence to be expected theoretically and, more significantly, that anharmonic coupling was necessary to produce a finite conductivity at any temperature. In 1929, Peierls[4] considered the discrete nature of the crystal lattice as well as the anharmonic coupling. His theory confirmed Debye's theory by means of a quantum-mechanical treatment and also predicted that the thermal resistivity should decrease exponentially with decreasing temperature. The intrinsic resistance is due to the "Umklapp" process, which becomes less probable at low temperatures. In 1938, Casimir[5] and Makinson[6] calculated the effect of the external crystal boundaries on the measured conductivity and showed that a crystal of finite size could not have an infinite thermal conductivity. The temperature range in which the crystal size is effective in limiting the conductivity is frequently called the boundary scattering region. The thermal conductivity of nonmetallic crystals is thus found to have a maximum at low temperatures, and the absolute value of this maximum can be quite large, as, for example, in Al_2O_3 (ref 7) or diamond.[8] Consequently, measurement of the thermal conductivity at low temperatures should be a very sensitive means of studying crystal imperfections, because the high values of thermal conductivity will be markedly reduced by any defect which disturbs the lattice vibrations. The manner in which the thermal conductivity of nonmetals, as well as the lattice component of the thermal conductivity of metals, will be decreased as a function of temperature depends on the type and concentration of the lattice imperfections.[9-11] Klemens[12] has shown that the temperature dependence of the thermal resistance arising from lattice imperfections is determined by the frequency dependence of their scattering cross section for lattice waves and has calculated the scattering by various types of static imperfections in alkali halides.[13]

The present investigation was undertaken to obtain information regarding the nature of the lattice defects produced by Co^{60} gamma rays and by pile-neutron irradiation. The choice of potassium chloride single crystals was made for the following reasons. First, KCl is a crystal which can be obtained in very pure form and is of simple structure. Second, some experimental work on the effect of impurities on the thermal resistivity had been made by Deviatkova and Stilbans[14] from 98 to 298°K. In addition, Slack[15] has recently carried out a careful study of the low-temperature conduction process in KCl to which varying amounts of divalent impurities have been added. He found agreement with the predictions of Klemens and, furthermore, suggested that an additional scattering due to the effect

[1] C. H. Lees, *Phil. Trans. Roy. Soc. London* **A204**, 433 (1905).

[2] A. Eucken, *Ann. Physik* **34**, 185 (1911).

[3] M. Planck *et al.*, *Vorträge über die kinetische Theorie der Materie und der Elektrizität*, Teubner, Leipzig, 1914.

[4] R. Peierls, *Ann. Physik* **3**, Ser. 5, 1055 (1929).

[5] H. B. G. Casimir, *Physica* **5**, 495 (1938).

[6] R. E. B. Makinson, *Proc. Cambridge Phil. Soc.* **34**, 474 (1938).

[7] R. Berman, E. L. Foster, and J. M. Ziman, *Proc. Roy. Soc. (London)* **A231**, 130 (1955).

[8] R. Berman, E. L. Foster, and J. M. Ziman, *Proc. Roy. Soc. (London)* **A237**, 344 (1956).

[9] R. Berman, in *Advances in Physics (Phil. Mag.* Supplement) **2**, 103 (1953).

[10] J. L. Olsen and H. M. Rosenberg, in *Advances in Physics (Phil. Mag.* Supplement) **2**, 28 (1953).

[11] W. R. G. Kemp *et al.*, *Proc. Phys. Soc. (London)* **A67**, 728 (1954).

[12] P. G. Klemens, *Proc. Roy. Soc. (London)* **A208**, 108 (1951).

[13] P. G. Klemens, *Proc. Phys. Soc. (London)* **A68**, 1113 (1955).

[14] E. D. Deviatkova and L. S. Stilbans, *Zhur. Tekh. Fiz.* **22**, 968 (1952).

[15] G. A. Slack, *Phys. Rev.* **105**, 832 (1957).

of isotopes limited the conductivity in the pure specimen.[16]

Effect of Strains. – In cleaved KCl crystals, it is found that, even for a high-purity crystal, a low thermal conductivity may be obtained, as shown in curve 1, Fig. 32. Following an anneal at 600°C for 1 hr and a slow cooling, a marked increase in conductivity was observed, as shown in curve 2, Fig. 32. Slack[17] has also observed an increase in the thermal conductivity of high-purity crystals after they were annealed near the melting point.

In another series of experiments, the effect of Co^{60} gamma-ray irradiations at room temperature upon the conductivity of a cleaved unannealed KCl crystal was studied. Following doses of 5.18×10^8 and 4.08×10^8 r, a marked increase in K over the temperature region from 3 to 18°K was observed, suggesting that annealing of cleavage strains during irradiation was occurring. Upon irradiation with an additional dose of 4.02×10^8 r, the resulting K values were then found to be less than the original unirradiated values. This indicates that on prolonged exposure the scattering from introduced lattice defects dominates the radiation annealing of strains.

[16] G. A. Slack, *Phys. Rev.* 105, 829 (1957).

[17] G. A. Slack, *Thermal Conductivity of Potassium Chloride Crystals Containing Calcium*, Doctoral Dissertation, Cornell University, 1956.

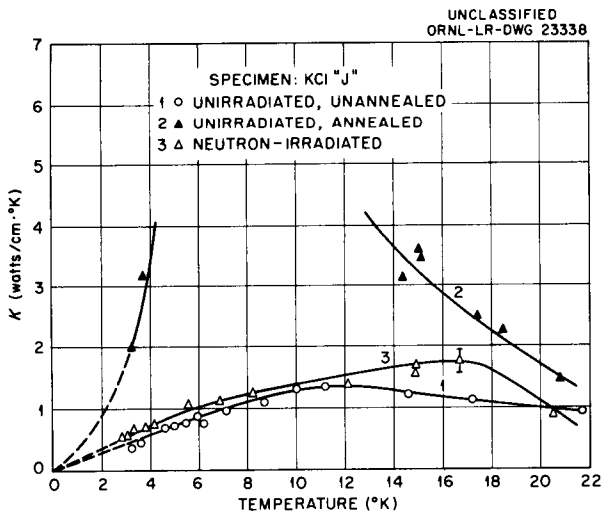

Fig. 32. Thermal Conductivity vs Temperature for KCl.

Effect of Irradiation with Co^{60} Gamma Rays. – With a well-annealed KCl crystal, the K vs T curve of which is very much like that of Slack's[17] pure crystal, the effect of Co^{60} gamma-ray bombardment at ambient temperature was studied. Above the temperature, T_m, at which the thermal conductivity has its maximum value, K_m, the thermal conductivity decreased upon an exposure of 3.95×10^7 r, somewhat as expected for point scatterers; the thermal resistivity in the boundary region, however, was greater than that expected on the basis of qualitative comparison with Slack's experiments,[15] where chemically introduced defects caused the scattering. Upon further bombardment (5.06×10^7 r) the measured K for $T > T_m$ decreased further. However, with an additional irradiation of 4×10^7 r, the decrease in K over the whole temperature range appeared to reach saturation. This may indicate an equilibrium between damaging and annealing processes. Care was taken following the irradiations to prevent ambient light from bleaching the color centers introduced by the gamma irradiation, although for periods of approximately 10 min during mounting exposure to light was unavoidable.

Irradiation with Fast Neutrons. – It was of interest to examine the effect of fast-neutron bombardment on the conductivity of KCl. The first experiment was carried out with the use of a short bombardment during which the integrated fast flux was 1.28×10^{16} neutrons/cm^2. The crystal of Fig. 32 was used after the anneal. Results of measurements made immediately after the bombardment are shown in curve 3 (Fig. 32). In another crystal it was found that, after a similar irradiation but with several hours of exposure to ambient light, the purple coloring of the crystal was bleached out. Subsequent K measurements showed the thermal conductivity to have returned to the initial unirradiated-annealed values over the entire temperature range of measurement. However, for longer bombardments, during which the KCl specimen was shielded with lead to diminish largely the effect of gamma rays, almost no decrease in K was observed over the region $T > T_m$. Below T_m, in the boundary scattering region, the decrease in K is already equal to that observed following gamma irradiations of 4×10^7 r. This suggests that clusters of lattice

defects are probably an important component of the damage produced by fast neutrons, as has been observed for other crystals.[9]

In summary, it has been observed that, even for high-purity KCl crystals, the scattering of phonons by strains introduced by cleaving may be considerable and that careful thermal annealing is effective in removing such thermal resistance. In addition, the fact that Co^{60} gamma rays are effective in annealing strains in such crystals suggests that mobile defects produced during bombardment are in some way able to relieve cleavage strains.

From experiments on annealed KCl crystals, it has been found that the Co^{60} gamma rays produce essentially point-defect scattering at $T > T_m$, and in the boundary region ($T < T_m$) an additional scattering which cannot be explained by point defects or by isotope effect. This may be in some way connected with the presence of dislocations or some other source of scattering which has been altered by gamma-ray exposure. The irradiations have been carried out at ambient temperatures, and since some annealing during the irradiation occurs, it appears that useful information relating to the mechanisms involved may be found from carrying out the irradiations and thermal measurements at, for example, liquid-helium temperatures. The experiments with fast neutrons indicate that point scattering is much less effective than with gamma rays, as evidenced by the fact that neutron bombardment produced almost no effect on the thermal conductivity of a KCl crystal at $T > T_m$ in the case where the crystal was shielded with lead. Whether clusters of defects are the cause for the scattering found at the lowest temperatures following neutron bombardment or whether it is due primarily to the same mechanism responsible for the extra scattering existing in the gamma-ray-bombarded crystals, is not as yet answered.

LOW-TEMPERATURE THERMAL CONDUCTIVITY OF NONMETALS

A. Foner Cohen

The thermal conductivity, K, of the purest available single crystals of KCl, SiO_2, LiF, CaF_2, MgO, Ge, and NaF has been measured at low temperatures. Table 5 gives the cross-sectional area of the crystals, the condition of the surfaces, the value of the thermal conductivity at the maximum, K_m, and the temperature, T_m, at which K_m occurs. The results with KCl, SiO_2, LiF, and Ge are in substantial agreement with those of other authors.[1-4] This author is unaware of other low-temperature measurements on CaF_2, MgO, or NaF crystals.

It was of interest to examine NaF because it should be free of isotope scattering and hence should exhibit an exponential K vs T dependence at temperatures higher than T_m. The only other scattering that would limit K would be that due to impurities or strains. Even though the K vs T dependence of NaF at $T > T_m$ is exponential in character, as shown in Fig. 33, comparison with theory[3,5,6] shows that the impurities which are present are sufficient to keep the theoretically expected K vs T values from being realized. [Semiquantitative analysis shows the presence of silicon, between 300 and 1000 ppm, and of the following elements (values within ±20%): Cu, 9 ppm; Fe, 36 ppm; Al, 50 ppm.] It is hoped that with higher-purity strain-free NaF crystals an experimental evaluation of the "Umklapp" scattering can be obtained. In addition, such a crystal would be particularly interesting to use for studying the effect of scattering by defects produced by gamma rays.

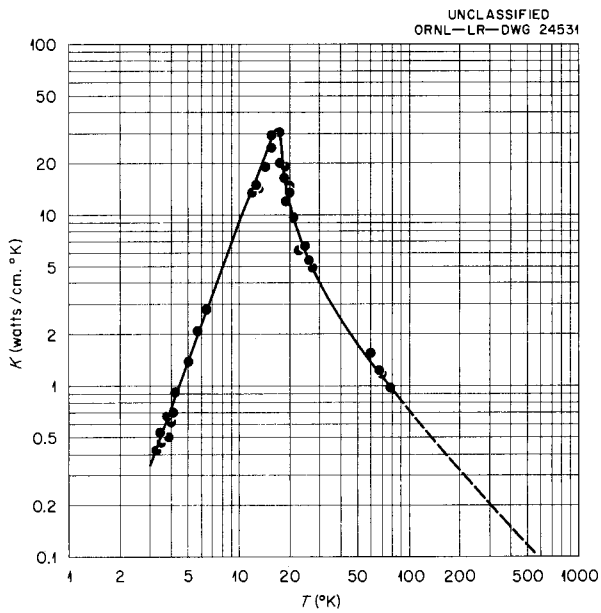

Fig. 33. Conductivity vs Temperature for NaF.

Table 5. Thermal Conductivity Maxima of Various Crystals

Crystal	Cross Section (mm^2)	Surface	K_m (watts/cm·°K)	T_m (°K)
KCl	16.00	Cleaved	8.2	6.2
SiO_2	19.75	Polished	15	12
LiF	18.15	Two surfaces cleaved	20	16
CaF_2	7.78	Polished	80	9–10
MgO	3.28	Cleaved	8	22
Ge	14.80	Polished	12	16
NaF	7.38	Cleaved	31	17

[1] G. A. Slack, *Phys. Rev.* **105**, 832 (1957).

[2] R. Berman, *Advances in Physics (Phil. Mag.* Supplement) **2**, 103 (1953).

[3] R. Berman and E. L. Foster, *Proc. Roy. Soc. (London)* **A237**, 344 (1956).

[4] J. A. Carruthers *et al.*, *Proc. Roy. Soc. (London)* **A238**, 502 (1957).

[5] G. Leibfried and E. Schlömann, *Nachr. Akad. Wiss. Göttingen Math.-physik. Kl. IIa. Math.-physik.-chem. Abt.* (4) 71 (1954).

[6] I. Pomeranchuk, *J. Phys.(U.S.S.R.)* **6**, 237 (1942).

LOW-TEMPERATURE THERMAL CONDUCTIVITY IN NEUTRON-IRRADIATED VITREOUS SILICA

A. Foner Cohen

At low temperatures the thermal conductivity, K, of crystalline, nonmetallic solids is limited by the scattering of phonons from lattice imperfections, that is, boundaries, impurity atoms, and lattice defects. Consequently, this property is a potentially powerful tool for investigating the nature of lattice defects introduced by fast-particle bombardment. Berman[1] has demonstrated the effectiveness of such an approach in his studies of neutron-bombarded quartz. The marked decrease of K which he observed in the low-temperature range has been analyzed by Klemens,[2] whose results indicate the presence of not only point defects, that is, interstitial atoms and lattice vacancies, but clusters of defects or disordered (vitrified) regions as well.

In contrast with that of crystalline solids, the conductivity of glasses is quite small at low temperatures. This is a natural consequence of the high degree of disorder in glassy substances. Klemens has constructed a theory for the conductivity in such materials which is in excellent agreement with experimental observation. At all but the lowest temperatures, K is dominated by a phonon mean free path which corresponds to the size of the basic SiO_4 tetrahedra, and hence K is proportional to the specific heat. At very low temperatures, however, phonons with wavelengths much greater than the ordered cell size become an important part of the phonon distribution, and, since the glass is a homogeneous substance, their scattering may be treated on the basis of plane-wave scattering, leading to a longer mean free path than that of the high-energy phonons.

Because of the highly disordered nature of fused quartz, K would be expected to be quite insensitive to additional imperfections. On prolonged fast-neutron bombardment, however, extensive structural changes are observed.[3-5] An increase in density is observed which saturates at 2.26 g/cm^3 (a 3% increase). The saturation density value is also attained after exposures in excess of 2×10^{20} fast neutrons/cm^2 by crystalline quartz[3] specimens, resulting in a 14% density decrease and a loss of crystallinity. Consequently, the saturation condition appears to represent an intermediate state of disorder. Lukesh[6] has observed changes in the intensity distribution of the x-ray pattern for vitreous silica after neutron irradiation. Moreover, Simon[7] made an analysis of the radial distribution of x-ray intensity in a heavily irradiated silica specimen and found a decrease in the Si–Si distances and a wider distribution in the O–O and Si–second-O distances after irradiation. Annealing studies by Wittels also attest to a qualitative difference in the structure of vitreous silica after irradiation to the saturation condition. He finds that a 900°C anneal subsequent to neutron bombardment produces a partial crystallization into the α-quartz structure.

On consideration of these structural modifications of fused silica by neutron bombardment, Klemens[8] has predicted that an appreciable increase in K would result in a longer phonon mean free path. The experimental results presented here confirm Klemens' prediction.

Thermal conductivity measurements on high-purity fused silica specimens of square cross section equal to 19.8 mm^2, obtained from the Corning Glass Works, were made by a static method at low temperatures before and after exposure to 1.71×10^{19} fast neutrons/cm^2 and later after an additional exposure to 4.13×10^{19} fast neutrons/cm^2. (The exposures were carried out in a water-cooled facility at the LITR.) As shown in Fig. 34, the

[1] R. Berman, *Proc. Roy. Soc. (London)* **A208**, 90 (1951).

[2] P. G. Klemens, *Proc. Roy. Soc. (London)* **A208**, 108 (1951).

[3] W. Primak, L. H. Fuchs, and P. Day, *Phys. Rev.* **92**, 1064 (1953).

[4] W. Primak, L. H. Fuchs, and P. Day, *J. Am. Ceram. Soc.* **38**, 135 (1955).

[5] M. Wittels, *Phys. Rev.* **89**, 656 (1953).

[6] J. S. Lukesh, *Phys. Rev.* **97**, 345 (1955).

[7] I. Simon, *J. Am. Ceram. Soc.* **40**, 150 (1957).

[8] P. G. Klemens, *Phil. Mag.* 1, Ser. 8, 938 (1956).

thermal conductivity following irradiation was significantly higher than before. The density (by hydrostatic weighing) of the silica before irradiation was 2.1994 g/cm^3, as compared with 2.2412 after 1.71×10^{19} neutrons/cm^2. Upon an additional exposure to 4.13×10^{19} neutrons/cm^2, the density increased to 2.2602 g/cm^3. The density after the second bombardment is approximately the limiting density for both crystalline quartz and fused silica after prolonged neutron exposure.[3,4,9] Measurements of the dimensions of fused silica before and after bombardment show that the density increase corresponds entirely to the decrease in dimensions. Since the thermal conductivity at low temperatures in fused silica does increase upon fast-neutron bombardment, it is seen that Klemens' prediction is correct.

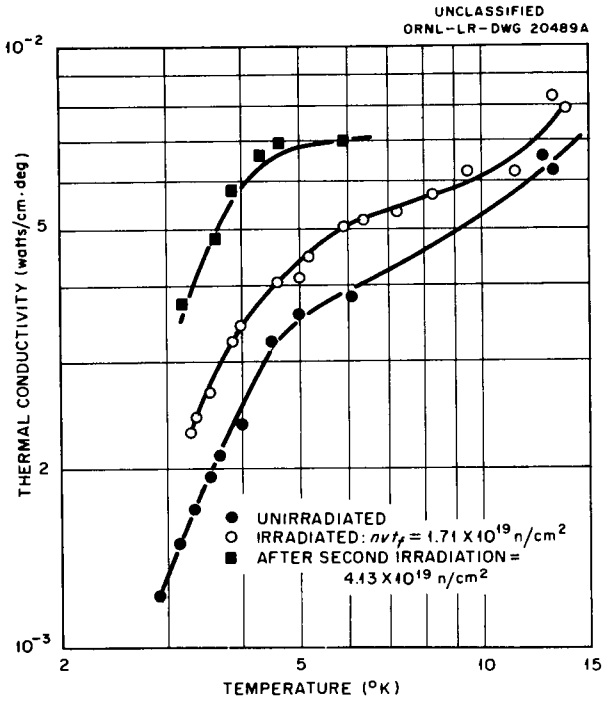

Fig. 34. Thermal Conductivity vs Temperature of Fused Silica Before and After Neutron Irradiation.

The experiments show an increase in the thermal conductivity of fused silica at low temperatures by a factor of 2 after bombardment with 5.84×10^{19} fast neutrons/cm^2, the increase being approximately linear with dose. On the other hand, the density is saturating at 2.26 g/cm^3 (a density increase of 3%) after exposure to 5.84×10^{19} neutrons/cm^2. It appears therefore that the increases in the density and the thermal conductivity upon irradiation are related in an indirect way. Further experiments to determine the extent to which the thermal conductivity of silica can increase upon fast-neutron irradiation are being carried out. Studies of the effect of further neutron irradiation and of the effect of subsequent high-temperature annealing on the low-temperature thermal conductivity of fused silica are in progress, and a further report will be submitted at the completion of these studies.

---

[9] M. C. Wittels and F. A. Sherrill, *Phys. Rev.* 93, 1117 (1954).

PROPOSED REACTOR BOMBARDMENTS AT 4°K

T. H. Blewitt R. R. Coltman
W. E. Busby J. T. Howe
C. E. Klabunde

Construction of a helium liquefier system which is to be inserted in the hole No. 12 cryostat is partially completed. With this system it is hoped that bombardments can be made in the vicinity of 4°K. This would make it possible to examine bombarded material for annealing processes which might occur below the presently obtainable temperature of 15°K. Also, those metals such as gold, platinum, and lead, whose temperature coefficient of resistivity is still appreciable at 15°K, may be examined more precisely at the lower temperature. The liquefier system will make use of the filtered, high-pressure, room-temperature helium gas from the compressor section of the present cryostat system. After passing through a counterflow heat exchanger, this gas will be further cooled to about 10 to 12°K by the present refrigerator. It will then enter another small counterflow heat exchanger which is terminated by a Joule-Thomson expansion valve. Here the final cooling and liquefaction will occur, and the helium gas-liquid mixture will be transported to a small sample chamber located in the sample chamber of the present cryostat at the center of the reactor. The helium will then return through the heat exchanger to the low-pressure side of the main compressor system via a vacuum pump and a small compressor. By using a vacuum pump on the low-pressure side of the liquefier system, it is hoped that a temperature somewhat below 4°K may be reached.

GAMMA-SOURCE FACILITIES

J. W. Cleland

Two gamma-source facilities have been constructed during the past year for room- and liquid-nitrogen-temperature irradiation of various materials. The first facility consists of a lead cylinder with provision for standard packaged units of Cs^{137} arranged in a ring 1 in. in inside diameter. The total activity employed was ~960 curies. The removal rate of conduction electrons from *n*-type germanium at ~35°C was determined as being less than 1×10^{-6} per incident 0.662-Mev photon in this assembly. A sliding cryostat with provision for electrical leads and replenishment of liquid nitrogen during prolonged irradiation was also constructed.

The second facility[1] consists of ~1880 curies of Co^{60}, arranged in 12 cylinders spaced concentrically around an exposure tube $1\frac{13}{16}$ in. in inside diameter and stored underground. Twenty-four right-cylindrical pellets of Co^{60} (1×1 cm) are employed and are currently arranged to obtain maximum intensity. The central intensity has been measured by the Analytical Chemistry Division, using cerous sulfate dosimeters. The value obtained was 2.26×10^6 r/hr at the center line of the Co^{60}, uniform within 10% over a vertical distance of 3 cm. This value corresponds[2] to a photon flux of $\sim 10^{12}$ gammas·cm^{-2}·sec^{-1}. Possession by ORNL of a standard shipping container permits repositioning of the present Co^{60}, or addition of more source material for other experiments if necessary. Twelve additional exposure tubes in which the intensity is $\sim 7.6 \times 10^5$ r/hr, or $\sim 3 \times 10^{11}$ gammas·cm^{-2}·sec^{-1}, are also available external to the 12 cobalt tubes that surround the central facility.

[1] M. Burton, J. A. Ghormley, and C. J. Hochanadel, *Nucleonics* 13(10), 74 (1955).

[2] C. D. Bopp and O. Sisman, *Nucleonics* 14(1), 46 (1956).

AUTOMATIC LIQUID-GAS LEVEL CONTROL

O. E. Schow

A device to maintain a constant level of liquid nitrogen in Dewar vessels is required in order to permit low-temperature storage over a protracted period. The liquid-level sensing element of the device is a flat spiral-wound tube of type 304 stainless steel, 40-mil OD, 3-mil wall thickness, filled with gaseous nitrogen. The spiral end of the tube is closed and is placed in the controlled Dewar. The other end of the tube opens into a pressure switch. If the spiral is below the liquid level in the Dewar, the gas inside the sensing tube is essentially at 0 psig, and the pressure switch is in the "off" position. When the spiral is above the liquid surface, the temperature of the spiral increases to some value above that of the liquefied gas, and the pressure switch is in the "on" position. In this temperature range, the pressure inside the spiral is quite sensitive to small temperature changes, but the device is not satisfactory because the gas immediately above the liquid level in the controlled Dewar is at essentially the same temperature as that of the liquefied gas. In order to make the device sensitive to the liquid level, a small, constant heat input is supplied to the spiral. The heat input must be of such a magnitude as to assure a significant pressure increase when the spiral is immediately above the liquid, but must be small enough to permit cooling by the liquid in the Dewar. Since this type of controller is sensitive to temperatures anywhere along its entire length, it is advisable to sheathe the element in a plastic sleeve, leaving only the spiral uncovered.

To keep the filling system free of moisture, the atmospheric vent on the three-way solenoid valve is connected to the liquid feed lines. Since only liquid is desired in the controlled Dewar, a cyclone separator was put into the system.

The controller described here has operated continuously for three months without failure and has therefore been found to be reliable. The device, as shown in Fig. 35, can maintain a level of liquid nitrogen in any Dewar to within limits of $\pm \frac{1}{4}$ in. and needs attention only when the main reservoir becomes empty. It is made of stock laboratory equipment and has sufficient flexibility for many applications.

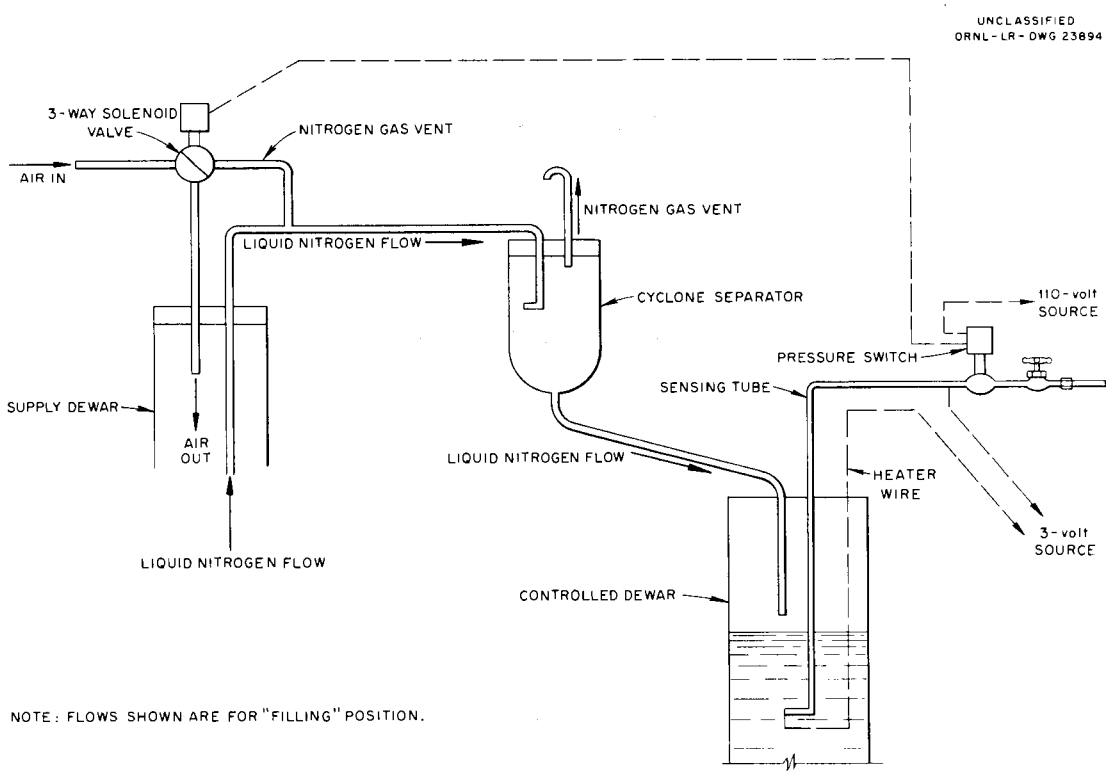

Fig. 35. Automatic Liquid-Gas Level Control.

HRP RADIATION METALLURGY

J. C. Wilson

R. G. Berggren F. M. Grizzell

The purpose of the HRP-supported radiation metallurgy program is to determine whether service conditions and the effects of irradiation may cause reactor structural materials to fail in a brittle manner, that is, rupture without appreciable plastic deformation. The greatest concern is for the steels used in the construction of the pressure vessel, upon which the reactor system depends heavily for its integrity and safety. For practical purposes, the pressure vessel must be made of carbon steel, a material that is capable of failing in a brittle manner under certain conditions of service. Further, radiation effects in carbon steels tend to reduce their ductility and to increase their tendency to show brittle behavior.

Quantitative evaluation of the brittleness or ductility of even an unirradiated steel has only recently become possible, and the subject is still not well understood. Many factors are influential: composition, heat treatment, temperature, design (particularly with respect to notches and stress raisers), and service conditions. To these must be added the effect of irradiation.

The approach to the problem has been as follows:

1. A large variety of possible structural steels have been irradiated, and the conventional mechanical property tests (used for evaluation under the Boiler Code[1]) have been performed. The test conditions – strain rate, temperature, etc. – have been varied to disclose behavior that might not be revealed in normal testing routines.

2. Neutron exposures equal to and in excess of expected service values have been employed.

3. The temperature of irradiation has been varied from room temperature to above maximum service temperatures to assess the effects of annealing and radiation-induced metallurgical reactions that may be temperature dependent.

4. Materials such as irons of high purity and steels of high purity (except for carbon) have been tested to aid in determining the mechanisms of the radiation effects and the dependence upon composition.

The following tentative conclusions have been reached:

1. The conventional mechanical properties of irradiated steels may be appreciably altered by a neutron dose of the order of 10^{18} cm^{-2} (energy greater than 1 Mev).

2. Irradiation by 10^{19} to 10^{20} neutrons/cm^2 will change the properties sufficiently to cause them to fall outside the limits of the applicable ASTM or ASME materials specifications.

3. The interrelationship between mechanical properties of steel is greatly altered by irradiation, and the general behavior during mechanical testing is that of an unfamiliar metal rather than that commonly exhibited by steels.

4. The temperature range over which the fractures in a steel change from predominantly ductile to predominantly brittle behavior is often increased by irradiation.

5. The sensitivity of property changes to irradiation appears to depend on composition and heat treatment in a manner that is still not clear.

6. The mechanical properties of irradiated high-purity iron are substantially different from those of irradiated medium-carbon steels.

7. Elevated irradiation temperatures (of the order of 600°F, the HRT service temperature) generally reduce the effects of irradiation, although some properties may be changed more during elevated-temperature irradiation.

The bulk of the data from which the above conclusions were drawn has been published.[2–4] Below are some significant additional facts disclosed in more recent tests.

Differences in the observed effects of irradiation on one class of carbon steels are typified by results obtained for three different heats of steel made to ASTM A-212 grade B specification. One of these was in the hot-rolled condition, one was

[1] American Society of Mechanical Engineers, *Rules for Construction of Unfired Pressure Vessels*, American Society of Mechanical Engineers, New York, 1949.

[2] J. C. Wilson and R. G. Berggren, *Am. Soc. Testing Materials Proc.* 55, 689 (1955).

[3] R. G. Berggren and J. C. Wilson, *Solid State Semiann. Prog. Rep. Aug. 30, 1956*, ORNL-2188, p 36.

[4] R. G. Berggren and J. C. Wilson, *Recent Data on the Effects of Neutron Irradiation on Structural Metals and Alloys*, ORNL CF-56-11-1 (Jan. 30, 1957).

normalized as ½-in. plate, and one was normalized as 4-in. plate. The increase in ductile-brittle transition temperature at about 10^{20} neutrons/cm^2 (>1 Mev) varied from 125°F to about 300°F, and the decrease in "ductile" fracture energy varied[3,4] by a factor of 3. Tensile test results also showed variations in the susceptibility to radiation effects, as evidenced by the uniform elongation.

The effect of grain size upon the sensitivity of a steel to neutron irradiation was studied by irradiation of two similar steels, one of which was aluminum-killed to secure a fine-grained structure. The results of these tests[4] indicate that the fine-grained steel was less sensitive to neutron irradiation. There is some evidence also that the radiation effects in the fine-grained steel saturate at a lower dosage.

A comparison of irradiation effects on base-metal and weld-metal properties was made by irradiation of notch-impact and tensile-test specimens of a 4-in.-thick carbon-steel weldment (E-7016 welding rod) in ASTM A-212 grade B steel made to fine-grain practice. The results[4] are shown in Figs. 36 and 37. The curves for the unirradiated specimens

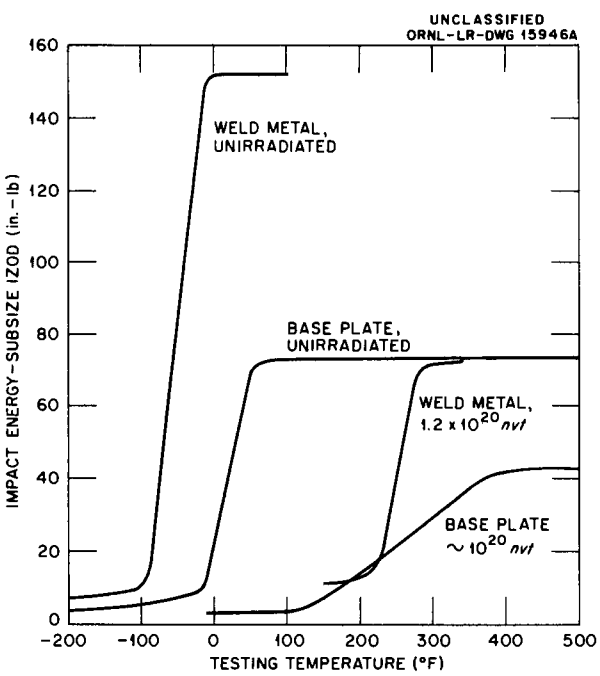

Fig. 36. Subsize Notch-Impact Results for Irradiated Carbon Steel Weld (E-7016 Rod) in ASTM A-212 Grade B Steel Plate (Items 65 and 65W).

show the better strength and fracture characteristics generally associated with weld metal in comparison with the base metal. The notch-impact tests of the irradiated metal (Fig. 36), however, show only a slight difference between the weld metal and the base metal. The same is true for the yield strengths of the weld and the base metal (Fig. 37). However, there was a marked difference in behavior during plastic deformation. The irradiated weld-metal specimens showed no observable uniform elongation, but localized deformation occurred immediately after initial yielding.

Several experimental heats of low-manganese steel were furnished for test by the Jones & Laughlin Steel Corporation.[5] These steels were made with a low manganese content to minimize the high-level, short-lived activation from manganese in reactor components or coolants. Analyses and mechanical properties are listed in Table 6; the impact tests have not yet been run. Some interesting characteristics were observed. Steel RH-1032 appears to be at least as resistant to irradiation-induced loss in ductility as any steel yet tested: this steel shows the greatest uniform elongation of any steel yet tested with a dose of 10^{20} neutrons/cm^2. Steels RH-1051 and RH-1053 have 1% or less uniform elongation after 10^{20} neutrons/cm^2, and the stress-strain curves (showing virtually no work-hardening) are similar to those of high-purity iron and irradiated E-7016 weld metal.[4] Since all these alloys (E-7016, high-purity iron, and steels RH-1051 and RH-1053) have low carbon contents compared with the bulk of the steels tested, there is preliminary indication that a carbon content of 0.20% or greater gives greater resistance to radiation effects than a carbon content of 0.06%. From the data on RH-1032, compared with a number of other steels with similar carbon contents, it appears that a high manganese-carbon ratio is not necessary for radiation resistance. All the Jones & Laughlin steels (RH-1032, RH-1051, RH-1053) were fully killed and of relatively high aluminum content. Aluminum-killing alone apparently is not sufficient to bestow radiation resistance upon a steel. Although all three steels would be regarded as fine-grained, heat RH-1032 had a finer grain size (ASTM 8) than the others (ASTM 6). The above

[5] H. F. Beeghly, "Low Manganese Steels for Nuclear Applications," paper presented at Engineers Joint Council Nuclear Congress, Cleveland, 1955.

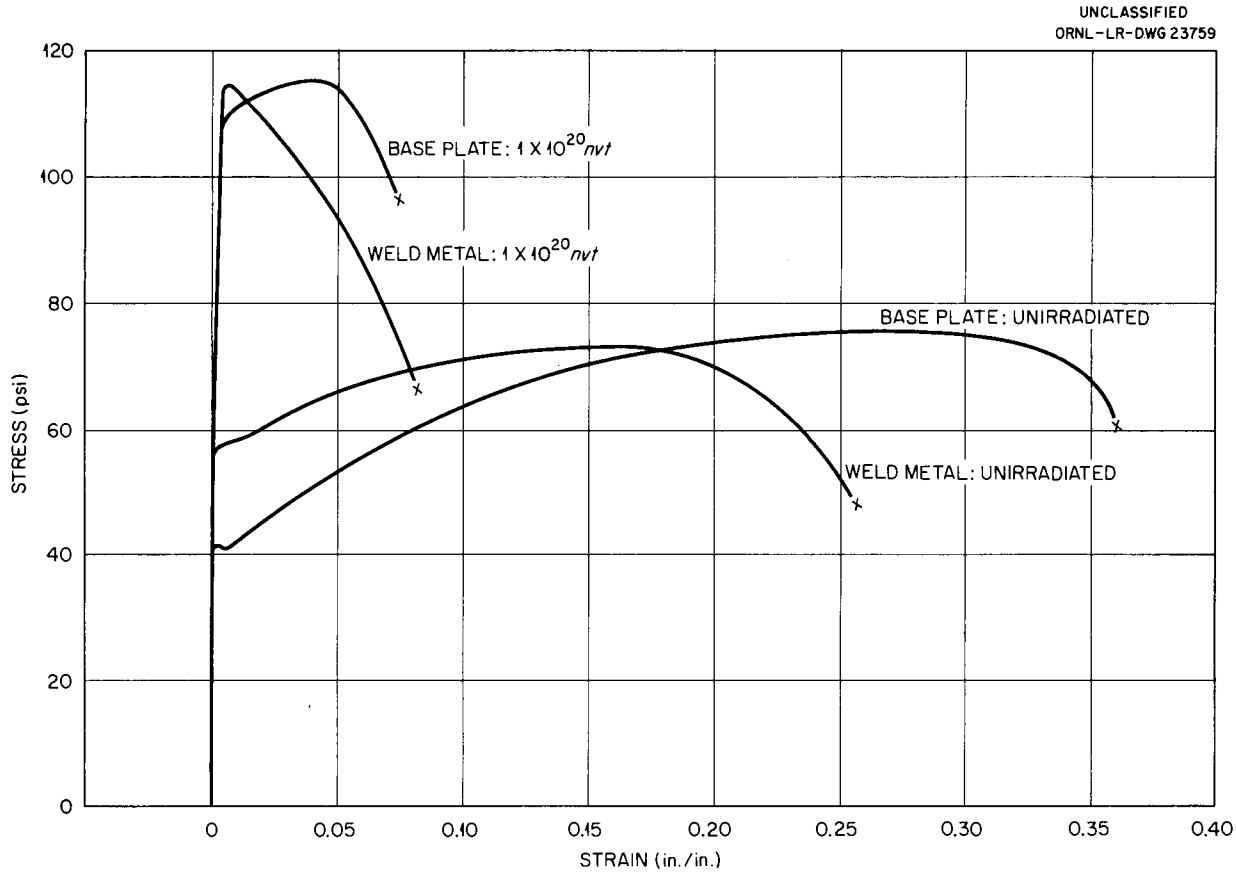

Fig. 37. Conventional Stress-Strain Curves for Irradiated E-7016 Carbon-Steel Weld Metal (Item 65W), in Fine-Grain ASTM A-212-B Carbon-Silicon Steel (Item 65).

Table 6. Tensile Properties of Low-Manganese Steel

Normalized from 1700°F and irradiated in the MTR below 200°F

Designation	Composition (wt %)	Integrated Fast (>1 Mev) Flux (*nvt*)	Yield Strength (psi)	Tensile Strength (psi)	Uniform Elongation (%)	Necking Elongation (%)	Total* Elongation (%)
RH-1032	0.21 C, 0.09 Mn, 0.009 P, 0.015 S, 0.18 Si, 0.009 Al, 0.14 Ti	0	57,200	78,000	17.4	10.8	28.2
		1.7×10^{19}	87,600	90,000	3.6	10.4	14
		1×10^{20}	85,800	101,200	7.8	5.8	13.6
RH-1051	0.07 C, 0.15 Mn, 0.011 P, 0.029 S, 0.07 Si, 0.048 Al, 0.39 Cu, 0.42 Ti	0	27,600	51,100	29.5	15.5	45
		1.7×10^{19}	82,600	82,600	0	9.5	9.5
		1×10^{20}	97,600	98,500	0.5	8.0	8.5
RH-1053	0.05 C, 0.08 Mn, 0.006 P, 0.018 S, 0.06 Si, 0.30 Al, 0.39 Cu, 0.33 Zr	0	45,600	55,500	25	10	35
		1.7×10^{19}	82,900	80,600**	0.5	10	10.5
		1×10^{20}	98,400	98,000**	1.0	6.5	7.5

*Elongation in approximately five diameters.
**Computed from maximum load reached after yield-point elongation.

information, while tentative, gives the first useful information yet obtained on the effect of composition and mill practice on radiation effects in steel.

The use of the conventional elongation in the tensile test as an index of ductility is frequently a part of metals specifications. The conventional elongation is made up of the uniform elongation that occurs up to the point where necking begins and of the localized elongation that takes place during necking. Since irradiation appears to reduce the uniform elongation more than the elongation during necking[4] (in a number of steels, high-purity iron, and weld metal, Fig. 37), the conventional elongation does not appear to be a sensitive or meaningful quantity to indicate the usable ductility of an irradiated steel. In Fig. 37 it may seem that the conventional (total) elongation of the base plate is about 7% at 10^{20} *nvt*. The total elongation of the weld metal is about 8% at the same dose. On the basis of the conventional elongation, the metals would be regarded as having about equal ductilities; but from the stress-strain curves it is obvious that the base plate is the better engineering material because, in the weld metal, necking would occur almost immediately upon stressing past the yield stress. Accordingly, the uniform elongation is recommended as a more useful ductility criterion than the conventional elongation in irradiated steels.

An unusual fracture appearance has been noted in Charpy V-notch impact specimens of irradiated steel: bright facets (indicating cleavage of grains) have appeared dispersed over a nominally ductile fracture surface. In unirradiated normalized steels this phenomenon is not observed; the faceted (cleavage) areas occur in certain well-defined regions of the fracture surface. Thus fracture appearance does not seem to be a useful criterion for comparing the ductile-brittle characteristics of irradiated and unirradiated metals because of the differences in fracture morphology. The change in fracture appearance is being studied by metallographic examination of sections taken through the fracture faces.

Irradiation and Testing Facilities

Most of the effort this year went into design, construction, and operation of irradiation apparatus. The backlog of specimens to be tested equals in number all the previous data combined; two experiments are presently under irradiation in the MTR and two more are under construction.

ORNL-MTR-10-5 was irradiated in the HB-3 facility of the MTR, and specimen testing has started. This experiment contained notch-impact and tensile specimens of four austenitic stainless steels, four carbon steels, a carbon-steel weld metal, four low-alloy steels, a Zircaloy-2 weld, and tensile specimens of Zr–15% Nb alloy in two conditions of heat treatment. The experiment was designed to utilize gamma heating in the reactor to maintain an elevated specimen irradiation temperature. The specimen chamber is shown in Fig. 38. Three layers of tensile and impact specimens are stacked on the opposite faces of the massive stainless steel wedge. The heat generated by gamma-ray absorption in the wedge and specimens is conducted out to the aluminum water jacket through the specimens. Specimens in contact with the wedge were at about 800°F during irradiation; specimens in contact with the water jacket were at about 400°F. The angle of the wedge is determined by the gamma-heating gradient so that uniform heating results.

ORNL-MTR-10-6 is being irradiated in a lattice piece of the MTR. This experiment contains 100 tensile specimens of titanium and various stainless steels. The specimens are maintained at approximately 100°F during irradiation.

ORNL-MTR-10-8 is currently being irradiated in the HB-3 facility of the MTR. This experiment contains Izod and Charpy impact specimens and tensile specimens of a number of carbon steels. Irradiation temperatures are less than 300°F. The experiment is designed to obtain data for comparison with those from ORNL-10-5 (above) as a function of irradiation temperature.

ORNL-10-9 is being assembled for irradiation in the MTR. It contains specimens of several carbon steels for comparison of the effects of specimen size and heat treatment.

ORNL-10-10 has been designed and construction will begin soon. This experiment will contain notch-impact and tensile specimens of a number of titanium and zirconium alloys and will operate at an elevated temperature (600°F).

Preparations are being made for irradiation of specimens in the HRT, ORR, and ETR.

UNCLASSIFIED
PHOTO 18805

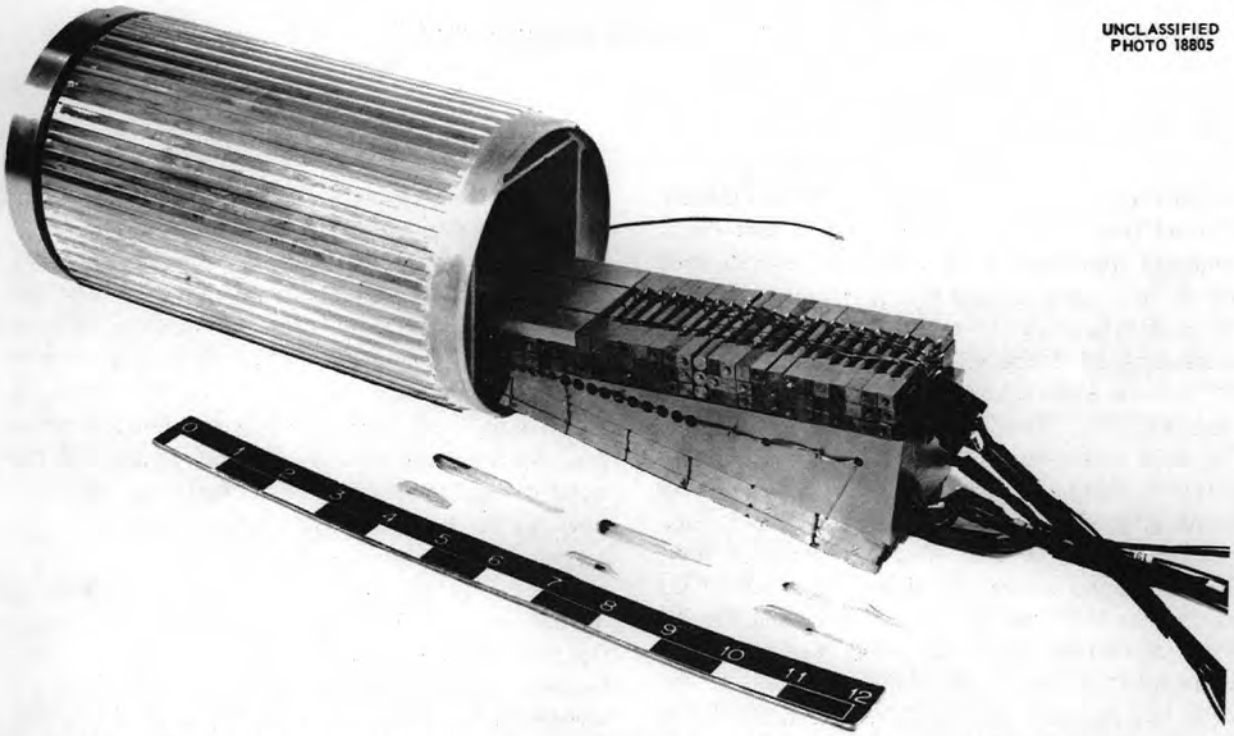

Fig. 38. Gamma-Heated Specimen Irradiation Apparatus for MTR Beam Hole Facility (ORNL-MTR-10-5).

Hot-cell testing of irradiated specimens has been delayed by mechanical failure of two items of hot-cell equipment, the impact machine and the remotely controlled extensometer. An improved, remotely controlled subsize impact machine has been built and has been placed in operation. Some comparison tests have been conducted in conjunction with the Naval Research Laboratory to correlate data from the subsize Izod test with the standard V-notch Charpy test. This study will be continued with irradiated specimens as soon as specimens and testing machines become available.

Procedures for photography of fractured radioactive test specimens and measurements of reduction of area and elongation have been developed.

The study of the effect of parameters such as metal composition, heat treatment, and irradiation temperature will be continued. Increased emphasis will be given to the properties of irradiated weldments, changes in fracture characteristics due to irradiation, and effects in relatively high-purity irons and steels.

RADIATION STABILITY OF CERAMIC MATERIALS

O. Sisman

C. D. Bopp R. L. Towns

A summary[1] has been given of radiation effects measured for a selection of ceramic materials. Exposures were conducted in a graphite-moderated reactor to integrated epithermal fluxes of 0.8×10^{20} *nvt* (exposure *A*) and 1.6×10^{20} *nvt* (exposure *B*), and in the MTR to 0.3×10^{20} to 0.6×10^{20} *nvt* (exposure *C*) and 2×10^{20} to 6×10^{20} *nvt* (exposure *D*). The spread in the flux for the *C* and *D* exposures is caused by the gradient across the test hole. The epithermal flux intensity for the MTR was about 3×10^{13} *nv*, and for the graphite reactor it was about one-fifth of this. For the graphite reactor the thermal flux was about 20% greater than the epithermal flux, and for the MTR the thermal flux was about ten times the epithermal flux. The ratio of the gamma-ray fluxes in the two reactors is roughly proportional to the ratio of the thermal fluxes. The temperature was less than 100°C for the exposures in both reactors.

For the *D* exposure, changes in some of the properties will be described here; for the other exposures, the x-ray diffraction, thermal conductivity, Young's modulus, and density were reported earlier. During the *A* and *B* exposures the materials were sealed in an inert atmosphere, but one material was subject to corrosion by decomposition products from the others; during the *C* and *D* exposures the materials were subject to corrosion by the reactor cooling water in which they were immersed. In order to study radiation effects in the absence of surface corrosion, an irradiation exposure is being made in which each material is sealed in a separate container. The irradiation containers are envelopes made of 20-mil aluminum sheet and are sealed by welding in an argon atmosphere. The exposure will be conducted under the higher flux conditions listed for the *C* and *D* exposures, and there will be some gamma heating. In order to keep the temperature as low as possible, thin specimens (20 mils) are employed, and the layer of specimens in a sample container is only one or two specimens thick.

Materials which were largely dissolved by the corrosive action of the water in the *D* exposure include pressed beryllium oxide, steatite, pressed magnesium oxide, and forsterite. Materials which broke up because of a large loss in strength were glass-bonded mica, asbestos, lead glass, and pyrex glass.

In Table 7 are listed the effects of radiation on the thermal conductivity and the density of the materials which remained intact for the *D* exposure. Changes for the *C* exposure have already been reported, but are also listed in Table 7 for comparison. The density was determined by weighing in air and in kerosene, as already described.[2] Density changes for sapphire were also determined by x-ray diffraction,[3] and the two methods agreed within the accuracy indicated in Table 7. The method of measuring thermal conductivity[4] was modified, in that the apparatus was not evacuated. The contact resistance between the mercury and the specimen is less and is more uniform in air than in a vacuum, and the low contact resistance makes possible measurements for thin specimens of such high-conductivity materials as sapphire and beryllium oxide. The conductivity of porous materials is more reproducible in air than in a vacuum. The dimensional stability of plate glass and of silica glass is poor under irradiation, and specimens of these materials were warped after exposure. This prevented sensitive thermal conductivity measurements.

The annealing characteristics of the radiation changes are important, both for predicting the effect of the temperature of irradiation and for studying the nature of the radiation-produced defects. Thermal conductivity measurements made on materials given the *C* exposure show only a small change between 350 days after removal from the reactor and 750 days after removal. An apparatus is being developed for the study of annealing

[1] *Ceramic Information Meeting Held at Oak Ridge National Laboratory on October 1, 2 and 3, 1956*, TID-7530 (Pt. 1).

[2] C. D. Bopp and R. L. Towns, *Solid State Semiann. Prog. Rep. Aug. 30, 1956*, ORNL-2188, p 31–32.

[3] Measurements by F. A. Sherrill, Solid State Div.

[4] O. Sisman, C. D. Bopp, and R. L. Towns, *Solid State Semiann. Prog. Rep. Feb. 28, 1955*, ORNL-1852, p 33–34.

Table 7. Effect of Radiation on Thermal Conductivity and Density

Material	Initial Value		Exposure *C*, *nvt* $\times 10^{19}$	After Exposure *C*		Exposure *D*, *nvt* $\times 10^{19}$	After Exposure *D*	
	Thermal Conductivity* (cal/°C·cm·sec) $\times 10^{-4}$	Density** (g/cm^3)		Thermal Conductivity* (cal/°C·cm·sec) $\times 10^{-4}$	Density** (g/cm^3)		Thermal Conductivity* (cal/°C·cm·sec) $\times 10^{-4}$	Density** (g/cm^3)
Sapphire	600 ± 200	3.983 ± 0.001	6	300 ± 60	3.969 ± 0.001	60	200 ± 30	3.944 ± 0.001
Al_2O_3 sintered	400 ± 100	3.559 ± 0.001	3	230 ± 40	3.553 ± 0.002	40	90 ± 5	3.80 ± 0.04
BeO	600 ± 200	2.84 ± 0.03	7	400 ± 100	2.85 ± 0.02			
Spinel	250 ± 50	3.60 ± 0.01	7	130 ± 10	3.60 ± 0.01	40	130 ± 10	3.60 ± 0.01
Forsterite 243	250 ± 50	3.056 ± 0.004	6	75 ± 10	3.03 ± 0.01			
Zircon 475	120 ± 10	3.73 ± 0.01	5	23 ± 1	3.48 ± 0.01	30		3.38 ± 0.01
Steatite	76 ± 5	2.796 ± 0.005	7	28 ± 1	2.760 ± 0.005			
Cordierite 202	73 ± 5		5	20 ± 2		30	20 ± 2	
TiO_2 192	165 ± 20	4.01 ± 0.01	6	110 ± 10	3.99 ± 0.01	30	65 ± 5	3.98 ± 0.01
Porcelain 576	270 ± 50	3.41 ± 0.01	6	120 ± 10	3.40 ± 0.01	40	85 ± 5	3.39 ± 0.01
Mica	17 ± 1	2.845 ± 0.001	4	12 ± 1	2.738 ± 0.002	20	28 ± 3	2.444 ± 0.002
Plate glass	25 ± 1	2.509 ± 0.001	3		2.530 ± 0.001	60		2.515 ± 0.001
Silica glass	35 ± 1	2.204 ± 0.001	7		2.255 ± 0.001	40		2.23 ± 0.01
Quartz, Brazilian		2.65 ± 0.01	5		2.27 ± 0.01	40		2.24 ± 0.01

*At 30°C.
**At 25°C.

at elevated temperatures both by dynamic property changes and by calorimetry. The work this past year has been confined to dynamic testing along the lines already described.[5] Provision has been made for changing the temperature between −100 and 500°C. The mode of bending in which the specimen vibrates is determined by the positions of clamping and driving the specimen; for this reason it is important that these positions shift as little as possible when the temperature is changed. Since the stress dependence of the elastic modulus and of the internal friction is simplest at low stresses, it is desirable to employ as low a stress as is permitted by the sensitivity of the vibration pickup. It has been found that sometimes, as the temperature is changed, the mode of vibration which is being followed disappears and a slightly different mode of vibration is favored. At intermediate temperatures both modes of vibration exist, and the two frequencies may be so close together as to give a resonance curve with a double peak. The appearance and disappearance of resonances introduce a complication in studying the temperature dependence of the dynamic properties. Different methods of clamping and driving are being investigated to determine the conditions under which double peaks occur least frequently.

A change in Knoop hardness (with the Tukon indenter) was measured for the materials listed in Table 8. The specimens were fine grained and highly polished, and a light load (100 g) was employed in order to prevent fracturing. It was necessary to employ a 2-kg load for coarser-grained pressed materials in order to obtain an impression which was distinguishable from the texture of the material. Even then the sensitivity of the measurement was less than would be required to detect a change of the same order as that measured for the Young's modulus.[6] It is not to be expected that the change in hardness and the change in modulus will run parallel for the coarser-grained materials, since the heavy load probably causes fracturing.

[5] C. D. Bopp and R. L. Towns, *Solid State Semiann. Prog. Rep. Aug. 30, 1956*, ORNL-2188, p 31, esp 33–35.

[6] C. D. Bopp, O. Sisman, and R. L. Towns, *Solid State Semiann. Prog. Rep. Feb. 29, 1956*, ORNL-2051, p 24, esp 27–29.

Table 8. Effect of Irradiation on the Knoop Hardness Number*

	Before Irradiation	After the *C* Exposure	After the *D* Exposure
Mica	113 ± 10		440 ± 10
Plate glass	120 ± 20	145 ± 10	440 ± 15
Quartz, Brazilian (polycrystalline)'	800 ± 100	500 ± 100	400 ± 100

*100-g load.

INFRARED SPECTRA OF PLASTICS AND ELASTOMERS AFTER IRRADIATION

W. W. Parkinson W. C. Sears[1] O. Sisman

As a part of the investigation of the physical and chemical changes produced in organic polymers by high-energy radiation, the infrared spectra of several materials have been measured before and after irradiation.[2,3] Irradiations of thin samples of poly-α-methylstyrene and polyethylene terephthalate (Mylar) have been continued in hole C-46 of the LITR in order to obtain usable specimens having appreciable doses. The polymethylstyrene specimens were found to deteriorate beyond usefulness at doses as low as 2×10^9 ergs/g (2×10^7 rads), and no spectra were obtained after irradiation. The infrared spectrum of a typical polyethylene terephthalate specimen after 3.9×10^{11} ergs/g (3.9×10^9 rads) is shown in Fig. 39. The specimens were contained in evacuated quartz tubes during irradiation, and the spectra after irradiation were measured, first without exposure to air, then after exposure to air for various periods.

Although the infrared spectrum does not show extensive changes after irradiation, the specimens were rendered so brittle that manipulation was difficult. The most important changes in the spectrum are the indications of chain cleavage and of a loss of crystallinity. The reduction in the band at 1125 cm^{-1} due to C–O stretching vibrations indicates a rupture of the ester linkage. The growth of a band at 1615 cm^{-1} suggests an increase in the carboxylate ion, so that it is not clear whether CO_2 is evolved, as in the case of radiolysis of simple acids and esters,[4,5] or whether decomposition is limited to breakage of the ester bond. Absorption is complete in the C=O stretching band at 1725 cm^{-1} and in the C–O stretching band at 1260 cm^{-1}, so that these bands are insensitive to small changes in concentration and cannot be useful in indicating loss of CO_2 in specimens of this thickness.

The loss of crystallinity resulting from irradiation is shown by changes in three peaks, that at 1345 cm^{-1}, due to the C–H bending vibration in the $\overset{H}{\overset{|}{C}}-O$ groups, and the bands at 975 and 1040 cm^{-1}. The band at 1040 cm^{-1} has been found to decrease slightly upon crystallization, while those at 1345 and 975 increase markedly.[6] In addition to the decrease in the crystalline-to-amorphous ratio, there is a conversion of $-CH_2-$ to $-CH_3$, shown by the decrease in the $-CH_2-$ deformation band at 1415 cm^{-1} and the increase in $-CH_3$ deformation at 1375. After exposure of vacuum-irradiated specimens to air for periods up to 30 days, the spectrum did not show formation of –OH oxidation products at 3400 cm^{-1}, and the C=O peak at 1725 cm^{-1} is saturated, so that increases in this species would not be perceptible.

The hydrocarbon polymers previously studied[2] showed significant changes in the infrared peaks associated with the C=C group, and the absorptivities of these peaks are being measured to derive quantitative relations from the spectra. The C=C group occurs in several isomeric arrangements in the polymers: cis, trans, terminal, and, in polyethylene, vinylidene, or side-chain. The attached hydrogen atoms have characteristic bending frequencies, but in practice there is a small amount of absorption by each species at the characteristic frequency of the others. This overlapping of peaks varies with the optical properties of the individual spectrophotometer. Therefore, in determining absorptivities from pure compounds containing only a single type of C=C group, not only must the absorptivity at the characteristic frequency be measured but also the absorptivities at the characteristic frequencies of each of the other isomeric types.

To determine the concentrations of the various C=C groups in a sample, the measured absorbances

[1] Consultant, University of Georgia.

[2] W. C. Sears, W. W. Parkinson, and W. K. Kirkland, *Solid State Semiann. Prog. Rep. Aug. 30, 1956*, ORNL-2188, p 26.

[3] W. C. Sears *et al.*, *Solid State Semiann. Prog. Rep. Feb. 29, 1956*, ORNL-2051, p 16.

[4] C. W. Sheppard and V. L. Burton, *J. Am. Chem. Soc.* 68, 1636 (1946).

[5] I. A. Breger, *J. Phys. & Colloid. Chem.* 52, 551 (1948).

[6] W. H. Cobbs, Jr., and R. L. Burton, *J. Polymer Sci.* 10, 275 (1953).

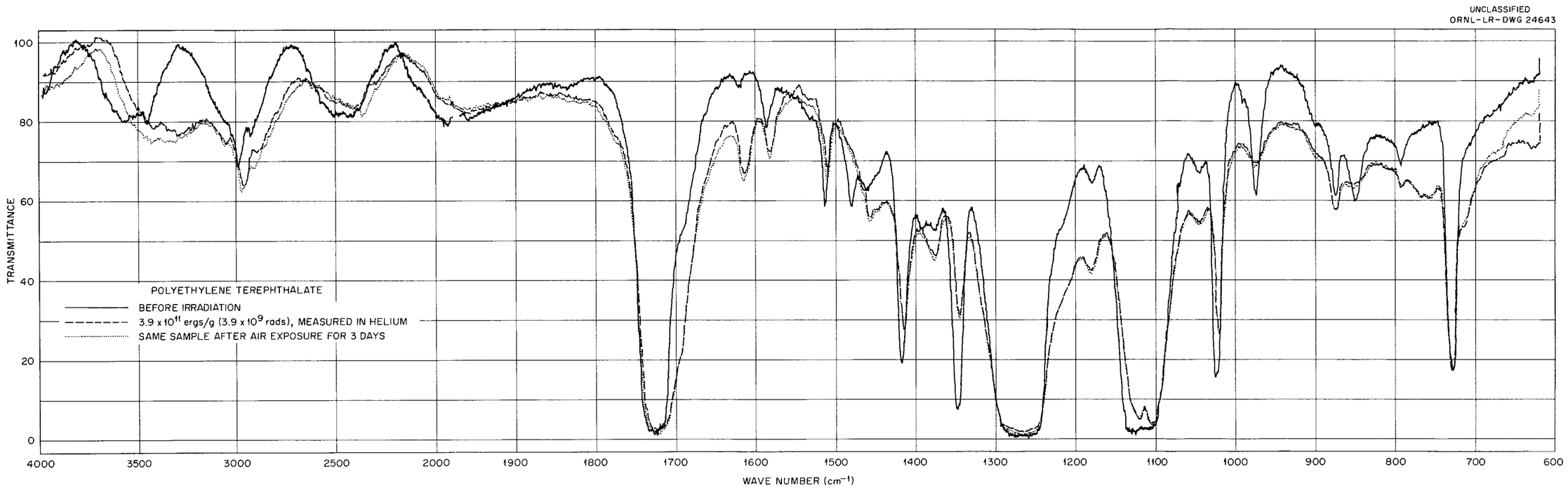

Fig. 39. Infrared Spectra of Polyethylene Terephthalate Before and After Irradiation in a Vacuum.

at the appropriate peaks can be related with the absorptivities of each C=C isomer by means of simultaneous equations of the type below (for the case of three C=C isomers):

$$A_1 = l\,(a_{1x}c_x + a_{1y}c_y + a_{1z}c_z)\ ,$$
$$A_2 = l\,(a_{2x}c_x + a_{2y}c_y + a_{2z}c_z)\ ,$$
$$A_3 = l\,(a_{3x}c_x + a_{3y}c_y + a_{3z}c_z)\ .$$

In these equations A is the measured absorbance, l is the thickness, a is the absorptivity for a single isomer determined from a pure compound, and c is the concentration of the isomer. The subscript numbers refer to frequencies, while the subscript letters refer to isomers.

The absorptivities of the C=C group were measured in four isomeric octenes. These absorptivities were used to calculate the concentrations of the three isomeric types in polybutadiene. These concentrations should total one C=C group per four-carbon monomer unit in high-molecular-weight material, but the experimental results were considerably lower than this. The discrepancy is due to inapplicability of the absorptivities determined on solutions of octenes in carbon disulfide to the absorbances of solid films. To obtain more precise analyses, absorptivities are being determined from solid polybutadiene standards of known C=C content which were obtained recently.

EFFECTS OF HIGH-ENERGY RADIATION ON POLYMERS

R. F. Hornbeck[1] W. K. Kirkland
W. W. Parkinson O. Sisman

The cross-linking and the scission of vinyl polymers have been investigated to determine the influence of initial molecular weight and radiation field intensity. Polystyrene, which is cross-linked by radiation, and polymethyl methacrylate, which undergoes scission, were selected as sample materials. Molecular weights were determined by measurements of the viscosity of dilute solutions of the polymers. The fractionation of stock material into samples of various molecular weights by precipitation techniques was described in the previous report.[2] After compression-molding to obtain bulk material from the fibrous fractionation product, the samples were sealed in evacuated quartz tubes for irradiation.

The scission study on polymethyl methacrylate was carried out in the ORNL Graphite Reactor (water-cooled hole 19), since low doses produce adequate effects. The doses were measured by the activation of cobalt foils irradiated with the specimens. Thermal-neutron activation was converted to energy absorbed in the polymer by the relation[3] $D = (2f + 0.2)\,\phi_t \times 10^{-7}$, where the absorbed energy, D, is in ergs/g, f is the weight fraction of hydrogen, and ϕ_t is the thermal-neutron exposure. After irradiation the molecular weights of the specimens were determined in order to indicate the amount of scission produced. The number-average molecular weights of the specimens were calculated from the measured solution viscosities by the following relation:

$$M_n = \frac{1}{1.9}\left(\frac{[\eta]}{5.7 \times 10^{-5}}\right)^{1.32},$$

where the constants are empirical, and the viscosity term $[\eta]$, in centipoise-deciliters per gram, represents the contribution of the polymer to the viscosity of the solution per unit of concentration, extrapolated to infinite dilution. The molecular weights, exposures, and energy required per scission are recorded in Table 9.

It was expected that the energy required per scission would be independent of molecular weight. However, the relation between the solution viscosities measured and the number-average molecular

[1]On loan from the Glenn L. Martin Co.

[2]W. W. Parkinson, W. K. Kirkland, and R. F. Hornbeck, *Solid State Semiann. Prog. Rep. Aug. 30, 1956*, ORNL-2188, p 30.

[3]C. D. Bopp and O. Sisman, *Nucleonics* 13(7), 28, esp 33 (1955), corrected as described at the end of this section.

Table 9. Molecular Weight Measurements of Irradiated Polymethyl Methacrylate of Various Molecular Weights

Molecular Weight		Number of Molecules per Gram		New Molecules or Scissions per Gram	Dose		Energy per Scission (ev)
Initial	Final	Initial	Final		Thermal *nvt*	Ergs/g	
$\times 10^6$	$\times 10^6$	$\times 10^{17}$	$\times 10^{17}$	$\times 10^{17}$	$\times 10^{16}$	$\times 10^{20}$	
1.81	0.63	3.32	9.6	6.3	0.30	0.69	110
1.31	0.50	4.60	12.0	7.4	0.30	0.69	92
0.96	0.42	6.3	14.3	8.0	0.30	0.69	86
0.42	0.22	14	27	13	0.077	0.172	13*

*This sample, the lowest molecular weight fraction, received different treatment in the final precipitation step. It is possible that this sample contained traces of a different solvent. It also received a lower total dose than the other specimens.

weight is somewhat dependent on molecular weight distribution. If the specimens had different molecular weight distributions, it is possible that the calculated molecular weights were not correct number-average molecular weights.

Samples of the same molecular weight distribution (stock polymethyl methacrylate) were irradiated for various times in the same manner as were the fractionated samples. The results of measurements of molecular weight, again by means of solution viscosities, are listed in Table 10.

The energy required per scission should not depend on exposure, and, again, it is possible that a change in the molecular weight distribution alters the relation between viscosity and average molecular weight. It has been reported that about five main-chain scissions per molecule are required to convert a uniform molecular weight distribution to a random distribution.[4] If the initial molecular weight distribution was far from random, then the moderate exposures listed would have produced different distributions in the various samples. To resolve the discrepancies in energy required for scission, further irradiations and different methods of molecular weight measurement are planned.

For measurements of cross-linking of polystyrene, irradiations were carried out in both hole 19 of the Graphite Reactor and hole C-46 of the LITR. Specimens were prepared and encapsulated in the same manner as for the polymethyl methacrylate. Both hole 19 and hole C-46 are water-cooled, but nuclear heating is an order of magnitude greater in C-46 than in 19. Cross-linking was determined by means of solvent swelling measurements as well as by viscosity determinations, since moderate radiation doses convert polystyrene to an insoluble three-dimensional network. The swelling measurements were performed by refluxing or soaking the irradiated specimens in toluene, allowing them to drain to surface dryness, and then weighing the swollen specimens. Finally, the specimens were thoroughly dried under vacuum and were weighed to obtain the ratio of swollen weight to dry weight. This ratio is an index of the number of monomer units between cross links.

The results of viscosity determinations of molecular weights of irradiated styrene are presented in Table 11. These results indicate that the energy required per cross link is independent of initial molecular weight and total dose, within the ranges covered.

The swelling-ratio determinations on two series of specimens, one irradiated in hole C-46 of the LITR and the other in hole 19 of the Graphite Reactor, do not lie on the same curve of swelling vs absorbed energy. The discrepancy could be due to an intensity effect but is in the direction to be expected if specimen temperatures were higher in the LITR. The specimen temperatures will be better controlled for the continuation of this investigation of the influence of radiation intensity and total exposure on cross-linking.

The energies required per scission or per cross link, as measured above for Graphite Reactor irradiations, indicated that a modification was needed in the equation of Bopp and Sisman,[3] which relates thermal-neutron flux in hole 19 to

[4] A. Charlesby, *Proc. Roy. Soc.* (London) A224, 126 (1954).

Table 10. Molecular Weight Measurements of Polymethyl Methacrylate Irradiated for Various Periods

Molecular Weight		Number of Molecules per Gram		New Molecules or Scissions per Gram	Dose		Energy per Scission (ev)
Initial	Final	Initial	Final		Thermal *nvt*	Ergs/g	
$\times 10^6$	$\times 10^6$	$\times 10^{17}$	$\times 10^{17}$	$\times 10^{17}$	$\times 10^{16}$	$\times 10^{20}$	
1.34	0.63	4.5	9.55	5.0	0.15	0.34	68
1.34	0.61	4.5	9.90	5.4	0.23	0.53	97
1.34	0.47	4.5	12.8	8.3	0.45	1.04	130

Table 11. Molecular Weight Changes in Irradiated Polystyrene

Molecular Weight		Number of Molecules per Gram		Difference, or Number of Cross Links per Gram	Dose (ev/g)	Energy per Cross Link (ev)
Original	Final	Original	Final			
$\times 10^5$	$\times 10^5$	$\times 10^{18}$	$\times 10^{18}$	$\times 10^{18}$	$\times 10^{20}$	
2.42	2.82	2.49	2.14	0.35	4.56	1350
6.27	10.6	0.96	0.57	0.39	4.56	1200
2.79	3.24	2.16	1.86	0.30	4.56	1550
1.09	1.17	5.53	5.15	0.38	4.56	1200
0.32	0.36	19.0	17.0	2.0	16.2	800
2.4	2.6	2.5	2.3	0.2	2.3	1150
2.4	3.5	2.5	1.7	0.8	9.4	1150

total energy deposited in a hydrocarbon. The use of the original equation,

$$D = (4.8f + 0.31)\,\phi_t \times 10^{-7} ,$$

with the symbols defined above, results in values about twice those reported in the recent literature. Gas-evolution measurements described below also show that the energies calculated from the equation are high. The equation was derived from calorimetric and flux measurements made in the center of the reactor. It did not allow for thermalization of the fast flux by the cooling water surrounding the sample containers and by the samples themselves. It has been found that for the average loading in hole 19 the thermal flux is about 30% higher than might be expected from flux distributions through the reactor. Hence the constant term in the original equation,

$$D = (4.8f + 0.31)\,\phi_t \times 10^{-7} ,$$

should be reduced by about 30%. The term including the hydrogen content accounts for energy from fast-neutron scattering, so that it should possibly be reduced by 60%. Then an approximate equation would be

$$D = (2f + 0.2)\,\phi_t \times 10^{-7} \text{ ergs/g} .$$

Calorimeteric measurements are planned for hole 19, to obtain a more accurate conversion from thermal flux to energy absorbed.

ANALYSIS OF GASES EVOLVED BY IRRADIATION OF POLYMERS

R. F. Hornbeck[1] W. W. Parkinson

An apparatus for vapor-phase chromatographic analysis was obtained and was calibrated for the probable products of radiation decomposition of organic polymers. The calibration was accomplished by introducing measured volumes of either pure compounds or known mixtures into the carrier gas stream of the apparatus. The determination of hydrogen was the most serious problem in the use of the apparatus, since sample detection was by thermal conductivity. The thermal conductivity of hydrogen is slightly higher than that of the helium carrier gas, while hydrocarbon gases have considerably lower conductivities than does helium. The response to hydrogen was therefore low and in the opposite sense from the response to other gases.

To improve the sensitivity to hydrogen, argon was tried as a carrier gas. The response to hydrocarbons was low with this carrier and was found to be strongly dependent on flow rate. Therefore the apparatus was calibrated for helium carrier gas, and a series of hydrogen samples was utilized to cover the region where the response to hydrogen was not linear. Mixtures ranging from hydrogen through hexanes, including unsaturated compounds, could be covered by three columns.

[1]On loan from The Glenn L. Martin Co.

Polypropylene and several types of polyethylene were irradiated in evacuated capsules in order to establish the range of compounds for which analytical columns would have to be calibrated. The yields of the gases evolved from these samples are listed in Table 12. In all cases the amount of hydrogen by direct analysis was about 99%, while the analysis by difference gave approximately 98%. The analyses in several cases are results from only one sample, and confirmatory work is planned. The high yield of butene, C_4H_8, from Alathon 10 is especially suspect.

The ordinary polyethylene showed a larger yield of C_4 gases than of C_3 or C_5, as has been noted by others. These relative yields reflect the predominance of four-carbon-atom side chains. Heating of samples after irradiation increased the yield of all gases and the proportion of the higher hydrocarbons. An increase in the surface-to-volume ratio (comparing strip and pellet samples) also increased the higher-hydrocarbon yield. Heating of unirradiated polyethylene for several weeks at 100°C liberated an imperceptible volume of gas. It is clear that radiation-product gases are dissolved in the bulk material and must be expelled for a valid analysis of decomposition products. Additional irradiations are planned after improvements have been made in the gas handling system.

Table 12. Gases Evolved by Irradiation of Hydrocarbon Polymers

Numbers listed are milliliters per gram of sample per week in the Graphite Reactor

Gas	Low-Density (Branched) Polyethylene			High-Density (Linear) Polyethylene			Polypropylene (Strips)
	Local Stock (Strips)	Du Pont Alathon-10 (Strips)	Du Pont Alathon-10, Heated* (Strips)	Koppers Super Dylan (Strips)	Koppers Super Dylan (Pellets)	Phillips Marlex 50 (Pellets)	
Total	15.0	5.8	8.2	18.0	20.0	18.0	22.0
CH_4	0.017	0.016	0.030	0.017	0.012	0.011	0.300
C_2H_6	0.093	0.010	0.037	0.007	0.026	0.065	0.015
C_3H_8	0.009	0.001	0.0057	<0.001	0.006	<0.001	0.011
n-C_4H_{10}	0.015	0.001	0.0115	<0.001	<0.001	<0.001	~0.001
i-C_4H_{10}	<0.0002	0.0003	~0.001				0.001
C_4H_8	<0.0002	0.0063	<0.001				0.022
n-C_5H_{12}	0.003	0.0003					0.0001
i-C_5H_{12}	0.0002	0.0002					0.0001
C_6H_{14}	0.002	<0.0002					~0.00005
H_2	Balance	Balance	Balance	Balance	Balance	Balance	Balance
Structural Data** (CH_3 Groups per 1000 C Atoms)							
Total	21.5			3	3	<1.5	~333
Terminal	4.6			~2	~2	<1.5	
Methyl branches	2.5						
Ethyl branches	14.4			1	1	<1	

*Heated to 60°C for 48 hr after irradiation but before opening.

**D. C. Smith, *Ind. Eng. Chem.* 48, 1161 (1956).

EFFECTS OF RADIATION ON ENGINEERING PROPERTIES OF POLYMERIC MATERIALS

W. W. Parkinson W. K. Kirkland

Fluorobutyl Acrylate Rubber

Irradiation and testing were completed[1] for samples of compounded polyfluorobutyl acrylate rubber (1,1-dihydroperfluorobutyl acrylate), which is of interest as a solvent-resistant gasket and sealant material. The samples were cut from sheets prepared according to the usual methods of rubber compounding, in the composition given below (in parts by weight):

Polymer	100
Philblack A	35
Paraffin	1
Sulfur	1
Triethylenetetramine	1.25

The mixture had been cured at 320°F for 30 min.

The material was tested according to methods described by Sisman and Bopp.[2] The properties before and after irradiation are listed in Table 13, in which the tabulated values are the averages for several specimens.

It is apparent from the increase in density despite a weight loss, and from the increase in hardness, that there is a net cross-linking effect. The weight loss and the rapid decrease in tensile strength and in dielectric properties indicate that there is extensive chemical decomposition in addition to the cross-linking.

Impregnated Asbestos Sheet

Asbestos mat or paper impregnated with various polymers to the extent of 25 to 30% by weight has applications as electrical insulation. These materials impregnated with polyvinyl acetate, polystyrene, or silicone proved to be interesting in that the tensile strength improved considerably during irradiation. This improvement was unambiguous, although several factors influenced the tensile properties. Aging, alone, for periods up to five or six months increased the tensile strength and decreased the elongation for polyvinyl acetate and polystyrene material. For this reason the properties of unirradiated samples of the same age as the irradiated specimens are plotted in Figs. 40 through 45, along with measurements on the irradiated materials. These measurements were made on specimens cut perpendicular to the fiber direction in the stock material. Samples cut parallel to the fiber direction were 15 to 30% stronger than the perpendicular specimens, but the changes from radiation were comparable.

Since aging increased the tensile strength in two of the materials, perhaps by increasing the

[1] W. W. Parkinson, W. K. Kirkland, and R. F. Hornbeck, *Solid State Semiann. Prog. Rep. Aug. 30, 1956*, ORNL-2188, p 30.

[2] O. Sisman and C. D. Bopp, *Physical Properties of Irradiated Plastics*, ORNL-928 (June 29, 1951).

Table 13. Effects of Radiation on Fluorobutyl Acrylate Rubber

Dose, thermal neutrons/cm^2	Unirradiated	0.23×10^{18}	0.45×10^{18}	1.73×10^{18}	5.1×10^{18}
ergs/g		0.58×10^{10}	1.1×10^{10}	4.3×10^{10}	13×10^{10}
Density, g/cc	1.6367	1.6410	1.6421	1.6467	1.6711
Weight loss, % of initial wt		0.15	0.73	2.2	4.4
Volume resistivity, ohm-cm	1×10^{10}	5×10^4	1×10^4	800	50
Tensile strength,* psi	1070 ± 75	840 ± 75	660 ± 40	560 ± 75	700 ± 160
Elongation at break, %	127	46	22	8	0
Dielectric strength, v/mil	86	0	0	0	0
Hardness, Shore durometer "A"	71	84	86	96	100

*The deviation listed is the average deviation. The increase for the longest exposure is caused by brittleness of the specimens.

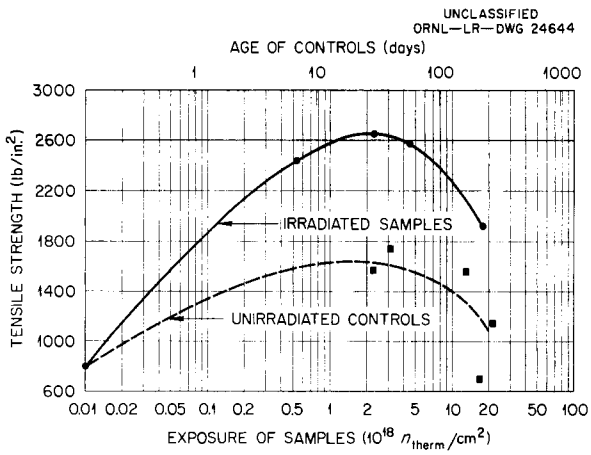

Fig. 40. Tensile Strength of Polyvinyl Acetate-Impregnated Asbestos.

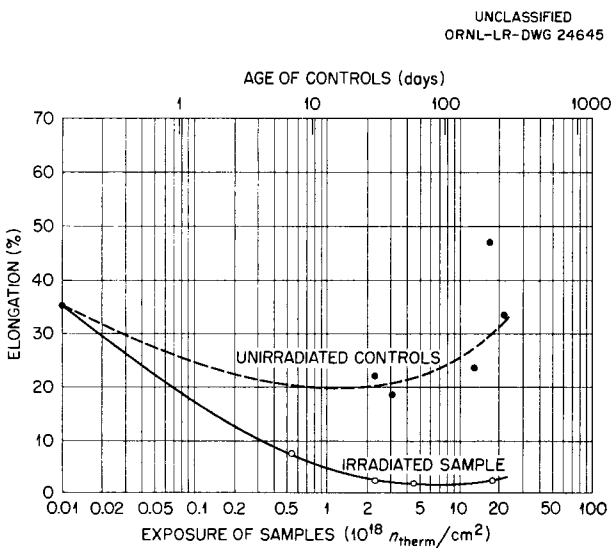

Fig. 41. Elongation of Polyvinyl Acetate-Impregnated Asbestos.

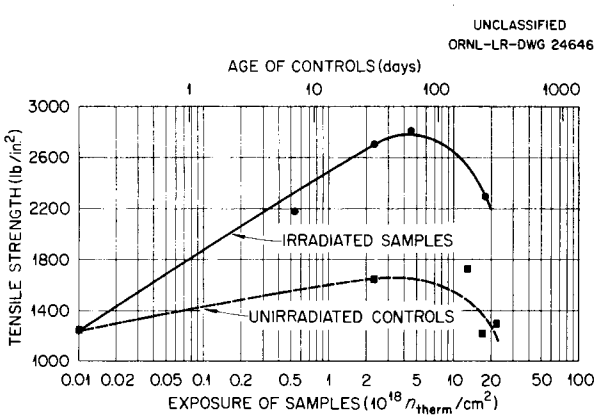

Fig. 42. Tensile Strength of Polystyrene-Impregnated Asbestos.

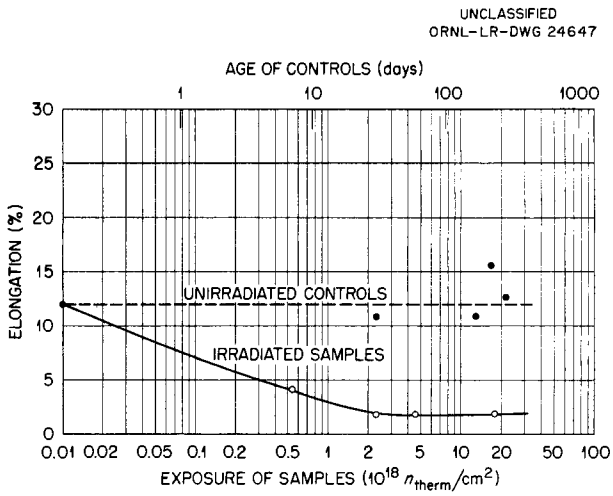

Fig. 43. Elongation of Polystyrene-Impregnated Asbestos.

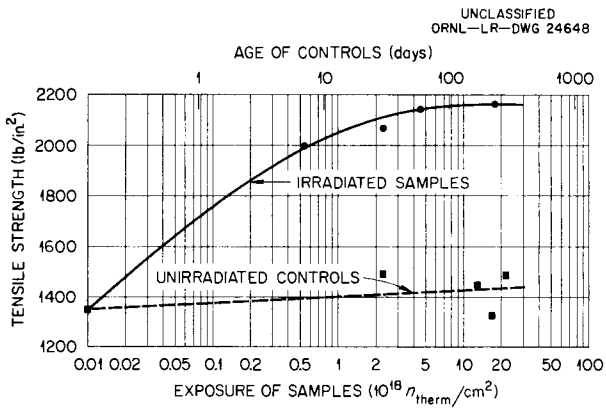

Fig. 44. Tensile Strength of Silicone-Impregnated Asbestos.

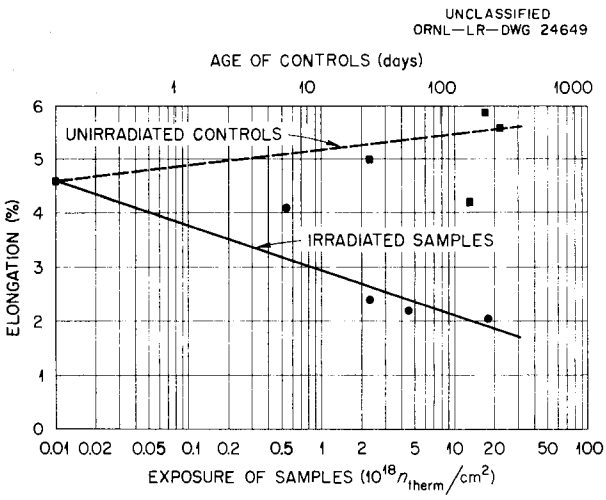

Fig. 45. Elongation of Silicone-Impregnated Asbestos.

degree of polymerization of the impregnant, samples were cured further by heating them for 8 hr at 100°C. This treatment increased the strength of silicone and polyvinyl acetate materials by about one-third the extent that radiation improved this property.

The decrease in strength for the last polyvinyl acetate and polystyrene unirradiated specimens is difficult to explain. Since temperature was controlled, but humidity was not controlled, in the testing environment, it is possible that variations in humidity affected the specimens. Samples conditioned for four days in a saturated atmosphere showed a considerable reduction in strength in the case of polyvinyl acetate material, but there was no effect on the other materials.

Radiation had an appreciable effect on the brittleness of the papers, as well as on tensile properties. Brittleness was tested by bending the specimens through 180 deg around mandrels of various radii in order to determine the minimum radius which would allow survival of 50% of the samples without visible signs of fracture. The results of the bend tests and of the usual engineering tests are listed in Table 14. The thickness of the sheet stock from which the samples were cut ranged from 4 to 6 mils.

High- and Low-Density Polyethylenes

To study the effect of physical properties on the radiation resistance of polymeric materials, two types of polyethylene have been irradiated in water-cooled hole 19 of the ORNL Graphite Reactor. The first material was low-density, or ordinary, polyethylene, while the second was high-density, unbranched material. These materials are characterized by a difference in crystallinity, about 65% in the low-density polymer and 85%

Table 14. Effects of Radiation on Impregnated Asbestos Papers

Dose (thermal neutrons/cm^2)	Tensile Strength (psi)	Elongation at Break (%)	Volume Resistivity (ohm-cm)	Dielectric Strength (v/mil)	Bend-Test Radius (in.)
		Polystyrene-Impregnated Asbestos			
0	1400	12	5×10^{12}	370	0
0.54×10^{18}	2200	4.2	6×10^{13}	340	0
2.3×10^{18}	2700	1.7	7×10^{13}	330	0.05
4.5×10^{18}	2800	1.7	8×10^{13}	320	0.07
18×10^{18}	2300	1.9		330	0.10
		Polyvinyl Acetate–Impregnated Asbestos			
0	800	20	6×10^{11}	390	0
0.54×10^{18}	2400	7.7	6×10^{12}	400	0
2.3×10^{18}	2700	2.5	2×10^{13}	340	0.08
4.5×10^{18}	2600	2.2	1×10^{13}	360	0.08
18×10^{18}	1900	2.7		430	0.10
		Silicone-Impregnated Asbestos			
0	1400	4.6	4×10^{12}	340	0
0.54×10^{18}	2000	4.1	9×10^{12}	320	0.01
2.3×10^{18}	2100	2.4	5×10^{12}	330	0.05
4.5×10^{18}	2100	2.1	6×10^{12}	340	0.07
18×10^{18}	2200	2.1		380	0.15

in the high-density polymer. Since the cross-linking process is presumed to require mobility of the molecular chains, the highly crystalline polymer should show this reaction to a lesser extent than does the ordinary polyethylene. Table 15 presents the results of measurements on the two materials before and after irradiation for various doses.

There is no conclusive evidence in these data to indicate that the cross-linking process is retarded at these dose levels in the more crystalline polymer. Such an effect has been reported for cross-linking by electron irradiation.[3] The density and hardness changes do indicate a difference in the behavior of the two materials, however. The density, which would be expected to increase as cross-linking proceeds, approaches maxima at different dose levels in the two materials. The more crystalline type of material cannot increase greatly in density from cross-linking in the amorphous regions before the radiation-produced irregularities in the crystalline regions reduce the density. The hardness measured on the Rockwell R scale, which permits recovery when the major load is removed, is sensitive to cross-linking in the amorphous regions. The α-scale measurement, performed with the total load applied, is the more indicative of crystallinity and actually shows a decrease for the highly crystalline polymer at large exposures.

[3]E. J. Lawton, J. S. Balwit, and R. S. Powell, paper presented at the American Chemical Society Meeting, Miami, Florida, April, 1957.

Polyethylene Terephthalate

The resistance of a polyester resin to radiation was investigated by measuring the tensile properties of specimens of polyethylene terephthalate (Du Pont Mylar). Specimens were cut parallel and perpendicular to the machine direction from

Table 15. Effects of Radiation on Two Polyethylenes

Dose, thermal neutrons/cm^2	0	0.24×10^{18}	0.55×10^{18}	1.1×10^{18}	3.6×10^{18}	6.5×10^{18}
ergs/g	0	1.2×10^{10}	2.6×10^{10}	5.2×10^{10}	1.7×10^{11}	3.1×10^{11}
Low-Density Polyethylene, Alathon-10 (Du Pont)						
Hardness, Rockwell R	1	26	46	76	95	98
Rockwell α	−118	−85	−74	−44	−16	17
Tensile strength, psi	1820	1780	1760	1820	770	660
Elongation, %	450	76	11	10	2	1
Shear strength, psi	1900	2100	2400	2600	2100	2200
Weight loss, %		0.05	0.13	0.26	0.70	0.95
Density, g/cc	0.923	0.926	0.928	0.928	0.923	0.924
High-Density Polyethylene, Super Dylan (Koppers)						
Hardness, Rockwell R	51	70	82	89	98	105
Rockwell α	12	36	48	55	24	23
Tensile strength, psi	3000	3600	4110	4180	2730	2530
Elongation, %	170	23	27	11	5	5
Shear strength, psi	2300	2900	3700	4000	2600	2300
Weight loss, %		0.02	0.10	0.19	0.55	0.74
Density, g/cc	0.958	0.961	0.961	0.958	0.944	0.938

0.004-in. sheet stock. Figure 46 presents the tensile strength and the elongation in terms of per cent of initial value. Except for the specimens having the two highest exposures, cross-head speed was 0.05 in./min up to 0.02 strain, then was 0.2 in./min (ASTM method D 638-46T). The specimens with the two highest exposures were brittle, and tensile measurements were subject to wide deviations, so cross-head speed was reduced to 0.01 in./min.

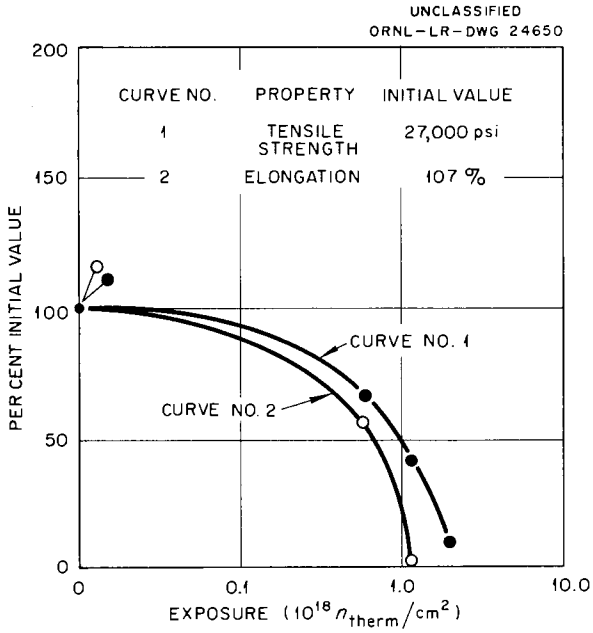

Fig. 46. Tensile Strength and Elongation of Polyethylene Terephthalate.

Infrared spectral measurements on polyethylene terephthalate have been discussed in the section "Infrared Spectra of Plastics and Elastomers After Irradiation," and it is planned to make density, viscosity, and gas-analysis studies as a further investigation of radiation-induced processes in a polyester.

Diisocyanate Polyester Rubber

Diisocyanate polyester elastomer has shown promise as a gasket material, and two sizes of O-rings of this material were tested at the suggestion of the Homogeneous Reactor Test project. The properties of the material were compared with those of natural rubber gaskets before and after irradiation under conditions simulating actual use. Samples were irradiated under compression at 135°C, and control specimens were heated at this temperature under the same compression for an equal length of time. The results of the tests are shown in Table 16. Compression-set measurements were performed according to a modification of ASTM method D395(B). Compression was only 10%, and for both materials, irradiated and unirradiated, compression set was 100%. The diisocyanate polyester, however, showed less tendency to increase in weight and hardness and therefore demonstrated a superiority to natural rubber under the test conditions.

Table 16. Comparison of Natural Rubber and Diisocyanate Polyester O-Ring Gaskets Under Radiation

	Before Treatment	Heated in Air, 135°C, 306 hr	Irradiated, 3×10^{10} ergs/g
Weight change, %			
Natural rubber (large)*		+0.80	+2.74
(small)		+1.55	+2.61
Polyester (large)		−1.16	−0.93
(small)		−1.49	−1.17
Hardness, Shore durometer			
Natural rubber (large)	68	90	95
(small)	70	90	95
Polyester (large)	72	70	77
(small)	72	71	76
Density, g/cc			
Natural rubber (large)	1.226 ± 0.004	1.272	1.274
(small)	1.223	1.277	1.275
Polyester (large)	1.245	1.236	1.248
(small)	1.252	1.249	1.249

*Refers to size of O-ring. Large rings had cross sections of 0.008 in.^{2}; small rings, 0.003 in.^{2}

MISCELLANEOUS POLYMER PROBLEMS

W. W. Parkinson
O. Sisman W. K. Kirkland

An apparatus is being designed for studying the stress-strain and stress-relaxation properties of certain plastics and elastomers while they are in the radiation field. The radiation source will be fuel elements from the ORR. The aims of these experiments are to separate the effects of cross-linking and cleavage and, by varying the temperature of irradiation, to study the effect of rigidity of the polymer on the rate of radiation-induced change. The experiment should be ready shortly after the ORR goes into operation.

A series of studies has been initiated to determine the effect of irradiation dose rate on the radiation damage rate in organic polymers. There appears to be some evidence that the changes in some materials may be dose-rate dependent. Dose rates varying by a factor of 100 are planned.

Since most of the change produced in polymers is by absorbed energy from ionizing radiation, it is most important in reactor studies on polymers to know the energy absorbed by the polymer from neutrons and from gamma radiation. These values are calculated from flux measurements. It is hoped that a much better value may be obtained for the energy absorbed in polymers by measuring it directly with hydrocarbon calorimeters. Two hydrocarbon calorimeters are now being constructed.

HIGH-FREQUENCY ELECTRICAL PROPERTIES OF SOME IRRADIATED PLASTIC MATERIALS

D. Binder R. A. Weeks

A survey of the effects of reactor and gamma-ray irradiation on the high-frequency electrical properties of some plastic materials has been completed. The materials selected for the survey were those in which the primary physical processes of chain cleavage and cross-linking have been shown to take place upon irradiation. Two others which are initially heavily cross-linked and one in which the energy imparted by irradiation with neutrons or gamma rays is absorbed without greatly altering the structure of the material were also examined. A report of this work has been prepared for publication, and an abstract of this paper is given below.

Effects of Neutron and Gamma-Ray Irradiation on the Dielectric Constant and Loss Tangent of Some Plastic Materials.[1] R. A. Weeks and D. Binder. – The loss tangent and dielectric constant of polyethylene, Teflon, polystyrene, nylon, phenol formaldehyde, and silica have been measured as a function of Co^{60} gamma-ray and reactor irradiation. The measurements were made at 4 Mc, 0.8, 1.0, 3.0, and 8.5 kMc. Relatively large changes in the loss tangent of Teflon and polyethylene were found at 0.8, 1.0, and 3.0 kMc for the maximum integrated flux used in the irradiations. The loss tangent of polystyrene, nylon, and silica did not change up to the maximum integrated flux used. A peak in the loss tangent as a function of frequency (at the maximum integrated flux) suggests the formation of polar molecular groups. The peak in the loss tangent of Teflon probably occurs at a higher frequency than in polyethylene. In heavily cross-linked materials, no effect on the molecular polarizability would be expected. The results on nylon and silica tend to confirm this suggestion.

[1] Submitted to *Nucleonics* Sept. 1957.

ATTEMPT AT THE SEPARATION OF NEUTRON AND GAMMA-RAY IRRADIATION EFFECTS BY MEANS OF A HYDROGENOUS ABSORBER

D. Binder W. W. Parkinson W. K. Kirkland

Irradiation effects in polymers may be induced by either neutrons or gamma rays.[1] The separation of these two effects in a reactor irradiation was made by Bopp and Sisman[2] by the addition of a known amount of gamma rays. Another possible technique is the degradation of the neutron energy by a hydrogenous absorber. If two polymers are irradiated with and without this absorber, a difference in irradiation effect should be detected. This difference would be caused by a diminution of the neutron effect, with little change in the gamma-ray effect. If the difference is large enough, the ratio of the neutron and gamma-ray effects could be derived. An experiment has been performed in which the change in solution viscosity of polymethyl methacrylate was used as an irradiation effect. The difference in this particular experiment was relatively small but observable.

To provide specimens irradiated with and without absorber, methacrylate sheets were packed with polyethylene sheets as the hydrogenous absorber in assemblies such as the one shown in Fig. 47. These sample assemblies were irradiated for 1 hr at full reactor power in holes 19 and 10 of the ORNL Graphite Reactor. Specimens of polymethyl methacrylate were cut from the interior of the center plate, from the top plate, and from the end pieces separated 1 to 2 in. from the polyethylene.

From the viscosities of dilute solutions of the specimens, the number-average molecular weights were calculated. The number of new molecules per gram is an indication of the number of scissions per gram, the primary radiation-induced event in the specimens. The results of the viscosity measurements are presented in Table 17. There is a reduction of the radiation effect by the polyethylene absorber or moderator. In hole 10, with its greater fluxes, there was a larger effect but less reduction in effect by the moderator. This can be explained on the basis of the temperature gradient in the assemblies. Nuclear heating and surface cooling produce higher temperatures at the center of the assemblies, and the rate of scissions increases with temperature. The less efficient cooling and higher fluxes of hole 10 produce larger temperature gradients, tending to vitiate the effect of the polyethylene, than does hole 19.

It is clear from the results of the hole-19 measurements that the gamma-ray effect cannot be larger than three-fifths of the total effect, the ratio of the number of scissions per gram for the center sample and the end sample. More definite conclusions await more efficient absorption of the neutron energy flux.

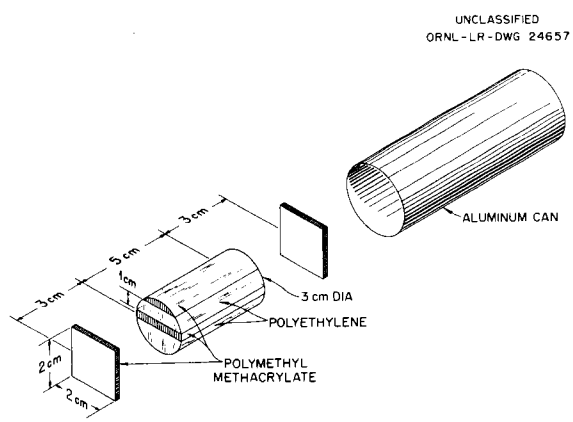

Fig. 47. Irradiation Assembly of Polymethyl Methacrylate and Polyethylene.

[1] C. D. Bopp and O. Sisman, *Nucleonics* 13(7), 28 (1955).

[2] C. D. Bopp and O. Sisman, *Radiation Stability of Plastics and Elastomers*, ORNL-1373, p 52 (July 23, 1953).

Table 17. Molecular Weight Measurements on Polymethyl Methacrylate

Reactor Position	Location in Assembly	Intrinsic Viscosity (centipoise-deciliters per gram)	Molecular Weight	Molecules per Gram	New Molecules or Scissions per Gram
			$\times 10^5$	$\times 10^{17}$	$\times 10^{17}$
Unirradiated		3.05	9.16	6.58	
Hole 19	Center	2.20	6.05	9.96	3.4
	Surface	2.05	5.42	11.12	4.5
	Separate end	1.95	5.08	11.87	5.3
Hole 10	Center	1.97	5.16	11.69	5.1
	Surface	1.90	4.93	12.25	5.7
	Separate end	1.86	4.76	12.68	6.1

AN INVESTIGATION OF THE PROPERTIES OF TWO URANIUM-BEARING ZEOLITES

J. G. Morgan M. T. Morgan

Recent syntheses of new zeolite species have produced structures with interesting properties.[1] Structurally, the zeolites of importance as adsorbents consist of a three-dimensional network of SiO_4 and AlO_4 tetrahedra with each oxygen shared with another tetrahedron so that the ratio O/(Al + Si) = 2. Electrical neutrality is achieved by the inclusion of alkali or alkaline earth ions such as Na^+ or K^+; interstitial voids contain water molecules which may be removed reversibly or may be replaced by other species. Depending on the size of these interstitial voids, other molecular species may be readily adsorbed, slowly adsorbed, or completely excluded. Two such zeolites were studied to determine the effectiveness of adsorption of fission-product gases when the structure contained uranium.

The two zeolite materials examined (6808-70-A and 6808-71-A) are referred to in this discussion as 70-A and 71-A, respectively. Material 70-A is a uranium trioxide–loaded sodium aluminum silicate, orange-yellow in color. Material 71-A is a uranium-exchanged sodium aluminum silicate, gray in color. The chemical and spectrographic analyses are given in Table 18. The 70-A material, having the higher uranium concentration, also contained considerable carbonate and nitrate. Random sampling showed that the materials were quite uniform in uranium concentration.

A thin film of each sample was placed on quartz as a water slurry. The films were weighed and counted at various stages of heating. Table 19 gives the results and indicates that, whatever volatility occurs, the uranium does not escape. Table 20 outlines the microscope observations at various stages of the heat treatment. In general both samples showed the first indications of sintering at about 650°C. Sample 70-A turned black as it went to higher temperatures (in air), while 71-A turned yellow. Both materials were too fine grained for petrographic examination.

Combustion Loss and Differential Thermal Analysis. – Combustion loss, in air, and differential thermal analysis (DTA) studies were made on both materials up to 1000°C. Figure 48 shows a total weight loss of 14.7% at 1000°C for sample 70-A and a 4.3% weight loss for sample 71-A. The DTA gives no indication of structural changes up to 1000°C (Fig. 49). The very broad and poorly defined endothermic peak in the DTA pattern for sample 70-A indicates the reduction step from UO_3 to U_3O_8, also indicated by the color change from yellow to black.

Irradiation Effects. – Both powder and pressed pellets were used in the irradiation studies. The pellets were formed by isostatic pressing at 35,000 psi and received no heat treatment. Each sample was sealed in an evacuated quartz capsule and irradiated for 10 min in the LITR for a total thermal *nvt* of approximately 13×10^{15} (see Table 21).

Table 18. Chemical and Spectrographic Analysis of Uranium-Bearing Zeolites

Constituent	Chemical Analysis		Spectrographic Analysis
	Sample 70-A	Sample 71-A	Both Samples
U[a]	43.5%[b]	5.8%[c]	
Al	5.19%	18.45%	
Si	9.20%	24.5%	
Na	4.43%	10.24%	
CO_3	9.23%	0.3%	
H_2O	1.79%	6.61%	
NO_3	17.37%	59 ppm	
SO_4	10 ppm	1 ppm	
F	37 ppm	38 ppm	
Cl	205 ppm	735 ppm	
Ce, Dy, Er, Gd, Ho, Nd, Pr, Tb			<0.3%[d]
La, Y.			<0.06%[d]
Eu, Tm, Yb			<0.03%[d]
Ca			0.01–0.1%

[a]As natural uranium.
[b]Random sampling gave 43.8, 42.9, and 45.4%.
[c]Random sampling gave 6.2%.
[d]Lower limit of detection.

[1]D. W. Breck *et al.*, *J. Am. Soc.* **78**, 5963 (1956).

Table 19. Weight Change and Activity Measurements on Uranium-Bearing Zeolites

Stage of Heat Treatment	Weight		Activity	
	Grams	Per Cent of Dry Weight	Counts·min^{-1}	Counts·min^{-1}·g^{-1}
		Sample 70-A		$\times 10^4$
Wet	0.9342	171.5	18,460.4	1.9
Dry	0.5447	100.0	21,809.6	4.0
Fumed	0.4902	89.9	16,872.3	3.4
Sintered at 427°C	0.4857	89.2	22,909.2	4.7
Sintered at 538°C	0.4797	88.1	23,528.2	4.9
Sintered at 649°C	0.4767	87.5	21,293.3	4.4
Sintered at 871°C	0.4532	83.20	23,409.4	5.1
Sintered at 1000°C	0.4512	82.83	21,766.3	4.8
		Sample 71-A		$\times 10^3$
Wet	0.5687	294.2	932.5	1.6
Dry	0.1933	100.0	987.7	5.1
Fumed	0.1914	99.0	1,053.3	5.5
Sintered at 427°C	0.1906	98.6	1,102.3	5.8
Sintered at 538°C	0.1901	98.3	1,095.5	5.8
Sintered at 649°C	0.1878	97.2	1,153.7	6.1
Sintered at 871°C	0.1606	83.08	1,207.9	7.5
Sintered at 1000°C	0.1605	83.03	1,507.3	9.3

The temperature was measured on the outside of the quartz capsule by means of a thermocouple. The samples were allowed to decay for 2 hr and then were taken to the hot cell for collection of fission gases. In the hot cell the capsules were sealed in the capsule breaker, and the system was evacuated by means of a vacuum pump (Fig. 50). Liquid nitrogen was then added to the charcoal trap, and the capsule was broken. Shielded radiation monitors were placed in the apparatus to show when the gas was released and to determine whether any gas was pumped out of the charcoal trap. The latter determination was negative in all cases. Gas was collected for 2 hr for the first sample and for 1 hr for the second sample. Since no appreciable difference was noted in the results, it was concluded that 1 hr for each capsule was sufficient.

The charcoal trap was sealed by means of valves, and the gas was analyzed by measuring decay curves both with a 100%-geometry ionization chamber and independently by means of a gamma-ray spectrometer.

Physical changes in the 70-A pressed pellets are shown in Fig. 51. The yellow 70-A pellets swelled and turned light in color on one end. The 70-A powder caked and turned light in color adjacent to the quartz. One 70-A pellet in a capsule which broke before or during irradiation suffered no apparent damage. An unirradiated 70-A pellet

Table 20. Microscope Examination of Uranium-Bearing Zeolites

Thin film on quartz glass capsule

Stage of Heat Treatment	Sample	Microscopic Observations
Dry	70-A	Smooth yellow cake, granular texture in cracks, grains ~10 μ.
	71-A	Gray cake, granular.
300°C	70-A	Yellow tinged, slightly anisotropic, first order yellow gray.
	71-A	Transparent fine granular material with some black opaque, 30–40 μ particles. Very slightly anisotropic.
427°C	70-A	Very fine transparent to yellowish to black agglomerates. Slightly anisotropic. First order yellow gray.
	71-A	Very fine transparent to black agglomerates. Slightly anisotropic.
538°C	70-A	Matrix of some very fine grained material with larger yellowish and black agglomerates. Slightly anisotropic. First order yellowish gray.
	71-A	Very fine grained transparent aggregates with some larger (~40 μ) black grains. Very slightly anisotropic.
649°C	70-A	Similar to 71-A (below) except more orange in color in plain transmittal light.
	71-A	Fine grained transparent to dark gray mostly about 2 or 3 μ festooned at sinter edge in a glassy material.
871°C	70-A	Material in center of film turned black – sharp larger crystals ~5 to 20 μ into sharp (angular) aggregates ~150 μ. Grains at edges are smaller and still yellow to orange. Fine material is anisotropic with yellow interference colors – fairly bright.
	71-A	Fine material ~5 μ aggregated to 150 μ in rounded particles. Interference color light dull yellow.
1000°C	70-A	Fine grained yellow to black through gray. Particle size ~8 μ predominant in larger agglomerates. Small amount of glassy material at extreme edge of fine material.
	71-A	More uniform transparent grains ~5 μ. Considerably more glassy material along the fine grain areas.

was heated in an evacuated quartz tube in an attempt to reproduce the changes noted in irradiated pellets. The pellet was heated to 400°C but suffered only a darkening in color. The change in density of 70-A pellets as the result of irradiation is listed in Table 22.

Because of the short irradiation times, no changes in the x-ray diffraction pattern were observed in material 71-A. The values of these patterns agree with those of aluminum calcium sodium silicate, with a few extra lines. The 70-A material gave a poor, unidentified pattern even in its unirradiated state.

Fission-Gas Analysis. – Fission gases analyzed for were Kr^{85m}, Kr^{88}, Xe^{135}, and Xe^{133}. Since the parent isotopes of Kr^{85} and Kr^{88} have short half lives and the time of irradiation was short, decay was neglected and the total krypton produced was calculated by the formula

$$Kr = nvtN\sigma_u Y_{Kr} ,$$

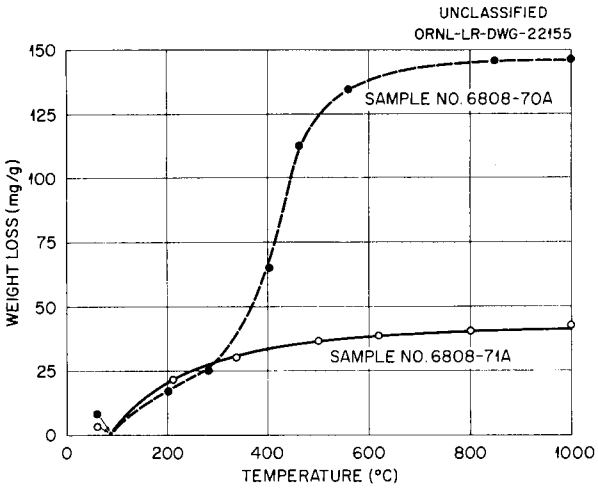

Fig. 48. Combustion Loss in Uranium-Bearing Zeolites.

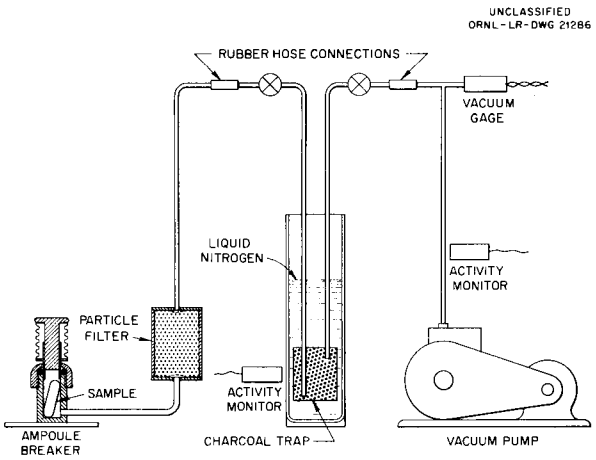

Fig. 50. Gas Collection Apparatus.

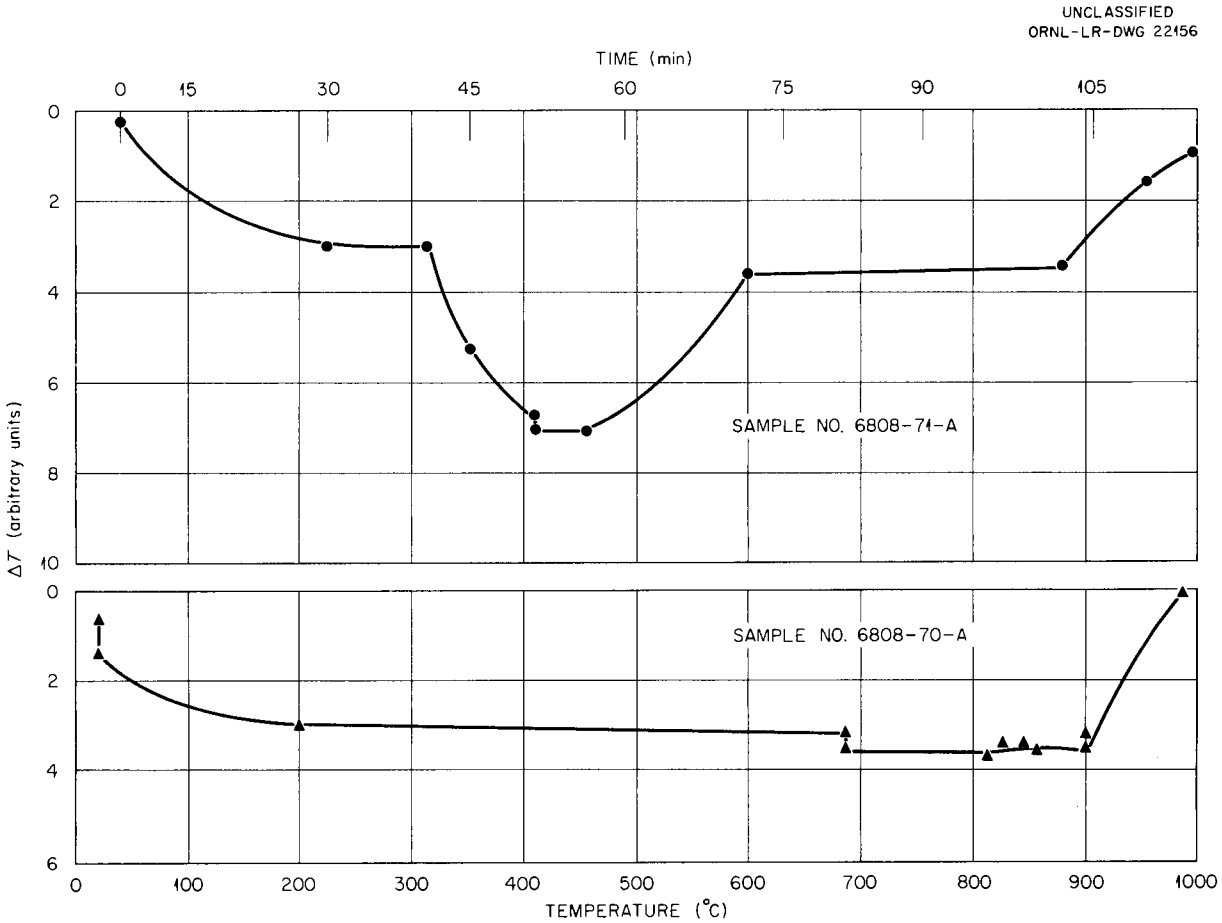

Fig. 49. Differential Thermal Analysis of Uronium-Bearing Zeolites.

Table 21. Irradiation Summary*

Sample No.	Type of Material	Weight (g)	nvt (neutrons/cm^2)	Irradiation Temperature** (°C)	Appearance
			$\times 10^{15}$		
70-A-1	Powder	1.592	8.2		Part next to quartz caked, turned light in color
70-A-2	Powder	1.138	11.9	210	
71-A-1	Powder	1.116	13.2		No apparent change
71-A-2	Powder	1.038	14.2	200	
70-A-P4	Pellet	0.709	12.6	180	Pellets swelled, surface crumbled, turned light in color at one end
70-A-P6	Pellet	0.628	13.5	160	
71-A-P2	Pellet	0.234	12.9	160	No apparent change
71-A-P3	Pellet	0.278	12.4	160	

*Each capsule was irradiated for 10 min.

**Temperatures were taken on the outside surface of the quartz capsules by means of thermocouples.

where

Kr = number of Kr atoms produced,

nvt = integrated neutron flux,

N = number of U^{235} atoms being irradiated,

σ_u = cross section of U^{235},

Y_{Kr} = yield for Kr isotope.

The measured activity of krypton gas was used to calculate the number of krypton atoms released from the uranium compounds at the time of irradiation.

Xenon-135 has a 6.7-hr I^{135} parent, and, therefore, a different method was used for calculating the amount produced. The equation for the decay of two successive radioactive isotopes is

$$\frac{dQ}{dt} = \lambda_1 P_0 e^{-\lambda_1 t} - \lambda_2 Q \ ,$$

(1)

$$Q = \frac{\lambda_1}{\lambda_2 - \lambda_1} P_0 \left(e^{-\lambda_1 t} - e^{-\lambda_2 t}\right) \ ,$$

where

P_0 = number of atoms of parent isotope at time zero,

Q = number of atoms of daughter isotope at time zero,

λ_1 = decay constant of parent isotope,

λ_2 = decay constant of daughter isotope,

t = decay time.

Xenon-135 is produced directly by neutron bombardment of U^{235} and also by decay of the fission product Te^{135}:

$$Te^{135} \longrightarrow I^{135} \longrightarrow Xe^{135}$$

Since Te^{135} has a half life of 2 min, compared with the I^{135} half life of 6.7 hr, it may be assumed that Te^{135} decays instantly to I^{135}. The number of atoms of I^{135} produced, neglecting decay, is

(2) $$I^{135} = nvt\sigma N\,(Y_I + Y_{Te}) \ ,$$

UNCLASSIFIED
PHOTO 41898

END SIDE

UNIRRADIATED

END SIDE

IRRADIATED
1.4×10^{16} *nvt*

Sample No. 6808-70-A

Fig. 51. Radiation Damage to Uranium-Bearing Zeolite Materials.

Table 22. Change in Dimensions and Density of Uranium-Bearing Zeolites*

Sample No.	Diameter (in.)		Length (in.)		Density (apparent)		
	Preirradiation	Postirradiation	Preirradiation	Postirradiation	Preirradiation (g/cc)	Postirradiation (g/cc)	Change (%)
70-A-P4	0.253	0.256	0.279	0.290	3.1	2.9	–6
70-A-P6	0.255	0.262	0.261	0.271	2.9	2.6	–9
71-A-P2	0.254	0.253	0.210	0.210	1.3	1.3	0
71-A-P3	0.258	0.259	0.230	0.230	1.4	1.4	0

*Change in weight not listed because of loss of some of the material from each pellet during handling.

the number of atoms of Xe^{135} formed by decay of I^{135} is

$$(3)\quad Xe^{135} = \frac{\lambda_I}{\lambda_{Xe} - \lambda_I}\,[nv t\sigma N(Y_I + Y_{Te})]\left(e^{-\lambda_I t_d} - e^{-\lambda_{Xe} t_d}\right),$$

and the number of atoms of Xe^{135} that had been formed directly by fission is

$$(4)\quad Xe^{135} = \frac{\sigma}{\sigma_{Xe}} N Y_{Xe}\left(1 - e^{-nv\sigma_{Xe} t}\right)\left(e^{-\lambda_{Xe} t_d}\right),$$

where

nv = neutron flux, neutrons·cm^{-2}·sec^{-1},

σ = cross section for fission, cm^{-1},

σ_{Xe} = cross section for xenon absorption, cm^{-1},

N = number of target atoms,

Y = isotopic yield, fraction of total,

t = irradiation time, sec,

t_d = decay time, sec,

λ = decay constant, sec^{-1}.

The total amount of xenon present at a given decay period was then calculated from the sum of Eqs. 3 and 4.

Values for Xe^{133} are not reported at this time because the spectrometer has not yet been standardized for Xe^{133}.

The number of atoms fissioned was determined by two independent methods, cobalt foil activation and analysis for Zr^{95}. The two results were in good agreement. The weight per cent of fissioned atoms was $(7.5 \pm 0.3) \times 10^{-4}$. Table 23 summarizes the results of the fission gas measurements. Three conclusions are apparent: (1) These two materials readily evolved their gaseous fission products during irradiation; (2) retention of the gaseous fission products was not increased by isostatically pressing the materials into pellets; (3) the materials appeared to retain xenon better than krypton.

Acknowledgments. – The authors wish to express their appreciation to A. J. Taylor, Ceramics Laboratory, for the combustion, microscopic, and differential thermal analysis data and for preparing the pellet samples; to W. R. Laing and W. R. Musick for the chemical and spectrographic analyses; and to S. A. Reynolds and E. I. Wyatt for the radioisotopic analyses.

Table 23. Escape of Fission Gases During Irradiotion

Sample No.	Type of Material	Amount Evolved (%)		
		Kr^{85}	Kr^{88}	Xe^{135}
70-A-1	Powder	70	61	27
70-A-2	Powder	89	83	30
70-A-4	Pellet	*	89	29
70-A-6	Pellet	*	*	67
71-A-1	Powder	89	65	55
71-A-2	Powder	61	65	38
71-A-P2	Pellet	68	59	61
71-A-P3	Pellet	81	68	54

*Determinations inconclusive.

FORCED-COOLING CERAMIC-FUELS EXPERIMENT

J. G. Morgan P. E. Reagan M. T. Morgan O. Sisman

An experiment is being designed for study of the radiation effects on ceramic fuels under conditions of high heat dissipation in the ORR. Fission-product retention, physical stability, and property changes will be studied. The fuel materials will generate 75,000 to 500,000 Btu/hr·ft^2 at surface temperatures of 1800 to 2500°F. The closed cooling cycle passes compressed gas (nitrogen) over the fuel elements (Fig. 52). The surface temperature of the elements is controlled by the exit pressure from the compressor storage tank. Upper-limit feasibility tests will be made on new fuel materials as they are developed. This research program is directed toward a study of the materials themselves and is not limited to a specific reactor cycle.

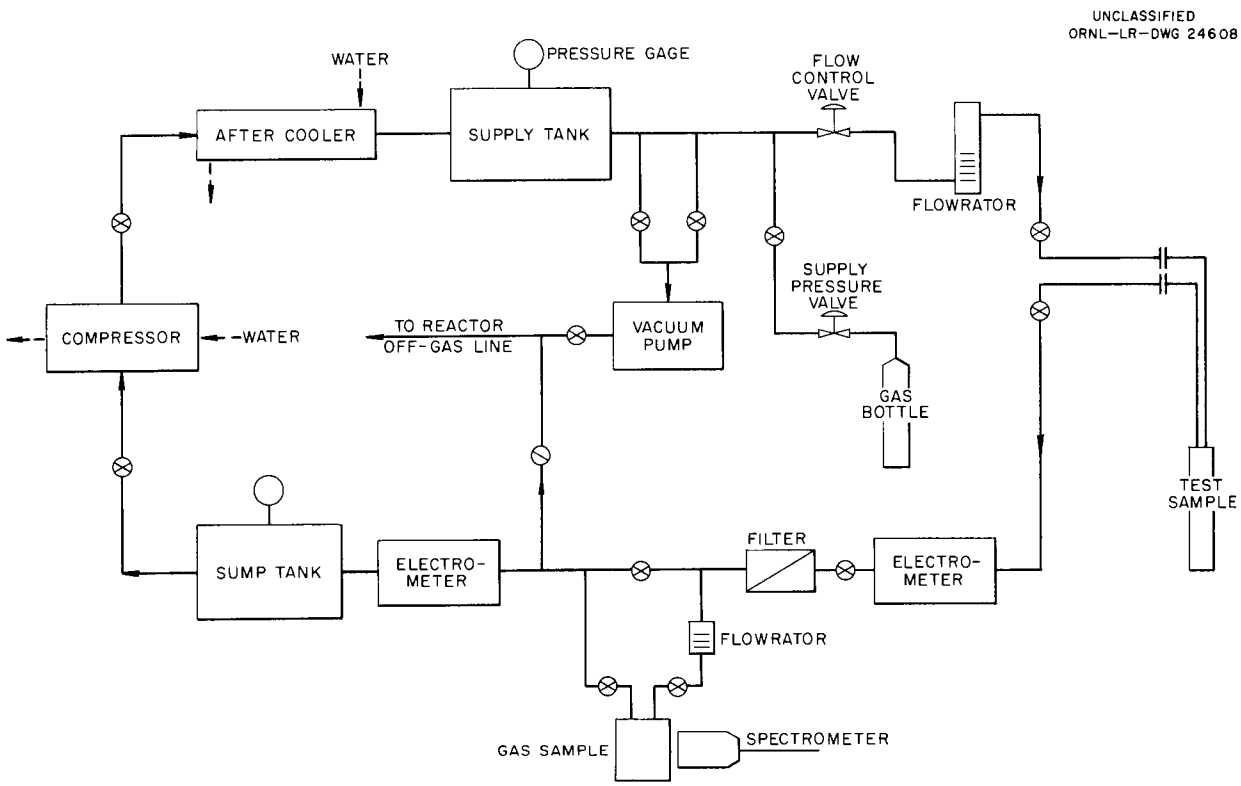

Fig. 52. Flow Diagram of Ceramic-Fuels Forced-Cooling ORR Experiment.

HIGH-TEMPERATURE CERAMIC FUELS

J. G. Morgan R. M. Carroll M. T. Morgan O. Sisman

SiC–Si–UO_2 Fuel Plates[1]

The first composite fuel system studied was siliconized, silicon carbide–clad UO_2. These plates were found to be dimensionally stable to radiation.[2] Metallographic examination of these fuel elements was hindered because no hot-cell apparatus was available which would allow sectioning of the plate without risk of damaging the structural integrity.[3] As a result, the observed fracturing of the ceramic elements cannot be attributed to irradiation or to in-pile thermal history.

Figure 53 shows a typical cross section of an irradiated and an unirradiated plate. This particular irradiated sample experienced a 4% U^{235} burnup at 1475°F with a maximum temperature of 1745°F. The silicon carbide grains surrounded by the lighter colored silicon can be seen in the cladding. The core appears to have suffered no damage as a result of the irradiation. Previous work showed that the UO_2 and solid fission products

[1]The ceramic and cermet fuel materials were developed and fabricated by the Ceramic Laboratory, Metallurgy Division.

[2]J. G. Morgan, M. T. Morgan, and R. M. Carroll, *Solid State Semiann. Prog. Rep. Aug. 30, 1956*, ORNL-2189, p 28 (classified).

[3]A. E. Richt and E. J. Manthos, ORNL CF-56-10-59, (Oct. 12, 1956) (classified).

UNCLASSIFIED
ORNL-LR-DWG 15996

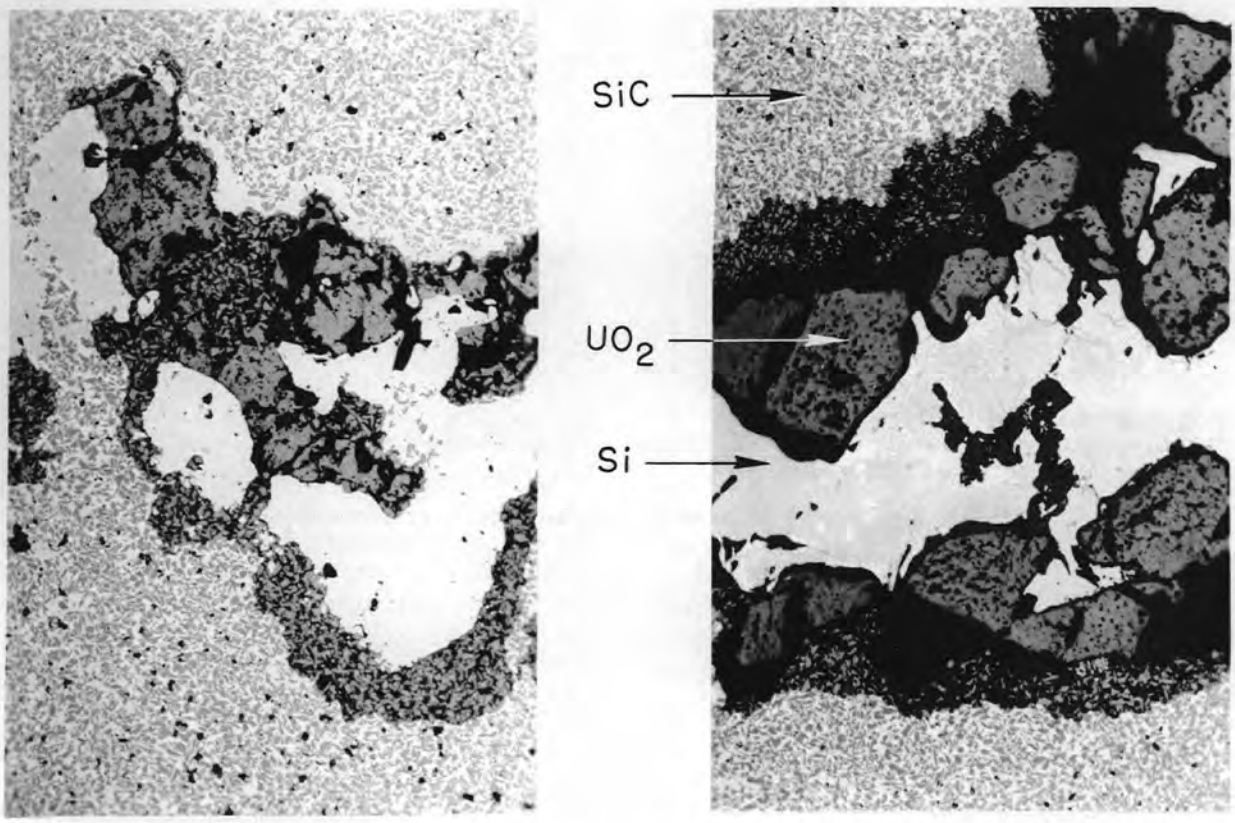

UNIRRADIATED IRRADIATED

Fig. 53. SiC–Si–UO_2 Specimen Core.

do not diffuse through the cladding, as detected by autoradiography. An experiment was performed to measure the escape of gaseous fission products. After irradiation the capsule containing the fuel plate was pierced remotely in the hot cell, and a portion of the gas surrounding the fuel plate was sampled. Because of the delay time necessary in the hot-cell transfer, gamma-ray spectrometer curves revealed only Xe^{133}. The activity of the xenon released from the fuel plate represented 1 part in 200,000 of the total Xe^{133} present in the plate at the end of the irradiation period. The cladding in these plates contained alpha activity when they were fabricated; so the actual cladding efficiency is somewhat greater. A better measure of cladding efficiency will be obtained from analysis of cooling gas as it is blown over the sample during irradiation.

Hardness Measurements on ThO_2–UO_2 Fuel Plates

The use of hardness as a radiation-sensitive property of ceramics was investigated. In testing a hard brittle ceramic, the older scratch methods permitted only a qualitative measurement.[4] The scale (due to Mohs) consists of ten standard minerals arranged in order of increasing hardness, each mineral being numbered according to its position in the series. To make the test, the sample is scratched in turn by the standard minerals of the series in decreasing number, until one fails to scratch the sample. The Mohs' scale number then lies between that number and the next higher one on the scale. The hardness is reported either as lying between these numbers or as the lower number plus five-tenths (e.g., Mohs' scale hardness between 6 and 7 or Mohs' scale hardness = 6.5).

Recently many investigators have used the indenter method, employing either the square-base diamond-pyramid indenter (DPH) or a pyramidal-shaped base (Knoop). Quantitative values thus obtained allow the experimenter to determine changes in hardness and brittleness. High-temperature hardness values for ceramics up to 1000°C have also been obtained[5] with a double-core diamond indenter. In testing brittle materials, subsurface and surface cracking may occur. A study[6] of such fractures on hard, transparent, brittle substances showed that the hardness value is valid only if the cracking is of a subsurface nature and if the specimen shows no perceptible amount of surface cracking. To minimize this cracking effect, the load should be as light as possible.

The following conditions are necessary in order to run reliable indentation hardness tests on ceramics:[7]

1. The sample must be highly polished and free from scratches; this is especially important in microhardness tests.
2. The testing surface must be normal to the indenter.
3. The material must be tested with the same load for comparable results to be obtained, since the Knoop hardness number often varies with the load applied on the indenter.
4. The crystal orientation of the diamonds should be the same so hardness values from two different machines can be compared precisely.
5. All vibration must be avoided in indenter tests on brittle materials.

Two types of ThO_2–UO_2 fuel elements, containing 2.5 wt % U^{235}, were tested with the DPH microhardness tester and the Tukon hardness tester with a Knoop indenter. The samples were fabricated as follows:[8]

Sample No. 1 ($\frac{1}{8} \times \frac{1}{8} \times 1\frac{1}{2}$ in.): Steam-oxidized UO_2 was thoroughly mixed with precalcined ThO_2 containing $\frac{1}{2}$ wt % CaO. To this mixture was added 1 wt % Carbowax 4000 as a binder. This mixture was pressed into the desired shapes at 8000 psi. The pieces were fired in a helium atmosphere at 1750°C and then machined to the final size.

Sample No. 2 ($\frac{1}{2}$ in. in diameter by $\frac{1}{2}$ in. long): Thorium oxide containing $\frac{1}{2}$ wt % CaO was calcined at 1600°C. One-fourth wt % CaO was added to the calcined material, and then steam-oxidized UO_2 was thoroughly mixed in. Rods were isostatically pressed from this mixture at 35,000 psi; no binder

[4] G. L. Kehl, *Principles of Metallographic Laboratory Practice*, 3d ed., McGraw-Hill, New York, 1949.

[5] J. H. Westbrook, *Application of Hot Hardness Testing to Ceramic Compounds*, General Electric Research Laboratory, unpublished work.

[6] V. E. Lysaght, *Indentation Hardness Testing*, Reinhold, New York, 1949.

[7] V. E. Lysaght, "The Knoop Indenter as Applied to Testing Nonmetallic Materials Ranging from Plastics to Diamonds," *ASTM Bull.* (Jan. 1946).

[8] A. J. Taylor to D. S. Billington, memo, June 12, 1956.

was used. The rods were fired in helium at 1765°C and then machined to their final size.

Both samples were mounted in epoxy resin, lapped on a cast-iron plate with the use of Al_2O_3, and polished on a cloth-covered wheel with the use of diamond dust in an oil carrier.[9] Their Mohs' scale hardness was 6.5, and their density was 9.10 g/cc. Sample No. 2 was tested on a microhardness tester with the Vickers projection microscope and a DPH indenter.[10] Any load above 5 g produced shattering and cracking. The results are summarized in Table 24. It was concluded from this test that the DPH is of no value for the irradiation experiments.

Both samples were then tested on the Tukon hardness tester with a Knoop indenter (Table 25), and heavier loads were obtained before cracking and chipping occurred. Sample No. 1 had 30% of its impressions cracking under a 100-g load. Sample No. 2 retained plastic deformation at 100 g load but was 100% chipped at 1000 g. The machine had no load range between 100 and 1000 g. The values at 100-g load are compared in Table 26 with those of other materials.

Figures 54 and 55 are photographs of the impressions obtained by the Knoop indenter at different loads. The heavy load stresses tend to be relieved by cracking around the actue angle of the indenter, by chipping, or by both.

[9] A. E. Richt, private communication.

[10] *Photomicrography with the Vickers Projection Microscope*, 4th ed., Cooke, Traughton & Sims, Ltd., York, England.

Table 24. Diamond Pyramid Hardness for Sample No. 2

Load (g)	DPH No.	Remarks
5	433 (392/454)	Plastic deformation
7	271 (257/298)	Slight cracking
10	279 (131/389)	Shattered
15	579 (433/673)	Chipped
20	801 (602/1040)	Shattered
25	822 (552/912)	Shattered
50	936 (701/1025)	Shattered

Table 25. Knoop Hardness Values for Samples Nos. 1 and 2

Load (g)	Average Knoop Hardness No.		Comments
	Sample No. 1	Sample No. 2	
10	630	496	Plastic deformation
25	800	735	Plastic deformation
50	790	790	Plastic deformation
100	890	891	Sample No. 1 cracking
1000		747	Sample No. 1 shattered

Table 26. Knoop Hardness Values for Various Materials Under a 100-g Load

Material	Mohs' Scale No.	Knoop Hardness No.
Diamond	10	7000
SiC	9–9.5	2400
Corundum	9	2000
ThO_2–UO_2	6.5	900

Because of the brittle behavior of the high-density ThO_2–UO_2 system, indenter hardness measurements are restricted to a qualitative treatment only. With a Knoop indenter and loads up to 100 g a comparison of unirradiated vs irradiated samples could be obtained. The hot-cell Tukon tester is not at present easily used with these light loads. It has been suggested[11] that the percentage of fractured impressions at one load could be used as a measure of change in brittleness. Young's modulus and breaking strength would seem to be the best properties to test for changes in elastic behavior under irradiation.

Specific Heat and Elastic Properties of ThO_2–UO_2 Fuel

Previous experiments on the ThO_2–UO_2 fuel materials were for determining retention of fission gases and changes in density and dimensions due to neutron irradiation. Information is presented

[11] D. Bopp, private communication.

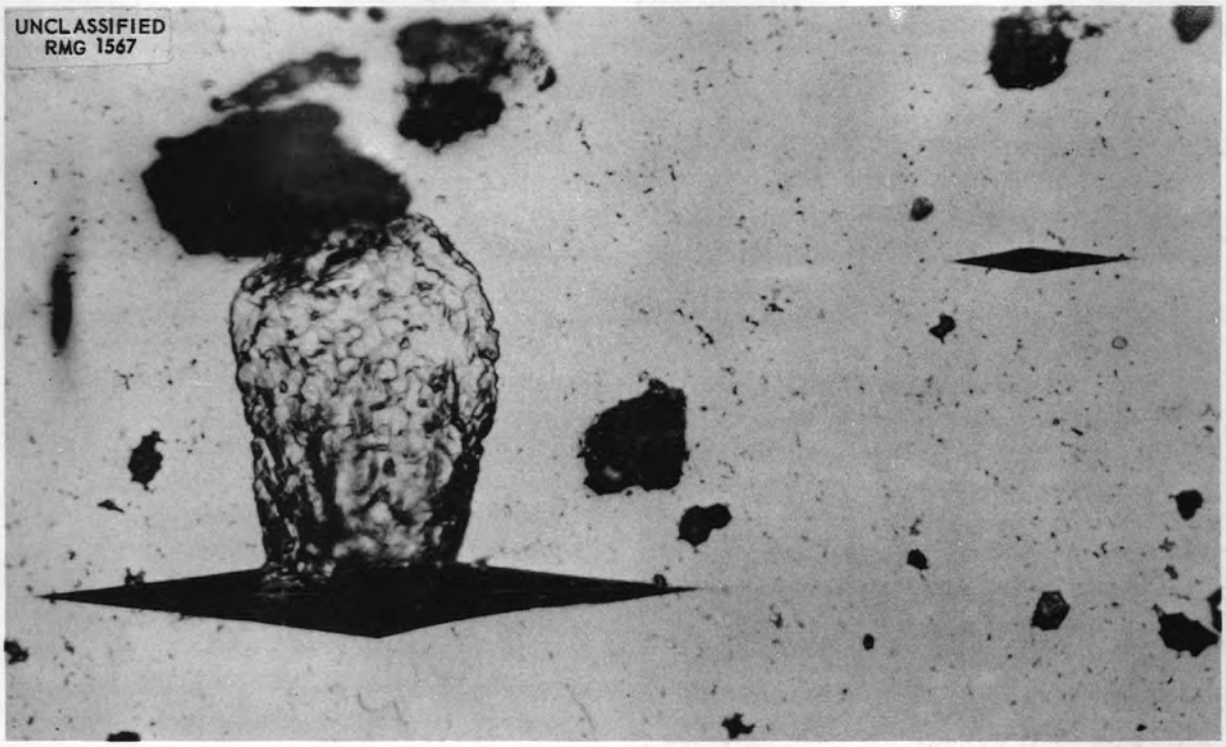

Fig. 54. Knoop Hardness Impressions in ThO_2–UO_2 (630X). Impression on left, with large chips, made by 1000-g load. Impression at upper right made by 100-g load.

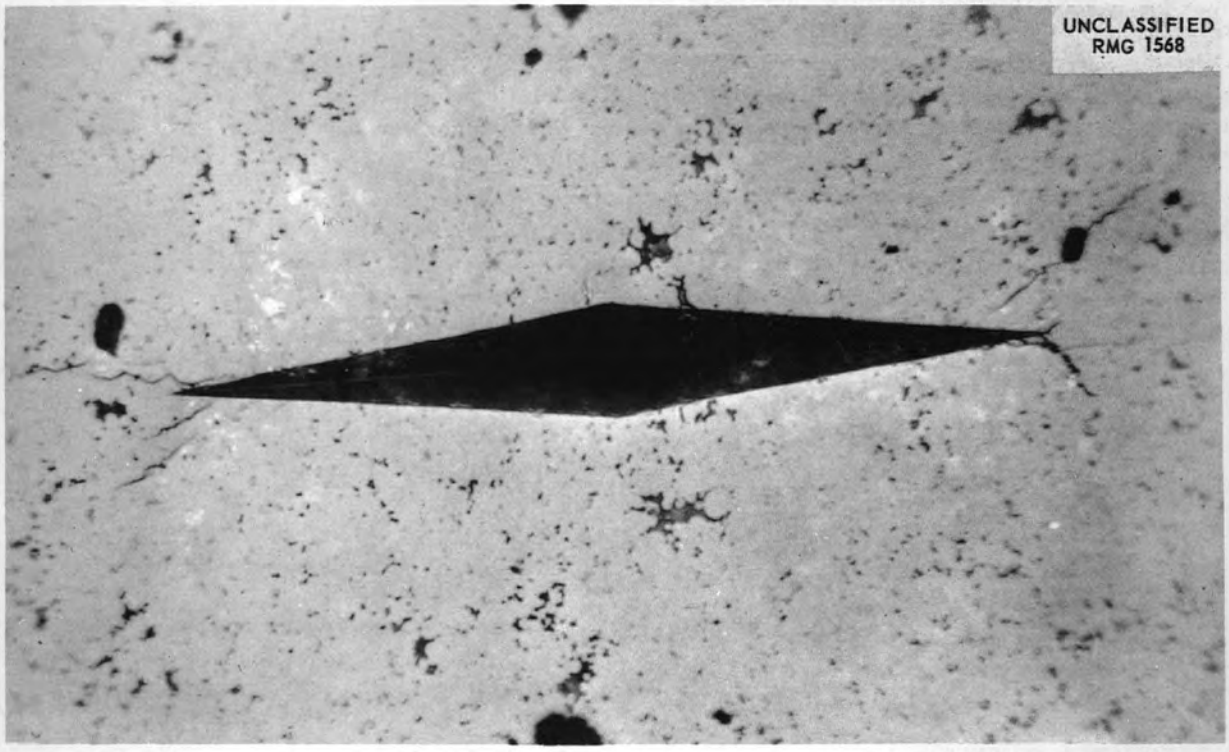

Fig. 55. Knoop Hardness Impression (750X) with Cracks at Acute-Angle Ends; 1000-g Load.

below concerning irradiation-induced changes in specific heat,[12] Young's modulus, and internal friction.

Irradiation of ThO_2–UO_2 for 557 hr in the LITR at a temperature of 740°C produced a change in specific heat of less than 2% (see Table 27). The samples were irradiated in a helium atmosphere. They were $\frac{1}{8} \times \frac{1}{8} \times 1\frac{1}{2}$ in. rectangular bars prepared from a mixture of 97.2% ThO_2 and 2.8% UO_2 (enriched) powders by isostatic pressing and firing at 1750°C.

The samples for elastic modulus tests were prepared as above but were 3 in. in length. Two of the samples were enriched in U^{235}. Irradiation for 700 hr in the LITR at 486°C for the unenriched samples and for 1079 hr at 1000°C for the enriched samples produced decreases in Young's modulus of less than 2% (Table 28).

The internal friction of these samples was calculated by the formula $\Delta n/\sqrt{3}N$, where Δn is the difference in resonant frequency at half amplitude and N is the resonant frequency.

The value of Δn was less than 1 cycle/sec and the resonant frequency was approximately 2700 cycles/sec for all samples. In the hot cells, vibration and other variations made Δn uncertain by ±0.2 cycles/sec; consequently the value of the internal friction is only approximate.

Young's modulus was measured by the dynamic method, transverse vibrations being used. The sample was suspended horizontally on cotton strings sprayed with plastic. The method is a variation of that developed previously by Kernohan.[13] A magnetostrictive driver was used to excite the sample, and a phonograph cartridge was

[12] J. G. Morgan, R. M. Carroll, and M. T. Morgan, *Solid State Semiann. Prog. Rep. Feb. 29, 1956*, ORNL-2052, p 11 (classified).

[13] R. H. Kernohan, *Effect of Fissionable Particle Size on Fission Damage in Graphite*, ORNL-1722, p 8 (April 21, 1954).

Table 27. Irradiation-Induced Change in Specific Heat of ThO_2–UO_2 Ceramic

Composition of samples: 97.2 wt % ThO_2, 2.8 wt % UO_2 (enriched)

Irradiation time: 557 hr in LITR

Thermal *nvt*: 6.4×10^{19} neutrons/cm^2

Number of heating cycles:* 13

Temperature: 740°C

	Sample No.	
	5	6
Density		
Before irradiation (g/cc)	9.14	9.12
Change (%)	0.2	0.2
Dimensional Change (in./in.)	±0.001	±0.0008
Specific heat 85–1800°F		
Before irradiation (cal/g·°C)	0.071	0.071
Change (%)	<2	<2

*Cycles to ambient temperature and back to operating temperature.

Table 28. Irradiation-Induced Change in Elastic Constants of ThO_2–UO_2

Sample*	Time Irradiated (hr)	Total *nvt* (neutrons/cm^2)	Number of Heating Cycles**	Average Temperature (°C)	Young's Modulus		Internal Friction	
					Before Irradiation (dynes/cm^2)	Change (%)	Before Irradiation	Change, Δn
YM-1-A	700	0.8×10^{20}	45	486	2.0×10^{12}	−1.5	1×10^{-3}	<0.4
YM-1-B	700	0.8×10^{20}	45	486	2.0×10^{12}	−1.5	1×10^{-3}	<0.4
YM-2-A	1079	1.0×10^{20}	42	1000	2.2×10^{12}	−1.8	1×10^{-3}	<0.4
YM-2-B	1079	1.0×10^{20}	42	1000	2.3×10^{12}	−0.9	1×10^{-3}	<0.4

*Composition was 97.2 wt % ThO_2 and 2.8 wt % UO_2. YM-1-A and YM-1-B were unenriched in U^{235}, and YM-2-A and YM-2-B were enriched in U^{235}.

**Cycles to ambient temperature and back to operating temperature.

used to receive the vibrations. Young's modulus was calculated by the formula

$$E = \frac{N^2 l^4 \rho}{1.057 t^2} ,$$

where

N = resonant frequency,

l = length of sample,

t = thickness of sample,

ρ = density of sample,

1.057 = constant for the fundamental mode of vibration.

$Cr-Al_2O_3-UO_2$ Fuel Material

A 70% chromium–30% alumina material has been developed[14] for high-temperature applications and seems promising for a UO_2 fuel plate cladding. The material, containing particles of Al_2O_3 surrounded by chromium, has attractive high-temperature strength and oxidation resistance. Fuel elements with a $Cr-UO_2$ core and clad with $Cr-Al_2O_3$ have been fabricated by the Ceramic Laboratory. A plate generating 150 w/in.^{2} at 1100°C is being irradiated in the LITR static test facility.

[14] T. S. Shevlin, *J. Am. Ceram. Soc.* **37**, 140 (1954).

RADIATION EFFECTS IN THERMOCOUPLE INSULATION

J. C. Wilson

W. W. Davis J. C. Zukas

As a check on the integrity of the insulation and insulation practices used in various in-pile experiments, the electrical resistivity of a number of insulating materials was checked under irradiation in hole HB-3 of the LITR in both helium and air atmospheres at temperatures up to 1600°F. From these tests it was concluded that the materials and practices used for thermocouple insulation have not led to errors during irradiation.

Glass-insulated thermocouple pairs (Chromel-Alumel, 30-gage wire) from two manufacturers were tested. In air or helium at room temperature the leakage resistances between the wires in the pairs were remarkably uniform at about 10,000 megohms (test voltage was about 20 v in all tests). The resistance dropped about a factor of 10 during irradiation and recovered the original value during reactor shutdowns. Similar commercially made insulated wire manufactured and tested several years ago showed changes 10 to 100 times greater. No long-term deterioration in the insulation resistance over a period of 700 hr was noted. From previous tests it had been expected that the leakage resistance of the pair in helium would decrease markedly as irradiation broke down the organic impregnant. This did not happen, and the conclusion is that a different impregnant is now being used.

A commercially available, glass-insulated thermocouple pair sheathed in a stainless steel tube (and reportedly made with no impregnant in the insulation) was irradiated in the range from 100 to 800°F. From a starting value of 2000 megohms the intra-pair leakage decreased to less than 600 ohms after 600 hr, and the resistance recovered only very slightly during reactor shutdowns after 300 hr. The insulation is being checked for the presence of organic materials that might have been broken down by heat or radiation. In tests of the glass-insulated pairs at elevated temperature (up to about 1800°F) the combination of radiation and temperature decreased the leakage resistance to about 0.1 megohms at 1500°F in helium, although only about 4 in. of the wire was at the elevated temperature. In air under the same conditions, the value was 1000 ohms. When the wire was cooled to room temperature (reactor off), the resistance of the insulation irradiated in helium rose 4 or 5 orders of magnitude; the insulation irradiated in air, however, generally showed only a factor of 2 recovery under the same conditions.

The high-temperature tests included Chromel-Alumel pairs in adjacent holes of stock ceramic insulators and a pair in swaged MgO insulation. Initial resistivity values were from 1000 to 10,000 megohms. After a week of irradiation at room temperature, the insulation was raised to 1500°F for the remainder of the tests except for short periods when the temperature was dropped for measurement of the recovery in resistivity. After 500 hr the insulation resistance was in the 1- to 10-megohm range for these ceramic materials, but when the temperature was reduced, the resistance recovered to 1000 to 10,000 megohms. There was some indication that the resistance and the amount of recovery of resistance on cooling were both decreasing with time.

CHEMICAL EFFECTS OF NUCLEAR REACTIONS

M. T. Robinson
W. A. Brooksbank
R. J. Carter
M. F. Osborne

In many systems, radiation effects show themselves primarily through chemical changes. The molten fluoride fuels recently described for use in nuclear reactors[1] are very stable towards radiation decomposition, but the fission-product elements produced in them significantly modify their behavior. Studies of the chemical states of the fission-product elements in molten fluorides constitute the major activity of this group. The principal experimental approaches are (1) studies of the evolution of gaseous fission products on treatment of molten fluorides with various gases and (2) electrochemical studies, primarily polarographic. Most of this work was commenced only within the past few months. A summary of previous work has recently been published.[2]

Several problems reported on in earlier progress reports have been discussed in the open literature.[3] An abstract of another report which has been prepared for publication is given below.

On the Conservation of Valency in Fission.[4] M. T. Robinson. – It is pointed out that on the average chemical valency must be conserved in the fission process. The consequences of this requirement are illustrated for two fuel materials: solid UO_2 and dilute solutions of UF_4 in molten fluorides. In both systems, changes with time of the valencies of several fission-product elements are sufficient to maintain valency conservation. In the molten fluorides, however, the situation is more complex than in the oxide, due to the possibility that certain fission-product species may react with the container. The importance of rare-gas removal in this regord is demonstrated.

Crystal Structures of K_2PO_3F and of K_2SO_4. – It was shown several years ago[5] that the room-temperature form of K_2PO_3F is isomorphous with β-K_2SO_4. This result has been verified by single-crystal x-ray methods. It was found that the published parameters[6] for β-K_2SO_4 gave only very poor agreement between calculated and observed structure factors for both compounds. A least-squares adjustment of the K_2SO_4 parameters was carried out on the Oracle[7] for the (010) and (100) zones. A spherically symmetrical temperature correction was made, as was a correction for secondary extinction. The final value of the agreement index,

$$R = \frac{\Sigma|F_{obs} - F_{calc}|}{\Sigma|F_{obs}|},$$

was 9.5%. The shifts of parameters from the previous values were small, no changes in the geometry of the SO_4^{--} ion being observed. A similar adjustment in the parameters of K_2PO_3F is in progress. It is not yet certain whether the correct space group is *Pnam* (D_{2h}^{16}) as it is for K_2SO_4 or whether it is the related acentric group $Pna2_1$ (C_{2v}^{9}). At present the agreement index in the former space group is about 29%.

---

[1] A. M. Weinberg *et al.*, *Molten Fluoride Reactors*, ORNL CF-57-6-69 (1957).

[2] M. T. Robinson *et al.*, ORNL-2374 (Aug. 28, 1957) (classified).

[3] M. T. Robinson and J. F. Krause, *Nuclear Sci. and Eng.* 1, 216–221 (1956); *Solid State Semiann. Prog. Rep. Feb. 29, 1956*, ORNL-2051, p 35–36; M. T. Robinson, *J. Phys. Chem.* 61, 120–122 (1957); *Solid State Semiann. Prog. Rep. Aug. 30, 1956*, ORNL-2188, p 42–43; M. T. Robinson and G. E. Klein, *J. Phys. Chem.* 61, 1004 (1957); *Solid State Quar. Prog. Rep. Aug. 10, 1952*, ORNL-1359, p 20–21 (classified); M. T. Robinson, *J. Am. Chem. Soc.* 79 (1957) (in press); *Solid State Quar. Prog. Rep. Feb. 10, 1953*, ORNL-1506, p 23–25 (classified).

[4] M. T. Robinson, *On the Conservation of Valency in Fission*, ORNL CF-57-8-46 (Aug. 21, 1957); to be submitted to *Nuclear Sci. and Eng.* for publication.

[5] M. T. Robinson and G. E. Klein, *Solid State Semiann. Prog. Rep. Aug. 31, 1953*, ORNL-1606, p 44 (classified).

[6] W. Ehrenberg and C. Hermann, *Z. Krist.* 70, 163–170 (1929).

[7] The assistance of W. R. Busing of the Chemistry Division in performing the Oracle computations is gratefully acknowledged.

ADSORPTION OF FISSION GASES BY ACTIVATED CHARCOAL

W. E. Browning
R. E. Adams
J. F. Krause
D. E. Guss

An investigation is being made of the holdup of fission gases flowing through activated-charcoal adsorption beds. Theoretical and experimental studies now under way are applicable to conditions of interest in the off-gas system of the Homogeneous Reactor Test and future homogeneous reactors.

The design of an adequate charcoal adsorption bed for a particular homogeneous reactor is at present a difficult problem because of the scanty experimental data on factors that influence the adsorption of fission gases on charcoal. It is the purpose of this investigation to provide these data. The function of a charcoal bed is to contain the fission gases for a definite period of time to allow the short-lived fission gases to decay almost completely before being vented to the atmosphere. The fission gases are not permanently adsorbed from a moving gas stream by the charcoal but are delayed in passing through the bed by the process of adsorption and desorption on the charcoal surface.

Various factors which influence the adsorption process are being or will be studied. This program is an extension of a previous study[1] of adsorption at temperatures ranging from +16 to −110°C, with nitrogen and helium used as sweep gases. The temperature range of interest in this study is from 25 to 150°C, with oxygen being used as the sweep gas; Kr^{85} is used to typify the fission gases.

Data thus far obtained[2] indicate the following: (1) The adsorptive capacity of charcoal decreases with increasing temperature of the charcoal; (2) adsorbed moisture decreases the adsorptive capacity of charcoal; (3) any deviation from complete filling in a horizontally mounted charcoal bed may lead to significant decreases in the holdup time of fission gases.

Comparative measurements were made on two grades of charcoal, one derived from coconuts and the other from bituminous coke. The different materials were found to be identical in their effectiveness for holding up krypton, provided that amounts of charcoal inversely proportional to their surface areas are used. These measurements have been reported.[3]

Other factors to be studied include trap geometry, other fission gases, different sweep gases, adsorber particle size, flow and flow perturbations, higher partial pressures of fission gases, different adsorber materials, and transfer of decay heat from the charcoal mass.

[1] W. E. Browning and C. C. Bolta, *Solid State Semiann. Prog. Rep. Feb. 29, 1956*, ORNL-2052, p 20 (classified).

[2] R. A. McNees *et al.*, *HRP Quar. Prog. Rep. July 31, 1957*, ORNL-2379, p 137.

[3] W. E. Browning, R. E. Adams, and D. E. Guss, *ANP Quar. Prog. Rep. June 30, 1957*, ORNL-2340, p 279 (classified).

INVESTIGATION OF SULFUR CONTAMINATION OF A DRY BOX BY NEOPRENE RUBBER

W. E. Browning

R. E. Adams H. L. Hemphill

During operation of a vacuum-type dry box containing high-purity helium, deposits of Cu_2S were observed on copper cooling coils inside the dry box. The Cu_2S was identified by chemical analysis and by x-ray diffraction measurements. Various materials exposed to the atmosphere inside the dry box were analyzed for sulfur, and the source was traced to neoprene rubber used in gloves in the dry box. Further tests in a separate vacuum system showed that the Cu_2S film was formed on copper exposed to the neoprene rubber only under vacuum conditions. The gaseous sulfur compound responsible for transport of the sulfur was not identified. Details of this investigation have been reported.[1]

[1] W. E. Browning, R. E. Adams, and H. L. Hemphill, *ANP Quar. Prog. Rep. March 31, 1957*, ORNL-2274, p 257 (classified).

NEUTRON FLUX MONITORING IN HIGH-TEMPERATURE IN-PILE EXPERIMENTS

D. E. Guss

A method has been developed for the measurement of thermal neutron flux in high-temperature in-pile experiments, the cobalt impurity in Inconel being used as the flux monitor. Inconel is of particular interest for this application because of its stability under a variety of environmental conditions at high temperatures. This material is stable in an air atmosphere and at temperatures greater than 1500°F and resists corrosive attack by many other materials. Inconel is quite frequently a material of construction in high-temperature experiments; in such cases it is not necessary to introduce a special flux monitor into the experiment, since use can be made of the structural parts of the apparatus. It is possible even to determine the flux to which an experiment has been exposed without advance preparation by collecting samples of Inconel after the irradiation is complete. It is necessary to assay the Inconel for cobalt and to establish the homogeneity of the Inconel with regard to cobalt composition. It has been determined that the interference from other components of Inconel is negligible, and the method has been shown to be accurate within 10% by comparison with flux values determined by other methods. Applications of this technique have been reported.[1] A description of the method is to be submitted for publication.[2]

---

[1] D. E. Guss, *ANP Quar. Prog. Rep. June 30, 1957*, ORNL-2340, p 278 (classified).

[2] D. E. Guss and G. W. Leddicotte, *The Use of Inconel as a High Temperature Corrosion Resistant, Thermal Neutron Flux Monitor* (to be published).

ORR EXPERIMENTAL FACILITY

W. E. Browning R. P. Shields

Engineering work is under way for auxiliary equipment to be used with in-pile experiments in the Oak Ridge Research Reactor. This equipment is planned to accommodate major reactor experiments such as the miniature vertical in-pile loop experiment. Specifications and cost estimates have been prepared for installing instruments, wire channels, control equipment, off-gas disposal facilities, and access leads through the reactor vessel.

FISSION REACTIONS AS THRESHOLD DETECTORS

D. Binder

The fission reactions in Pu^{239}, Np^{237}, and U^{238} were used to measure the fast-neutron flux in hole 51N of the ORNL Graphite Reactor. Measurements were made in and near the cylindrical uranium converter, or "donut," to test the assumption that the donut adds a fission spectrum to the reactor spectrum outside the donut. The number of fissions in the three reactions was measured by a method developed by Hurst *et al.*[1]

The Pu^{239}, Np^{237}, and U^{238} foils were enclosed in a 1.4-g/cm^2 B^{10} shield, which made the effective threshold for Pu^{239} fission 1 kev. The effective threshold for Np^{237} is 0.6 Mev, and that for U^{238} is 1.5 Mev, the B^{10} shield merely excluding competing reactions such as $Np^{237}(n,\gamma)Np^{238}$ and the fission of the U^{235} impurity in the U^{238} foil. The fission-product gamma rays having an energy greater than 1.2 Mev were observed after irradiation for the three fast fissions and compared with the gamma rays from the thermal fission of Pu^{239} in a known thermal flux. If it is then assumed, as in the work of Hurst *et al.*,[1] that the gamma-ray spectra are the same, the fast-neutron flux above 1 kev, 0.6 Mev, and 1.5 Mev may be derived from the data.

The results are shown in Fig. 56, where the various integral fluxes are plotted against distance in units of turns of a handle that controls the sample holder's motion into the reactor. One turn equals 10.1 in., and the edge of the donut is near 21.3 turns. In Figs. 57, 58, and 59 the assumption that a fission flux is added by the donut is borne out. In Figs. 57 and 58, respectively, the changes in the >1-kev flux are plotted against the changes in the >0.6-Mev and the >1.5-Mev fluxes, with the 20.8-turn point as a base point. The dashed lines represent the constant ratio to be expected from a fission spectrum, and are in agreement with the data. In Fig. 59 the total fluxes above 0.6 Mev and above 1.5 Mev are plotted against one another. Within experimental error, the fluxes agree with the fission ratio.

Since the measurements of Fig. 59 are of the total flux, that is, reactor flux plus donut flux, it would follow that the reactor flux at 20.8 turns

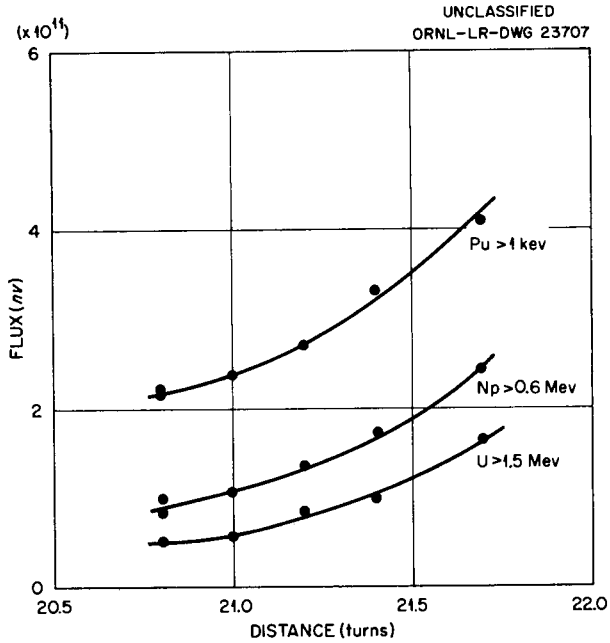

Fig. 56. Neutron Flux vs Distance into Hole 51N, as Measured by Pu^{239}, Np^{237}, and U^{238} Fission Foils in a B^{10} Shield.

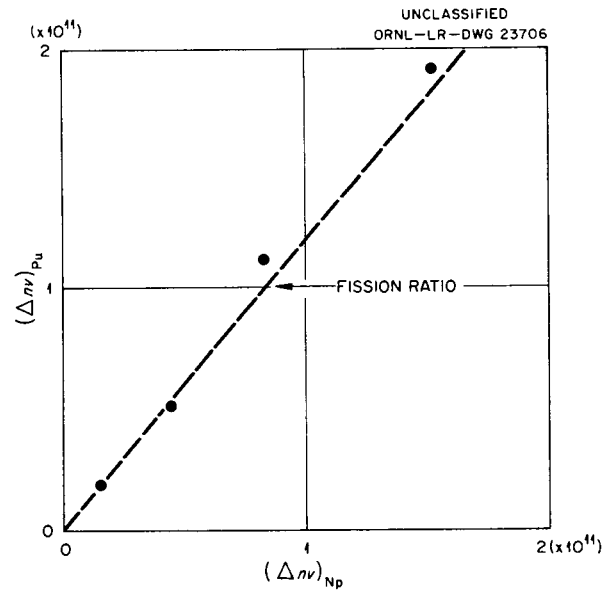

Fig. 57. Comparison of Increases in Neutron Flux as Measured by Pu and Np Foils.

[1] G. S. Hurst *et al.*, *Rev. Sci. Instr.* **27**, 153 (1956).

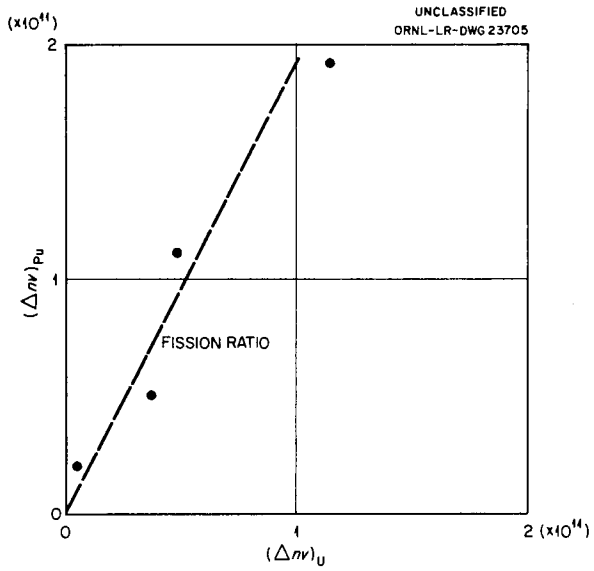

Fig. 58. Comparison of Increases in Neutron Flux as Measured by Pu and U Foils.

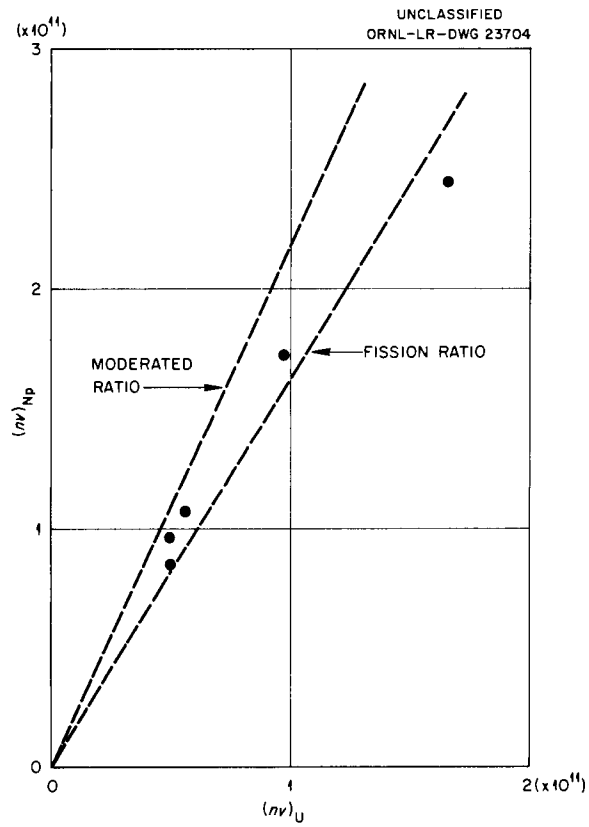

Fig. 59. Comparison of Total Neutron Fluxes as Measured by Np and U Foils.

having an energy >0.6 Mev agrees with a fission spectrum within experimental error. In order to test the sensitivity of this result, another reactor spectrum was calculated which included moderation. Starting with a fission spectrum $f(E')$, a $1/E$ spectrum was extended from each differential element of $f(E')$ from E' to zero energy. All the $1/E$ spectra were then summed to obtain a "moderated" spectrum $\phi(E)$. Analytically,

$$d[\phi(E)] = \frac{E'f(E')\,dE'}{E} ,$$

or

$$\phi(E) = \frac{1}{E}\int_E^{\infty} E'f(E')\,dE' .$$

The ratio of the flux above 0.6 Mev to the flux above 1.5 Mev calculated from $\phi(E)$ is plotted as the "moderated ratio" in Fig. 59. Within experimental error, it agrees with the first three points. But the moderated ratio is not in agreement with the remaining points which correspond to positions closer to, or inside, the donut.

The data indicate then that the donut adds a fission spectrum to a reactor spectrum outside the donut. The data are not yet sufficiently accurate to indicate the nature of the reactor spectrum.

The size of the B^{10} shield (roughly 2 × 3 × 3 in.) places a restriction on the use of this technique inside reactor test holes. Although substituting a cadmium cover eliminates the 1-kev-threshold Pu^{239} detector, the U^{238} reaction may be utilized, provided that the U^{235} content in the foil is sufficiently low. The use of the Np^{237} fission reaction is dependent on exclusion of the activity from the 2-day Np^{238} isotope resulting from the (n,γ) reaction. This was accomplished previously by (1) counting gamma rays above 1.2 Mev, (2) the $1/v$ absorption of the B^{10} shield, and (3) short irradiations. The counting was done directly on the aluminum foil on which the neptunium was deposited, and the activities induced in the Al^{27} were subtracted by the use of a control foil.

The 0.4-ev cutoff of cadmium is insufficient to mask the Np^{238} activity on the aluminum foil with the Np^{237} deposit, and therefore a catcher technique was developed. An aluminum foil was used to catch the fission products, and the Np^{238} recoils were stopped by a thin aluminum absorber. Since

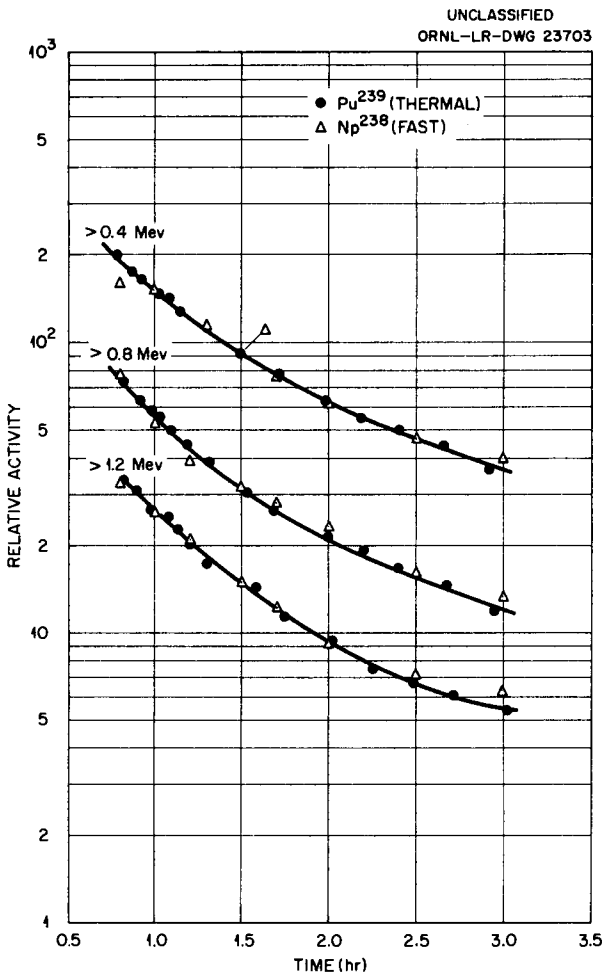

Fig. 60. Decay of the Fission-Product Gamma Rays from the Thermal Fission of Pu^{239} and the Fast Fission of Np^{238}.

the Np^{238} range is unknown, an absorber was chosen whose thickness was about 10% of the average of the measured fission-product ranges, or about 0.3 mg/cm^2 of aluminum.

To show that this method is sufficient to mask the Np^{238} activity as compared with the fission-product activity, the same catcher technique was used for a 10-min thermal irradiation of Pu^{239} as was used for an irradiation of Np^{237} in hole 51N. The relative gamma-ray activities are plotted for both reactions in Fig. 60 with integral biases of >0.4 Mev, >0.8 Mev, and the previously used >1.2 Mev. The two reactions are normalized at a time 1 hr after the irradiation for the >0.4-Mev bias. The curves are drawn through the Pu^{239} points. The Np^{238} activity would have appeared as a discrepancy gradually increasing with time and becoming most pronounced at the >0.8-Mev bias. The actual agreement is excellent, with the discrepancies at long times mostly counting errors.

The technique has been found satisfactory in the Graphite Reactor for irradiations up to 30 min and for three days to one week. It is limited by the 14-hr activity induced in the catcher by the $Al^{27}(n,\alpha)Na^{24}$ reaction, which is subtracted by the use of a control foil. This reaction must either be limited by a short irradiation or be allowed to decay after a long irradiation.

HOT LAB STUDIES

A. E. Richt E. S. Schwartz S. E. Dismuke

Throughout the past year the Hot Cell Group has continued to function basically as a service organization for various intralaboratory groups. Starting July 1 this group has been functioning strictly as a service group without a budget of its own; the charges made each month against the various accounts are based on the percentage of the total work that is done for each account. In other respects the operation of the Hot Lab Section will remain more or less unchanged, with the actual performance of the experiment being a cooperative effort between this section and the requesting group.

During the last year metallographic preparation and examination of approximately 400 radioactive specimens were completed, and the results have been reported.[1] In general, these results were published on a limited-distribution basis to the originating organization, which, in turn, issued a final complete report. Metallographic preparation and examination of approximately 100 nonradioactive specimens have also been made during this period. These specimens generally serve as preirradiation controls, and the results are usually included in the applicable hot-cell report.

In addition to the metallographic work, 53 experiments were completed in the hot cells. This work included disassembly and examination of loop experiments and other in-pile assemblies, machining operations, physical measurements, mechanical and metallurgical testing, and preparation for chemical analysis. A large majority of these experiments were requested by members of the Solid State Division, but work was also requested by members of the Applied Nuclear Physics, Electronuclear Research, Health Physics, Metallurgy, Physics, and Reactor Experimental Engineering Divisions, and included most of the major reactor projects at the Laboratory. Data concerning the use of the hot cells are shown in Table 29.

The dark room has been greatly improved by remodeling and enlarging. Equipment improvements have been made in the metallographic lapping and polishing units. The Solid State Metallurgical Section has constructed a subsize remote impact unit.

Major difficulties were caused by manipulator breakdown, decontamination of cutoff wheel, and operation of specimen cleaner.

Table 29. Hot Cell Utilization

	1956 (%)	January–June 1957 (%)
Installation and testing of equipment and techniques	4	6
Experimental (actual disassembly, data-taking, examination, etc.)	26	30
Decontamination and removal of material	7	5
Maintenance		
Scheduled	9	3
Emergency	6	6
Miscellaneous	3	3
Operational down time (cell occupied but not actually in use)	41	38
Vacant	4	9
Total	100	100

[1] A. E. Richt and J. O. Stiegler, *Metallographic Examination of Components and Coupons from HRP In-Pile Loop L-4-11*, ORNL CF-56-9-116 (Sept. 28, 1956); J. O. Stiegler, *Metallographic Examination of Components, Coupons and Stress Corrosion Specimens from HRP In-Pile Loop L-4-8*, ORNL CF-56-12-113 (Dec. 28, 1956); *Metallographic Examination of Components, Coupons and Stress Corrosion Specimens from HRP In-Pile Loop L-4-12*, ORNL CF-57-2-88 (Feb. 19, 1957); *Metallographic Examination of Components and Coupons from HRP In-Pile Loop L-2-10*, ORNL CF-57-3-42 (March 9, 1957); *Metallographic Examination of Components and Coupons from HRP In-Pile Loop "GG,"* ORNL CF-57-3-83 (March 19, 1957); *Metallographic Examination of Components and Coupons from HRP In-Pile Loop L-4-13*, ORNL CF-57-3-140 (March 29, 1957); *Metallographic Examination of Components, Coupons and Stress Corrosion Specimens from HRP In-Pile Loop L-2-15*, ORNL CF-57-5-103 (May 22, 1957); *Supplementary Metallographic Examination of Titanium Stress Corrosion Specimens from HRP In-Pile Loop L-4-12*, ORNL CF-57-8-54 (Aug. 9, 1957); E. S. Schwartz, *Fifth Hot Laboratories and Equipment Conference, March 14–15, 1957*, p 91, 1957 Nuclear Congress, Philadelphia, 1957.

Plans for next year include setting up a semihot lab, installing a master-slave-type manipulator and periscopes in cells Nos. 1, 2, and 3, and installing a vacuum cleaning system for the hot cells. Plans also include construction of a dry storage facility and improvement of remote equipment, particularly a metallurgical specimen cutoff wheel and specimen cleaner. The effort to improve operating techniques and equipment will be continued, with particular attention given to means of reducing personnel exposure.